MICROFLUIDIC REACTORS FOR ARTIFICIAL PHOTOSYNTHESIS OF CARBOHYDRATES USING CALVIN CYCLE

ZHU YUJIAO

PhD

The Hong Kong Polytechnic University

2019

THE HONG KONG POLYTECHNIC UNIVERSITY

DEPARTMENT OF APPLIED PHYSICS

MICROFLUIDIC REACTORS FOR ARTIFICIAL PHOTOSYNTHESIS OF CARBOHYDRATES USING CALVIN CYCLE

ZHU Yujiao

A thesis submitted in partial fulfilment of the requirements for

the degree of Doctor of Philosophy

August 2018

Certificate of Originality

I hereby declare that this thesis is my own work and that, to the best of my knowledge and belief, it reproduces no material previously published or written, nor material that has been accepted for the award of any other degree or diploma, except where due acknowledgement has been made in the text.

_____ (Signature)

ZHU Yujiao (Name of candidate)

Abstract

Natural photosynthesis (NPS) in green plants relies on Calvin cycle to convert CO_2 into carbohydrates, but the energy efficiency is extremely low. The first step of Calvin cycle catalysed by the enzyme Ribulose-1,5-bisphosphate carboxylase/oxygenase (RuBisCO), though most important in plants, poses to be the major bottleneck due to its low enzymatic efficiency. This PhD research aims to produce basic food materials by realizing Calvin cycle *in vitro* using microreactors. The core technique here is the immobilization of RuBisCO into the microreactors, which enables to overcome the long-standing problems of enzymes and inherits many merits of microfluidics. This research developed three designs of microfluidic reactors for RuBisCO immobilization to produce the glucose precursor, 3-phosphglycerate (3-PGA) using the first step of Calvin cycle. It is original and new since little similar work can be found in literature.

The first design is a PDMS microfluidic reactor (PMR), which directly immobilizes RuBisCO on the inner surface by physical adsorption. It produces 3-PGA at the production rate of 0.011 nmol·min^{-1} and presents a great feasibility in 3-PGA production. But the reusability is quite weak. Only ~20.3% of the initial activity can be attained after 5 cycles of reuse.

The second design (RI-DPMR) utilizes polydopamine to modify the inner surface of microreactors for RuBisCO immobilization via covalent binding. It greatly increases the

surface area from a nanoscopic aspect and significantly enhances the 3-PGA production rate to be as high as 0.122 nmol·min^{-1}, presenting an 11-fold enhancement as compared to that of the first design. Experimental results also show that the immobilized RuBisCO presents enhanced storage stability, thermal stability and reusability as compared to the free RuBisCO in solution.

In the third design (RI-SPMR), the microreactor is formed by compressing porous PDMS sponge into a confined space. Polydopamine is used for RuBisCO immobilization as well. This monolithic structure provides much larger surface area for RuBisCO immobilization, ensuring the highest 3-PGA production rate (0.715 nmol·min^{-1}, 65-fold enhancement as compared to the first design) of the three designs.

In summary, three designs of microfluidic reactors have been developed to improve the surface area and the enzyme immobilization technique for glucose precursor synthesis. Compared with the bulk reaction using free enzyme in solution, the microfluidic reactors have shown enhanced thermal stability, storage stability and reusability. Moreover, the use of microfluidic reactors allows easy control of reaction by changing the flow rate and continuous production of 3-PGA with small amount of RuBisCO. Once scaled up, they would enable to produce large amount of basic food materials in a low-cost, convenient and durable way, which would relieve the food crisis and prepare for future space colonization. Furthermore, the ideas can be applied to other bio-enzymatic systems, expanding the application of enzyme engineering and microfluidics in industry.

List of Publications

Journal publications

1. **Zhu, Y.**, …, Zhang, X., Continuous artificial synthesis of glucose precursor using enzyme-immobilized microfluidic reactors. (under revision)

2. **Zhu, Y.**, Zhang, X., Microfluidic immobilized enzyme reactors for continuous biocatalysis. (to be submitted to Reaction Chemistry & Engineering)

3. Chen, Q., Li, T., **Zhu, Y.**, Yu, W., & Zhang, X. (2018). Dielectrophoresis-actuated in-plane optofluidic lens with tunability of focal length from negative to positive. Optics express, 26(6), 6532-6541.

4. Ma, S., Chiu, C. P., **Zhu, Y.**, Tang, C. Y., Long, H., Qarony, W., ... & Tsang, Y. H. (2017). Recycled waste black polyurethane sponges for solar vapor generation and distillation. Applied Energy, 206, 63-69.

5. Huang, X., Hao, H., Liu, Y., **Zhu, Y.**, & Zhang, X. (2017). Rapid Screening of Graphitic Carbon Nitrides for Photocatalytic Cofactor Regeneration Using a Drop Reactor. Micromachines, 8(6), 175.

6. Huang, X., Liu, J., Yang, Q., Liu, Y., **Zhu, Y.**, Li, T., ... & Zhang, X. (2016). Microfluidic chip-based one-step fabrication of an artificial photosystem I for photocatalytic cofactor regeneration. RSC advances, 6(104), 101974-101980.

7. Huang, X., **Zhu, Y.**, Zhang, X., Bao, Z., Lei, D. Y., Yu, W., ... & Wang, Y. (2016). Clam-inspired nanoparticle immobilization method using adhesive tape as microchip substrate. Sensors and Actuators B: Chemical, 222, 106-111.

8. Huang, X., **Zhu, Y.**, Tsoi, C. C., & Zhang, X. (2015, April). Experimental study on microfluidic nanoparticle immobilization using a biomimetic method. In Design, Test, Integration and Packaging of MEMS/MOEMS (DTIP), 2015 Symposium on (pp. 1-4). IEEE.

9. Zhang, H. Y., **Zhu, Y. J.**, Hu, X. Y., Sun, Y. F., Sun, Y. L., Han, J. M., ... & Zhou, M. (2014). An investigation on the biotribocorrosion behaviour of CoCrMo alloy grafted with polyelectrolyte brush. Bio-medical materials and engineering, 24(6), 2151-2159.

Conference presentations

1. **Zhu, Y.**, Huang, X., Zhang, X., Glucose precursor generation with immobilized enzyme on gold nanoparticles in microfluidic reactors, The 26th IUPAC Symposium on Photochemistry, ***Oral,*** Apr 2016, Osaka, Japan.

2. **Zhu, Y.**, Huang, X., Zhang, X., Artificial Photosynthesis for Carbohydrates Generation with Immobilized Enzyme on Gold Nanoparticles Patterned Microfluidic Reactors, 8th International Symposium on Microchemistry and Microsystems, ***Poster (CHEMINAS Poster Award),*** May 2016, Hong Kong, P.R. China.

3. **Zhu, Y.**, Huang, X., Zhang, X., Artificial Photosynthesis on a Chip: Enzymatic

Synthesis of Glucose Precursor with RuBisCO Immobilized, The 19th Conference of The Physical Society of Hong Kong, ***Oral,*** Jun 2016, Hong Kong, P.R. China.

4. **Zhu, Y.**, Huang, X., Zhang, X., Microfluidic reactors with immobilized enzymes for glucose generation, The 6th International Multidisciplinary Conference on Optofluidics, ***Poster (Nomination Certificate for Best Poster Awards),*** Jul 2016, Beijing, P.R. China.

5. **Zhu, Y.**, Long, J., Zhang, X., Microfluidic reactors for conversion of CO_2 into glucose precursor, Asia-Pacific Conference on Transducers and Micro-Nano Technology (APCOT 2018), ***Oral,*** Jun 2018, Hong Kong, P.R. China.

6. **Zhu, Y.**, Zhang, X., Generation of Glucose Precursor from CO_2 with Microfluidic Reactors, The 8th International Multidisciplinary Conference on Optofluidics 2018, ***Poster,*** Aug 2018, Shanghai, P.R. China.

Acknowledgments

Firstly, I would like to express my sincere gratitude to my advisor **Dr. Zhang Xuming** for the continuous support of my PhD study and related research, for his patience, motivation, and immense knowledge. His guidance helped me in all the time of research and writing of this thesis. I could not have imagined having a better advisor and mentor for my PhD study.

My sincere thanks also go to Prof. Yao Zhongping, Dr. So Pui-Kin, and Dr. Wu Qian from Department of ABCT, and Mr. Zhao Hui from Phenomenex Company, who gave me the access to their laboratory and research facilities and gave me the suggestions in HPLC analysis. I thank all my group members, my friends and colleagues for their great help during my Ph.D. study and all the fun we have had in the last four years, including Dr. Wang N., Dr. Tan F., Dr. Huang X., Dr. Chen Q., Dr. Li T., Mr. Tsoi C. C., Mr. Wong S., Miss Jia H., Dr. Chen L., Dr. Long H., Miss Ma S. and Mr. Wang X..

At the same time, I am also very grateful to those who insist on their dreams. It is their music, their stories, and their spirits that bring joy to me in this boring research life, so that I can still stick to myself. In the future, I will definitely become a better self. To be the chief of life, to reach the unreachable star.

Last but not the least, I would like to thank my parents for supporting me spiritually throughout my PhD study life and writing this thesis in general.

Table of Contents

Certificate of Originality ..... **I**

Abstract ..... **II**

List of Publications ..... **IV**

Journal publications IV

Conference presentations V

Acknowledgments ..... **VII**

Table of Contents ..... **VIII**

List of Figures ..... **XV**

List of Tables ..... **XXVII**

CHAPTER 1 INTRODUCTION **1**

1.1 Overview of artificial photosynthesis 1

1.2 Microfluidic reactors for artificial photosynthesis 5

1.3 Objectives and motivations 7

1.4 Organization of thesis 9

1.5 References 11

CHAPTER 2 LITERATURE REVIEW 15

2.1 Brief 16

2.2 Fabrication of microfluidic reactors 19

2.2.1 Materials for microfluidic reactors 19

2.2.2 Configuration design of microfluidic reactors 21

2.3 Internal structure designs of microfluidic channel 23

2.3.1 Wall-coated type channel 24

2.3.2 Packed-bed type channel 26

2.3.3 Monolithic type channel 27

2.4 Enzyme immobilization techniques 30

2.4.1 Surface binding 35

2.4.2 Encapsulation 44

2.5 Multi-enzymes systems 46

2.6 Summary and outlooks 50

2.7 References 54

CHAPTER 3 MATERIALS AND METHODOLOGY 66

3.1 Chemicals and reagents 66

3.2 Instruments 67

3.2.1 Ultraviolet-visible spectrophotometer 67

3.2.2 Scanning electron microscopy 70

3.2.3 Attenuated total reflection-Fourier transform infrared spectroscopy .. 71

3.2.4 Raman spectroscopy 73

3.2.5 Fluorescence microscopy 74

3.2.6 Ultra-high-performance liquid chromatography-electrospray ionization triple quadrupole mass spectrometer 75

3.3 Determination of reaction time 78

3.4 Determination of protein concentration 78

3.5 Determination of RuBisCO activity 80

3.5.1 RuBisCO activity determination by NADH decreasing 80

3.5.2 RuBisCO activity determination by NADH decreasing with amplification method 82

3.5.3 RuBisCO activity determination by HPLC-MS/MS 84

3.6 Summary 86

3.7 References 87

CHAPTER 4 PDMS MICROFLUIDIC REACTORS FOR 3-PGA PRODUCTION 88

4.1 Brief 88

4.2 Experimental methods 90

4.2.1 Fabrication of PMRs 90

4.2.2 Immobilization of RuBisCO 91

4.2.3 Comparison between pristine and plasma-treated PMRs for RuBisCO immobilization 92

4.2.4 Optimal condition investigation 92

4.2.5 Feasibility of 3-PGA generation with RI-PMRs 92

4.2.6 Reusability of RI-PMRs for 3-PGA production 93

4.3 Results and discussions 93

4.3.1 Comparison between pristine and plasma-treated PMRs for RuBisCO immobilization 93

4.3.2 Optimal condition investigation for RI-PMRs fabrication 96

4.3.3 Feasibility of RI-PMRs for 3-PGA production 98

4.3.4 Reusability of RI-PMRs for 3-PGA production 99

4.4 Summary 100

4.5 References 102

CHAPTER 5 PDA-PDMS MICROFLUIDIC REACTORS FOR 3-PGA PRODUCTION ... 104

5.1 Brief 104

5.2 Experimental methods 105

5.2.1 Fabrication of RI-DPMRs 105

5.2.2 Confirmation of RuBisCO immobilization 106

5.2.3 Determination of protein loading capacity 107

5.2.4 Assay of RuBisCO activity 107

5.2.5 Feasibility of 3-PGA production with RI-DPMRs 108

5.2.6 Storage and thermal stability of RI-DPMRs 108

5.2.7 Reusability of RI-DPMRs 109

5.2.8 Continuous production of 3-PGA from RI-DPMRs 109

5.3 Results and discussions 110

5.3.1 Fabrication of RI-DPMRs 110

5.3.2 Confirmation of RuBisCO immobilization 111

5.3.3 Determination of protein loading capacity and kinetic parameters .. 115

5.3.4 Feasibility of the RI-DPMRs 118

5.3.5 Storage and thermal stability of the RI-DPMRs 119

5.3.6 Reusability of the RI-DPMRs 121

5.3.7 Continuous production of 3-PGA from RI-DPMRs 122

5.4 Summary 123

5.5 References 125

CHAPTER 6 SPONGE PDMS EMBEDDED-MICROREACTOR FOR 3-PGA PRODUCTION 127

6.1 Brief 127

6.2 Experimental methods 129

6.2.1 Fabrication of SPMRs 129

6.2.2 Immobilization of RuBisCO into SPMRs 131

6.2.3 Determination of SPMRs volumes 132

6.2.4 Optimal condition investigation for RI-SPMRs fabrication 132

6.2.5 Feasibility of 3-PGA production with RI-SPMRs 133

6.2.6 Reusability of RI-SPMRs 133

6.3 Results and discussions 133

6.3.1 Characterization of SPMRs and RI-SPMRs 133

6.3.2 Determination of SPMRs volumes 136

6.3.3 Optimal condition investigation for RI-SPMRs fabrication 138

6.3.4 Feasibility of 3-PGA production with RI-SPMRs 141

6.3.5 Reusability of RI-SPMRs 142

6.4 Summary 143

6.5 References 145

CHAPTER 7 CONCLUSIONS AND FUTURE WORK 148

List of Figures

Figure 1.1 The detailed processes of (a) natural photosynthesis and (b) artificial photo-synthesis. 2

Figure 1.2 The detailed reactions of Calvin cycle which consists of three phases. 3

Figure 1.3 Schematics of different microfluidic reactor structures. (a) The high surface area optofluidic microreactor with micro-pillar structure. (b) Cross section of the staggered micro-pillars in the reaction chamber. [23] (c) The PDMS based optofluidic microreactor with the micro-grooved structure. [24] 6

Figure 2.1 Representative configuration designs of microfluidic chips. 22

Figure 2.2 Typical designs for the internal structure of microfluidic channels. 24

Figure 2.3 Examples of wall-coated microchannels for enzyme immobilization. (a) Schematic of the sucrose phosphorylase immobilized on the nanosprings microreactor with enhanced enzyme activity [48]; (b) Process of immobilization of CAL-b based on self-oxidation of dopamine and LBL method. Long chains with positive charges represents PEI, and the circles represents the lipase [28]. 25

Figure 2.4 Examples of packed-bed microchannels for enzyme immobilization. (a) Reaction scheme for ring-opening polymerization of ε-caprolactone to polycaprolactone. (b) Schematic of the microreactor setup. (c) Image shows the photograph of a typical microreactor used in this study. CAL-b immobilized solid beads (macroporous polymethyl methacrylate) were filled in the channel [52]. (d) Scheme representation of the construction and analytical procedure of GOx–MNPs–MD. BR, buffer reservoir; SR, sample reservoir; DR, detection reservoir; WE, working electrode; RE, reference electrode; AE, auxiliary electrode. [61] 27

Figure 2.5 SEM of monolithic and coating in capillary: (a, b) monolithic, (c, d) coating. (e) Lineweaver–Burk plots for L-Asnase immobilized in the monolithic (A, ■) and coating (B, ●) enzymatic microreactors [63]. 28

Figure 2.6 Different enzyme immobilization techniques. 31

Figure 2.7 Schematic representations of enzyme immobilization by ionic binding via different polycations and polyanions. (a) Adenosine deaminase (ADA) immobilization of by PEI and alginate [94]. (b) Trypsin immobilization by HA and chitosan [27]. (c) Trypsin immobilization by PDDA and negatively charged graphene oxide [47]. 37

Figure 2.8 Schematic representations of enzyme immobilization by His-tag/metal binding (a) Diagram of enzyme immobilized by the His-tag/Ni-NTA binding [84]; (b) Chemical structures of the building blocks and scheme for the step-wise assembly process. Ethylene glycol-based mono-adamantyl linker (1) for minimizing the non-specific protein adsorption, biotinylated bisadamantyl linker (2) for the first assembly step and streptavidin (3) as the second assembly step. Biotinylated ALP (bt-ALP, 4) is immobilized onto these streptavidin-biotin surfaces [86]; (c) Schematic diagram of the photo-immobilization process. (Top) Enzyme patches are formed on the top and bottom of a microchannel using the following procedure: (i) Passivation of the surface with a fibrinogen monolayer is followed by (ii) biotin-4-fluorescein surface attachment. This is accomplished by photobleaching with a 488-nm laser line. (iii) Next, the binding of streptavidin-linked enzymes that can be exploited to immobilize catalysts and (iv) to monitor reaction processes on-chip [106]..... 40

Figure 2.9 Covalent binding for enzyme immobilization. (a) Commonly used covalent bonds: mechanisms of the Schiff chemistry and the Carbodiimide chemistry [9]; (b) Preparation of laccase-immobilized membrane on the inner wall of a PTFE microtube; (c) Parabolic

velocity profile characteristic of the laminar flow inside the microtube, and (d) confocal acquisition of the sectional view of the laccase-immobilized microreactor (dry state) [111]..... 43

Figure 2.10 Examples of enzyme immobilization by encapsulation. (a) Schematic illustrations of the microreactor with immobilized lipase–nanoporous material (FSM) composite particles; (b) Lipase molecules encapsulated in the FSM pores [91]; (c) Schematic diagram of the flow-induced gelation in a microfluidic filter device (left) and a typical microscope image showing the nanogel production at a flow rate of 10 ml h^{-1} (right) [112]. 44

Figure 2.11 Examples of enzyme immobilization in multi-enzyme systems. (a) Diagrams of three different configurations of microfluidic reactors. In reactor I, GOx and HRP were co-immobilized on a single set of beads. In reactor II, GOx-immobilized beads and HRP immobilized beads were loading sequentially. In reactor III, the two beads were mixed in the reactor; [120] (b) Schematic of enzyme cascade reaction confined in a microchannel. β-galactosidase and glucose oxidase were assembled on the Au-films with controllable distances (up). Graph of the normalized response currents of H_2O_2 as a function of the concentration of lactose with different gap distances in the

experiment (down). [92] (c) Localization of GOx (yellow) and HRP (purple) at defined distances on the surface of DNA origami tiles (up). An increased catalytic activity was observed when the inter-enzyme distance was decreased to 10 nm, as analyzed with d-glucose, $ABTS_2$–(2,2'-azinobis(3-ethylbenzothiazoline-6-sulfonate)) and O_2 as substrates at pH 7.2 (down). C_1 and C_2 refer to the tiles without nucleic acid and free enzymes, respectively. [118] (d) A three-enzyme cascade was performed in a microchannel using the two immobilized enzymes Cal-b and HRP in combination with GOx, which was added in solution together with the substrates (up). [121] The graph plotted the measured product absorbances of a three-enzyme cascade reaction at different flow rates and different distances between the immobilized enzyme Cal-b and HRP. [87]..... 47

Figure 3.1 Schematic (a) and photograph (b) for an ultraviolet-visible spectrophotometer. 68

Figure 3.2 Photography of JEOL field emission scanning electron microscopy. 70

Figure 3.3 Mechanism of the ATR accessory (a) and photography of the Bruker Vertex-70 FTIR (b)..... 72

Figure 3.4 Photograph of the LabRAM HR 800 Raman Spectrometer. 74

Figure 3.5 Photograph of the Olympus BX41 fluorescence microscope. 75

Figure 3.6 Diagram (a) and photography (b) of the LC-MS system. 76

Figure 3.7 Calibration curve of protein amount determined from BSA solutions by the Bradford method. 78

Figure 3.8 Principle of the stoichiometric determination of 3-PGA by the spectrophotometer. 80

Figure 3.9 (a) UV-Vis spectral absorbance of NADH over time during the reaction; (b) 3-PGA production and polynomial fit of the produced 3-PGA. 81

Figure 3.10 Decrease of the NADH absorbance at 340 nm after the assay mixture except for RuBisCO is flowed through the RuBisCO-immobilized microreactor. 82

Figure 3.11 Principle of the amplification signal assay for RuBisCO activity. 83

Figure 3.12 Calibration for the determination of 3-PGA amount by UV-Vis spectrophotometer. (a) The absorbance decreasing at 340 nm at different concentrations of 3-PGA. (b) Calibration curve for the 3-PGA determination by the decreasing rate of absorbance at 340 nm. 83

Figure 3.13 Calibration for the determination of 3-PGA amount by HPLC-

MS/MS. (a) HPLC-MS/MS chromatography of the standard RuBP and 3-PGA. (b) Calibration curves of the RuBP (red circle) and 3-PGA (black square) signals by the areas of the peaks. 85

Figure 4.1 Schematics for the fabrication of RI-PMRs. (a) Process flow of the fabrication of the PMRs using soft lithography. (b) Three-dimensional diagram of the RI-PMRs. (c) Illustration of the procedures for RuBisCO immobilization by physical adsorption. 90

Figure 4.2 Water contact angle measurement of pristine/plasma-treated PDMS surfaces. All data are presented as mean ± s.d. (n = 3). 94

Figure 4.3 SEM images of the surfaces of (a) pristine PDMS, (b) RuBisCO-immobilized pristine PDMS, (c) plasma-treated PDMS and (d) RuBisCO-immobilized plasma-treated PDMS. 95

Figure 4.4 Comparisons of the protein loading efficiency and the RuBisCO activity between the pristine and plasma-treated PDMS microfluidic reactors. RuBisCO concentration is 1 $\mu g \cdot \mu L^{-1}$ with the immobilization time of 4 h. 0.5 mM RuBP is injected at the flow rate of 7 $\mu L \cdot min^{-1}$. 96

Figure 4.5 Protein loading efficiencies and RuBisCO activities as a function of the immobilization time. RuBisCO concentration is 1 $\mu g \cdot \mu L^{-1}$. 0.5

mM RuBP is injected at the flow rate of 7 μL·min^{-1}. 97

Figure 4.6 Protein loading amount (a) and loading efficiencies (c) and RuBisCO activities as a function of the concentration of injected RuBisCO. The immobilization time is 4 h. 0.5 mM RuBP is injected at the flow rate of 7 μL·min^{-1}. 98

Figure 4.7 Feasibility of RI-PMRs: 3-PGA production amount as a function of the reaction time. The error bars represent the standard deviations of three repeated experiments. RuBisCO concentration is 2 μg·μL^{-1} with the immobilization time of 4 h. 99

Figure 4.8 Reusability of the RI-PMRs. RuBisCO concentration is 2 μg·μL^{-1} with the immobilization time of 4 h. 0.5 mM RuBP is injected at the flow rate of 7 μL·min^{-1}..... 100

Figure 5.1 Schematics of the fabricated RI-DPMRs. (a) Three-dimensional diagram and the photo (inset) of the RI-DPMRs, the scale bar of the inset is 1 cm. (b) Illustration of the procedures of RuBisCO immobilization. 110

Figure 5.2 Surface characterization of RI-DPMRs inner surfaces. (a), (b) and (c) are the SEM images of the pristine PDMS surface, PDA-modified PDMS surface, and RuBisCO-immobilized PDA-PDMS surface,

respectively. The top right insets are the optical microscopic images of the corresponding microfluidic reactors and the bottom right insets are the water contact angle results of the corresponding surfaces. 112

Figure 5.3 SEM images with larger magnification of (a) PDA-modified PDMS surface, and (b) RuBisCO-immobilized PDA-PDMS surface, respectively. 112

Figure 5.4 Raman spectra (a) and ATR-IR spectra (b) of the PDMS channels before (black line) and after (red line) RuBisCO immobilization. 113

Figure 5.5 Fluorescence experiments for confirming the RuBisCO immobilization. (a) Fluorescence images of the empty microchannel, the RuBisCO-FITC filled microchannel, and the rinsed microchannel. (b) The corresponding fluorescence intensity profiles obtained along the observation lines. (c) Fluorescence images of the the RuBisCO-FITC filled in the pristine PDMS microchannel, and the rinsed pristine PDMS microchannel. (d) The corresponding fluorescence intensity profiles obtained along the observation lines. The scale bar is 500 μm. 114

Figure 5.6 Protein loading amount and loading efficiency as a function of the

concentration of injected RuBisCO. Immobilization time is 6 h. 116

Figure 5.7 Feasibility of the RI-DPMRs for 3-PGA production. (a) Production amount of 3-PGA as a function of the reaction time for the RI-DPMRs (red solid line) and the BI-DPMRs (black dash-dotted line). (b) HPLC-MS/MS chromatography of RuBP and 3-PGA from the production solutions obtained in 5 min. 119

Figure 5.8 Characterizations of the immobilized RuBisCO. (a) Storage stability of immobilized (red line) and free RuBisCO (black line). (b) Thermal stability of immobilized (red line) and free RuBisCO (black line). (c) Reusability of the RI-DPMRs with the flow rates of the injected RuBP at 7 μL/min (grey bar) and 1.4 μL/min (red bar), the reaction times are 1 min and 5 min, respectively. 120

Figure 5.9 Production amount of 3-PGA as a function of the volume of used reactant mixture solution, the black line is the reaction in the bulk reactor with free RuBisCO and the red line is the reaction in the RI-DPMRs with the immobilized RuBisCO. 123

Figure 6.1 Process flow of the fabrication of sp-PDMS embedded microreactors. 130

Figure 6.2 Design of the aluminum mold for PDMS pattern fabrication, the unit

is mm. 131

Figure 6.3 Illustration of the procedures for RuBisCO immobilization on SPMRs by PDA. 131

Figure 6.4 SEM images of (a) the g-CAM, porous PDMS sponge with the g-CAM to PDMS solution ratio of (b) 1:1, (c) 5:1 and (d) 7:1. 134

Figure 6.5 Photographs of the PDA modified-PDMS sponges in different procedure orders (a) and the RI-SPMRs (b). 1#: PDMS sponge was embedded first in microreactor then modified with PDA. 2#: PDMS sponge was modified with PDA first and then embedded in microreactor. 3#: PDMS sponge was formed in-situ in the microreactor and then modified with PDA. 135

Figure 6.6 SEM images of the inner surfaces of (a), (b) the PDA-modified SPMRs and (c), (d) the RI-SPMRs. 135

Figure 6.7 Volume determination of the SPMRs. (a) Weight change of SPMRs after infusion by different solutions having different densities. The thickness of the sp-PDMS used here is 1 mm. Calculation of the volumes of SPMRs fabricated by different thicknesses of sp-PDMS with the g-CAMs/PDMS ratio of (b) 3:1, (c) 5:1, (d) 7:1. 137

Figure 6.8 3-PGA production by RI-SPMRs fabricated in different procedures.

The flow rate of injected RuBP solution was 7 μL·min^{-1}..... 139

Figure 6.9 3-PGA production amount from the RI-SPMRs fabricated in different conditions with RuBP solution injected in 7 μL·min^{-1}. (a) 3-PGA production amount changes as a function of the thickness of sp-PDMS when 1 μg·μL of RuBisCO is injected for immobilization. (b) 3-PGA production amount changes as a function of the injected RuBisCO concentration by SPMRs fabricated with 2 mm-thick sp-PDMS. 140

Figure 6.10 3-PGA production amounts when RuBP solution is injected at different flow rates. The thickness of sp-PDMS is 2 mm, RuBisCO concentration is 2 μg/μL. 141

Figure 6.11 Reusability of the microreactor when the flow rate of the injected RuBP is set as 7 μL·min^{-1}. The thickness of sp-PDMS is 2 mm, RuBisCO concentration is 2 μg/μL. 142

List of Tables

Table 2.1 Summary of recent μ-IMERs studies. 31

Table 5.1 Summary of different parameters of the RI-DPMRs reaction and bulk reaction. 116

Table 7.1 Comparison of the microfluidic reactors developed in this PhD research..... 148

CHAPTER 1
INTRODUCTION

1.1 Overview of artificial photosynthesis

There have been enormous demands for researchers in the field of energy generation to convert solar energy into chemical energy thanks to its greenhouse-gas-free property. Moreover, the chemical energy can be stored and used for biological activities on demand [1]. Food, as the major source of chemical energy in our daily life, is of ultimate importance to human beings. However, the food shortage problem has long been overshadowing the history of mankind. For instance, the food and feed production needs to increase by 70 percent by 2050 in order to satisfy the world's food demands according to the Food and Agricultural Organization (FAO) of the United Nations [2]. The fundamental mechanism behind the food production is natural photosynthesis (NPS) by plants. It is a process in which sunlight is captured and converted into the energy in carbohydrates [3]. It includes light-dependent and light-independent reactions. The light reaction of NPS, known as the "Z-scheme" [1], as shown in **Figure 1.1** (a), utilizes two pigments P680 and P700 linked by a complicated electron transport chain to change two absorbed photons into one excited electron. Then, the $NADP^+$ reductase captures two electrons and one H^+ ion to reduce one $NADP^+$ molecule into NADPH. Next, NADPH is used as a reductant for the light-independent reactions, also called the Calvin Cycle, to assemble carbon dioxide and water into energy-rich carbohydrates. However, NPS suffers

some drawbacks including low energy efficiency (~1%) and severe limits of soil, climate, water and labor [4]. It is urgently needed to find a scientific solution for the food production.

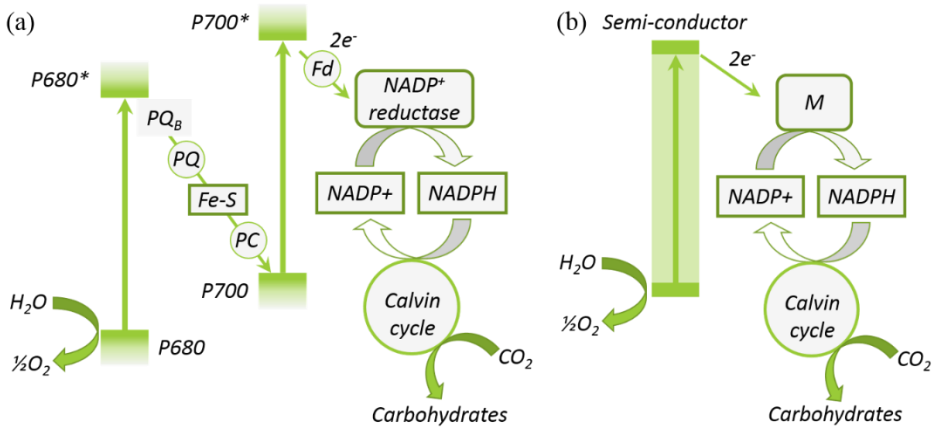

Figure 1.1 The detailed processes of (a) natural photosynthesis and (b) artificial photo-synthesis.

Recently, artificial photosynthesis (APS) has become a potentially more controlled substitute for the solar-to-chemical energy-conversion process, which aims to mimic the green plants to produce energy-rich chemicals using sunlight but with much higher efficiency (~12%) and simplicity [5]. It may break the limits of NPS by using man-made nanomaterials and engineered photosynthetic reactors, thus attracting increasing research interests. Most efforts of these studies have been put into hydrogen generation by water splitting [1, 6-9] and biofuel production[10-14]. This Ph.D study, which differs obviously from these previous studies, intends to mimic the NPS to produce the glucose precursor, rather than generate hydrogen or grow algae or cyanobacteria. **Figure 1.1** (b) shows the main idea of APS process, here a semiconductor photocatalyst is utilized to absorb the

photons, an electron mediator M to regenerate NADPH and the same Calvin cycle to convert carbon dioxide into carbohydrates. Comparing the two figures, one can see the obvious differences: the electron transfer processes and its mediator are much simplified in the APS. But Calvin cycle, a series of biochemical redox reactions, remains the same.

The Calvin cycle [15], which is also called Calvin–Benson–Bassham (CBB) cycle, reductive pentose phosphate cycle or C3 cycle, is a series of biochemical redox reactions that convert carbon dioxide and other compounds into glucose. It is also known as the light-independent reactions; the detailed reactions are schemed in **Figure 1.2** [16]. These reactions occur in the stroma, the fluid-filled area of a chloroplast outside of the thylakoid membranes. These reactions utilize the products (ATP and NADPH) of light-dependent reactions and perform further chemical processes.

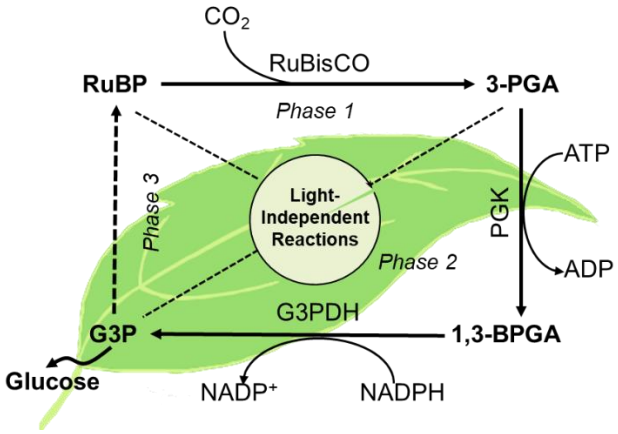

Figure 1.2 The detailed reactions of Calvin cycle which consists of three phases.

The light-independent reactions can be divided into three phases: carbon fixation, reduction reactions, and ribulose 1,5-bisphosphate (RuBP) regeneration. Here are the

detailed descriptions:

Phase 1: Referring to **Figure 1.2**, the enzyme ribulose-1,5-bisphosphate carboxylase oxygenase (RuBisCO, EC 4.1.1.39) catalyzes the carboxylation of RuBP, (a 5-carbon compound) by carbon dioxide (a total of 6 carbons) into two molecules of 3-phosphoglycerate (3-PGA, a 3-carbon compound). Then, the enzyme phosphoglycerate kinase (PGK) catalyzes the phosphorylation of 3-PGA by ATP (which is already produced in the light-dependent stage). The products are 1,3-bisphosphoglycerate (1,3-BPGA, glycerate-1,3-bisphosphate) and ADP are the products;

Phase 2: The enzyme glyceraldehyde-3-phosphate dehydrogenase (GAPDH) catalyzes the reduction of 1,3-BPGA by NADPH (which is another product of the light-dependent stage). Glyceraldehyde 3-phosphate (G3P, a 3-carbon compound) is produced, and the NADPH itself is oxidized into NADP+. Two of G3Ps can form the end product glucose ($C_6H_{12}O_6$);

Phase 3: RuBP is regenerated using a series of enzymatic reactions, which are complicated and beyond the scope of this research. The details are not presented here.

The general reactions of Calvin cycle are as follows:

$$6\,CO_2 + 12\,NADPH + 10\,H_2O + 18\,ATP \rightarrow 2\,G3P + 4\,H^+ + 12\,NADP^+ + 18\,ADP + 16\,Pi \quad (1.1)$$

$$2\,G3P \rightarrow Glucose \quad (1.2)$$

In the absence of Phase 3, the general reaction becomes

$$RuBP + CO_2 + 2\,NADPH + 2\,ATP \rightarrow 2\,G3P + 2\,H^+ + 2\,NADP^+ + 2\,ADP + 2\,Pi \quad (1.3)$$

In Eq. (1.3), the fixation of each CO_2 molecule can produce two molecules of G3P. It is more productive as compared to the full Calvin cycle in Eq. (1.1), which needs to fix six CO_2 molecules to get two G3P molecules. However, it is at cost of consumption of RuBP.

1.2 Microfluidic reactors for artificial photosynthesis

In fact, NPS is naturally a microfluidic system as it occurs in microscale chloroplasts and bacteria-filled fluids, implying the feasibility to be mimicked by man-made microfluidic structures. This inspires me to propose this work to develop integrated microfluidic chips for the APS of glucose precursor generation from CO_2. The microchannel reaction systems are regarded as the new and promising technology in chemistry, chemical engineering and biotechnology [10] by offering several advantages over traditional technologies in performing chemical reactions, such as small consumption of reactant solutions, large surface-area-to-volume ratio [17], high efficiency, superior repeatability [11,12], and precise reaction control [18]. The key advantages of microsystems are rapid heat exchange and fast mass transfer [19-21], which are hard to achieve by the conventional bulk system. Therefore, many researchers have applied microfluidic chips to the APS for water splitting [22-24], biofuel production [25-27], or other organic compounds production [28, 29].

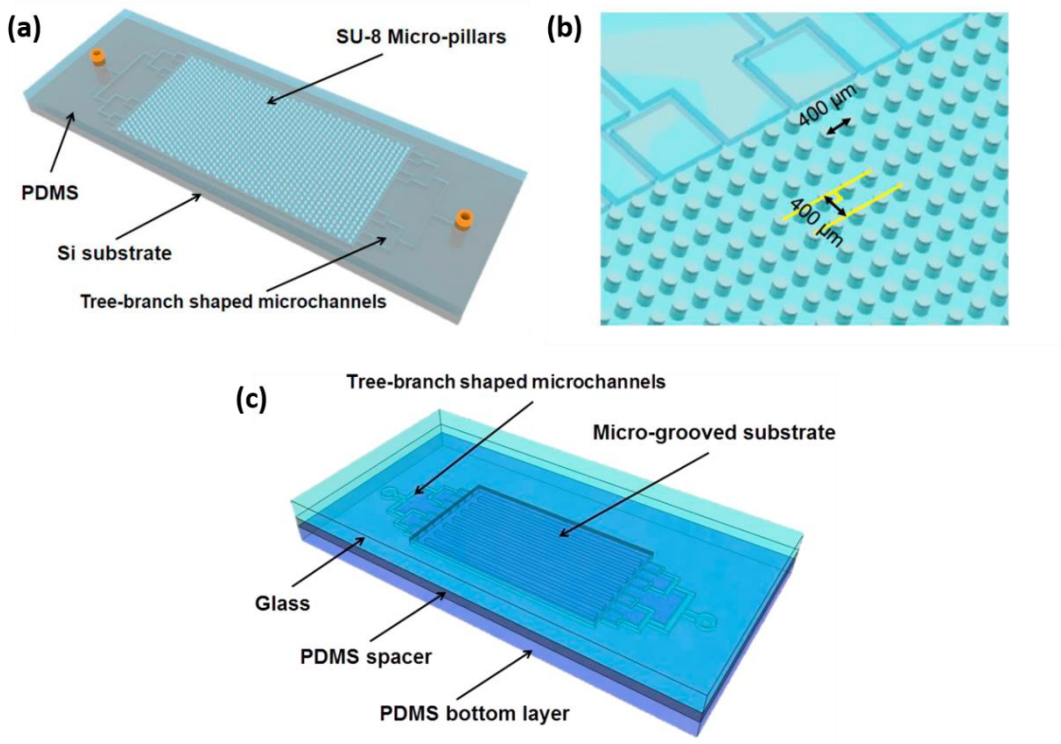

Figure 1.3 Schematics of different microfluidic reactor structures. (a) The high surface area optofluidic microreactor with micro-pillar structure. (b) Cross section of the staggered micro-pillars in the reaction chamber. [23] (c) The PDMS based optofluidic microreactor with the micro-grooved structure. [24]

In the previous studies of APS in microfluidics, the catalysts are usually immobilized in the microchannels for high reaction efficiency, enhanced reusability and superior stability during reaction, leading to a considerable improvement in the reaction rate as compared to that of the traditional bulk reactions. It has also been demonstrated that when the surface area of the microfluidic reactors is enlarged, as shown in

Figure 1.3, more catalysts can be loaded, resulting in a rapid solution mixing, an increased reaction rate and an enhanced mass transfer as compared to the planar microreactors [23, 24].

1.3 Objectives and motivations

This research aims to produce the glucose precursor in microfluidic reactors by replicating the Calvin cycle reactions of plants with much higher efficiency and simplicity, which is different from the previous studies. As we all know that the world is moving rapidly into food crisis due to the extreme weather, shortage of energy and population explosion. The mechanism of food production by plants is glucose production by Calvin cycle from light energy and carbon dioxide. Calvin cycle is a series of cascaded reactions with kinds of enzymes as the catalysts. Enzymes in living organisms often have the disadvantages of being inefficient because of their functional diversity to meet the requirements of biological evolution [30]. RuBisCO, as the most abundant enzyme in plants, catalyzes the first carbon fixation phase in light-independent reactions. Even so, the low catalytic rate and poor specificity of RuBisCO seriously limits the agricultural productivity[30]. Although many studies have been conducted to overcome the inefficiency of RuBisCO, they are mainly designed for *in vivo* biological systems[31, 32]. Lots of energy and labor are consumed to balance the metabolic pathways in intact cells. For the industrial cell-free application with the demands of sustainability and scalability, immobilizing and concentrating RuBisCO into man-made structures would be a more promising method to enhance the overall catalytic efficiency [33, 34]. Enzyme immobilization has many advantages, such as high enzyme-to-reactant ratio, enhanced enzyme stability, admirable enzyme reusability, weakened feedback inhibition and

possible modulation of catalytic property [35-37]. On account of these benefits, this research plans to constitute the NPS system for glucose precursor production with the first phase reaction by immobilizing RuBisCO. As can be seen from the previous APS with microfluidics, immobilization of enzymes in microfluidic reactors with large surface area would be a promising solution to the APS of glucose precursor with Calvin cycle with many advantages: small dimension which saves sample and cost, large surface to volume ratio which enhances the reaction rate, well defined reaction time and easily controlled reaction conditions, and easy cascading of several reactions in separated reactors. The technique can also overcome the enzymes' low stability in solution, the gradually decreased activity in storage, the feedback inhibition of reactions, and the cross-contamination of enzymes [38].

Basically, we want to streamline the first phase reaction in microfluidic reactors by immobilizing RuBisCO on the inner surfaces of reactors comes out for the foundation of basic food production with bio-mimic systems. The detailed objectives are listed as below:

- To explore the reaction pathway of Calvin cycle for glucose precursor synthesis;
- To optimize the RuBisCO immobilization technique so as to maintain the RuBisCO activity without denaturation, and to allow repeated use of RuBisCO;
- To design microfluidic reactors with different internal structures for RuBisCO immobilization;

- To produce glucose precursor in a continuous mode by developing an integrated, enzyme-immobilized microfluidic chip;
- To simplify Calvin cycle for more efficient and environmentally friendly synthesis processes.

1.4 Organization of thesis

The chapters of the thesis are organized as follows:

Chapter 1 starts with an overview of the mechanisms of NPS and APS and their comparison. Then, the significance of microfluidics to APS are presented. At the end, the objectives and organizations of the thesis are discussed.

Chapter 2 reviews different enzyme immobilization techniques in microfluidic reactors, which will be adopted into this work, with a comprehensive study of related works.

Chapter 3 presents the characterization equipment and the usual methods used in the work.

Chapter 4 reports a simple design of microfluidic reactors made by sealing patterned PDMS layer with another flat PDMS layer. The enzyme RuBisCO is directly immobilized on the PDMS surface by physical adsorption.

Chapter 5 presents an improved design of microfluidic reactors, in which

polydopamine is used to immobilize RuBisCO onto the microchannel surfaces for the production of glucose precursor. Then, the performances of the immobilized RuBisCO are compared with free RuBisCO. In addition, the microfluidic RuBisCO immobilized reactors are demonstrated to produce 3-PGA in the continuous mode with much higher production efficiency as compared to that in the bulk reaction due to the cumulative effect.

Chapter 6 proposes a new design of microreactor embedded with a polydopamine-modified porous PDMS. It has much increased surface area for more RuBisCO loading, leading to larger 3-PGA production. In this case, the properties of immobilized RuBisCO and 3-PGA production efficiency are also investigated and compared with the first design.

Chapter 7 summarizes this work of glucose precursor production using microfluidic reactors. The limitations of this work and some suggestions for future work are presented as well.

1.5 References

[1] Y. Tachibana, L. Vayssieres, and J. R. Durrant, "Artificial Photosynthesis for Solar Water-Splitting," *Nature Photonics,* vol. 6, pp. 511-518, 2012.

[2] E. Northoff. (2009). *2050: A Third More Mouths to Feed*. Available: http://www.fao.org/news/story/en/item/35571/icode/

[3] J. M. Berg, J. L. Tymoczko, and L. Stryer, *Biochemistry*, 7th ed. New York, USA: W. H. Freeman, 2012.

[4] C. A. Carter, "China's Agriculture: Achievements and Challenges," *Agricultural and Resource Economics Update,* vol. 14, pp. 5-7, 2011.

[5] J. J. Concepcion, R. L. House, J. M. Papanikolas, and T. J. Meyer, "Chemical Approaches to Artificial Photosynthesis," *Proceedings of the National Academy of Sciences,* vol. 109, pp. 15560-15564, 2012.

[6] E. S. Andreiadis, M. Chavarot‐Kerlidou, M. Fontecave, and V. Artero, "Artificial Photosynthesis: From Molecular Catalysts for Light‐Driven Water Splitting to Photoelectrochemical Cells," *Photochemistry and Photobiology,* vol. 87, pp. 946-964, 2011.

[7] D. Gust, T. A. Moore, and A. L. Moore, "Solar Fuels Via Artificial Photosynthesis," *Accounts of Chemical Research,* vol. 42, pp. 1890-1898, 2009.

[8] N. S. Lewis and D. G. Nocera, "Powering the Planet: Chemical Challenges in Solar Energy Utilization," *Proceedings of the National Academy of Sciences,* vol. 103, pp. 15729-15735, 2006.

[9] A. J. Bard and M. A. Fox, "Artificial Photosynthesis: Solar Splitting of Water to Hydrogen and Oxygen," *Accounts of Chemical Research,* vol. 28, pp. 141-145, 1995.

[10] R. Razeghifard, *Natural and Artificial Photosynthesis: Solar Power as an Energy Source*: John Wiley & Sons, 2013.

[11] A. M. Ruffing, "Engineered Cyanobacteria: Teaching an Old Bug New Tricks," *Bioengineered Bugs,* vol. 2, pp. 136-149, 2011.

[12] E. I. Lan and J. C. Liao, "Metabolic Engineering of Cyanobacteria for 1-Butanol Production from Carbon Dioxide," *Metabolic Engineering,* vol. 13, pp. 353-363, 2011.

[13] A. M. Kunjapur and R. B. Eldridge, "Photobioreactor Design for Commercial Biofuel Production from Microalgae," *Industrial & Engineering Chemistry*

Research, vol. 49, pp. 3516-3526, 2010.

[14] A. Magnuson, M. Anderlund, O. Johansson, P. Lindblad, R. Lomoth, T. Polivka, *et al.*, "Biomimetic and Microbial Approaches to Solar Fuel Generation," *Accounts of Chemical Research,* vol. 42, pp. 1899-1909, 2009.

[15] I. Wikimedia Foundation. (2015). *Light-Independent Reactions*. Available: https://en.wikipedia.org/wiki/Light-independent_reactions

[16] D. B. P. State. (2004). *Energy V - Photosynthesis (Calvin Cycle)*. Available: https://wikispaces.psu.edu/pages/viewpage.action?pageId=97552146

[17] K. S. Elvira, X. C. i Solvas, and R. C. Wootton, "The Past, Present and Potential for Microfluidic Reactor Technology in Chemical Synthesis," *Nature Chemistry,* vol. 5, p. 905, 2013.

[18] M. Oelgemöller and O. Shvydkiv, "Recent Advances in Microflow Photochemistry," *Molecules,* vol. 16, pp. 7522-7550, 2011.

[19] G. M. Whitesides, "The Origins and the Future of Microfluidics," *Nature,* vol. 442, p. 368, 2006.

[20] N. Wang, X. Zhang, Y. Wang, W. Yu, and H. L. Chan, "Microfluidic Reactors for Photocatalytic Water Purification," *Lab on a Chip,* vol. 14, pp. 1074-1082, 2014.

[21] R. Gorkin, J. Park, J. Siegrist, M. Amasia, B. S. Lee, J.-M. Park, *et al.*, "Centrifugal Microfluidics for Biomedical Applications," *Lab on a Chip,* vol. 10, pp. 1758-1773, 2010.

[22] S. S. Ahsan, A. Gumus, and D. Erickson, "Redox Mediated Photocatalytic Water-Splitting in Optofluidic Microreactors," *Lab on a Chip,* vol. 13, pp. 409-414, 2013.

[23] L. Li, R. Chen, Q. Liao, X. Zhu, G. Wang, and D. Wang, "High Surface Area Optofluidic Microreactor for Redox Mediated Photocatalytic Water Splitting," *International Journal of Hydrogen Energy,* vol. 39, pp. 19270-19276, 2014.

[24] R. Chen, L. Li, X. Zhu, H. Wang, Q. Liao, and M.-X. Zhang, "Highly-Durable Optofluidic Microreactor for Photocatalytic Water Splitting," *Energy,* vol. 83, pp. 797-804, 2015.

[25] X. Cheng, R. Chen, X. Zhu, Q. Liao, X. He, S. Li, *et al.*, "Optofluidic Membrane Microreactor for Photocatalytic Reduction of Co2," *International Journal of Hydrogen Energy,* vol. 41, pp. 2457-2465, 2016.

[26] X. Cheng, R. Chen, X. Zhu, Q. Liao, L. An, D. Ye, *et al.*, "An Optofluidic Planar Microreactor for Photocatalytic Reduction of Co2 in Alkaline Environment," *Energy,* vol. 120, pp. 276-282, 2017.

[27] R. Chen, X. Cheng, X. Zhu, Q. Liao, L. An, D. Ye, *et al.*, "High-Performance Optofluidic Membrane Microreactor with a Mesoporous Cds/Tio2/Sba-15@ Carbon Paper Composite Membrane for the Co2 Photoreduction," *Chemical Engineering Journal,* vol. 316, pp. 911-918, 2017.

[28] J. S. Lee, S. H. Lee, J. H. Kim, and C. B. Park, "Artificial Photosynthesis on a Chip: Microfluidic Cofactor Regeneration and Photoenzymatic Synthesis under Visible Light," *Lab on a Chip,* vol. 11, pp. 2309-2311, 2011.

[29] X. Ren, H. Lu, J. G. Zhou, P. L.-G. Chong, W. Yuan, and M. Noh, "Porous Polydimethylsiloxane as a Gas–Liquid Interface for Microfluidic Applications," *Journal of Microelectromechanical Systems,* vol. 26, pp. 120-126, 2017.

[30] R. J. Ellis, "Biochemistry: Tackling Unintelligent Design," *Nature,* vol. 463, pp. 164-165, 2010.

[31] G. K. Sidhu, R. Mehrotra, and S. Mehrotra, "Carbon Concentrating Mechanisms: In Rescue of Rubisco Inefficiency," *Acta Physiologiae Plantarum,* vol. 36, pp. 3101-3114, 2014.

[32] E. Carmo‐Silva, J. C. Scales, P. J. Madgwick, and M. A. Parry, "Optimizing Rubisco and Its Regulation for Greater Resource Use Efficiency," *Plant, Cell & Environment,* vol. 38, pp. 1817-1832, 2015.

[33] S. Chakrabarti, S. Bhattacharya, and S. K. Bhattacharya, "Immobilization of D‐Ribulose‐1, 5‐Bisphosphate Carboxylase/Oxygenase: A Step toward Carbon Dioxide Fixation Bioprocess," *Biotechnology and Bioengineering,* vol. 81, pp. 705-711, 2003.

[34] S. Satagopan, Y. Sun, J. R. Parquette, and F. R. Tabita, "Synthetic Co 2-Fixation Enzyme Cascades Immobilized on Self-Assembled Nanostructures That Enhance Co 2/O 2 Selectivity of Rubisco," *Biotechnology for Biofuels,* vol. 10, p. 175, 2017.

[35] R. C. Rodrigues, C. Ortiz, Á. Berenguer-Murcia, R. Torres, and R. Fernández-Lafuente, "Modifying Enzyme Activity and Selectivity by Immobilization," *Chemical Society Reviews,* vol. 42, pp. 6290-6307, 2013.

[36] U. T. Bornscheuer, "Immobilizing Enzymes: How to Create More Suitable Biocatalysts," *Angewandte Chemie International Edition,* vol. 42, pp. 3336-3337, 2003.

[37] R. A. Sheldon and S. van Pelt, "Enzyme Immobilisation in Biocatalysis: Why, What and How," *Chemical Society Reviews,* vol. 42, pp. 6223-6235, 2013.

[38] E. Magnan, I. Catarino, D. Paolucci-Jeanjean, L. Preziosi-Belloy, and M.-P. Belleville, "Immobilization of Lipase on a Ceramic Membrane: Activity and

Stability," *Journal of Membrane Science,* vol. 241, pp. 161-166, 2004.

CHAPTER 2
LITERATURE REVIEW

Biocatalysis has attracted significant attention owing to their environmental-friendly nature, high efficiency and remarkable selectivity during reactions. However, enzymes, one powerful catalyst used in biocatalysis, also suffer from low stability for long time operation in solution and gradual decrease of activity in storage. On the other hand, microfluidic reactors are devices known for small dimension, large surface to volume ratio and well-defined reaction time. Enzymes immobilized in the microfluidic reactors can significantly improve both the reaction rate and the storage stability, not to mention the decreased autolysis and the ease of use. The use of microfluidic immobilized enzyme reactors (μ-IMERs) offers several advantages over traditional technologies in performing biocatalytic reactions, such as low consumption of reactant solutions, rapid heat exchange, fast mass transfer, and high efficiency and superior repeatability. In this chapter, the strategies to increase the enzyme stability and reusability in microfluidic reactors will be discussed and investigated by a top-down approach. First, from the macroscopic perspective, different designs of the microfluidic reactors are categorized by the materials and the overall layout. Then, from the microscopic point of view, several strategies are discussed to increase the surface area of the microreactors so as to increase the enzyme loading amount and to reduce the substrate diffusion path. Finally, when we move to a nanoscopic level, attention is paid to the choice of enzyme immobilization technique to

increase the stability and reusability as well as to preserve its activity. This chapter is intended to provide a guide to the biocatalysis in microreactors and to expedite the progress of this important research area.

2.1 Brief

Biocatalysis is the catalytic reaction that uses natural catalyst to catalyze chemical reactions. Enzyme is one important kind of natural catalysts which owns many excellent characteristics that artificial catalysts are lack of, such as high efficiency, great selectivity, environment friendly and the ability to favor biocatalysis under mild conditions [1]. The applications of enzyme for green and sustainable chemical synthesis in industry have been widely investigated and have infiltrated into our daily life. Despite their excellent catalytic ability, in many cases it is necessary to improve certain aspects of the enzyme, such as reusability and activity recovery for economic effects, long-term operation and storage stability, inhibition of certain reaction products, and selectivity to non-native substrates, prior to the mass production of industrialized products [2]. Moreover, the separation of enzyme from products after the completion of reaction is always an indispensable part of work. It can avoid possible contamination of the products and can reduce the overall operational costs of industrial production, however it often requires a lot of time and effort [3]. Fortunately, these drawbacks can be overcome by enzyme immobilization, which greatly simplifies the separation and recovery of enzyme. Additionally, it has been demonstrated that the enzyme immobilization can improve the enzyme activity, stability

and selectivity to some extents [4]. Furthermore, the enzyme immobilization also makes it easy to precisely control the reaction condition and the whole processes. Researchers have devoted lots efforts to studying various enzyme immobilization techniques so far, such as physical adsorption, affinity bonding, covalent binding, and encapsulation [5-8]. However, inappropriate enzyme immobilization would also cause conformational change, block of active sites and diffusion resistance, which in turn leads to activity loss. Considering the structural diversity, complexity and variability of enzymes and their sensitivity to environmental conditions, different immobilization techniques may have different impacts on different enzymes. Therefore, it remains an important area of scientific research to explore simple, efficient and more adaptable enzyme immobilization methods.

In laboratory research of enzyme immobilization, it has been pointed out that when the products are separated from the enzymes in time and the substrates are continuously injected, a higher yield of productions can be obtained with less sample used in reactions [9]. Therefore, the combination of microfluidic reactors and enzyme immobilization, regarded as microfluidic immobilized enzyme reactors (μ-IMERs), attracts a lot of research interests. Microfluidic reactors are devices with small dimension, large surface area to volume ratio and well defined reaction time [10]. The microchannel reaction systems are regarded as a new and promising platform in chemistry, chemical engineering and biotechnology [11] by offering several advantages, such as low consumption of

reactant solutions, high efficiency and improved repeatability [12, 13], as compared to traditional technologies in performing chemical reactions. The key advantages of microsystems are rapid heat exchange and fast mass transfer, which are hard to achieve by the conventional bulk system. In addition, microchannel reaction systems provide large surface and interface areas, which are advantageous for the enzyme loading. And different microchannel types (e.g., wall-coated type, packed-bed type, and monolithic type) also provide various possibilities for the integration of immobilization carriers into micro space. When the enzyme is immobilized in microfluidic reactors, there is no need to separate the enzyme loaded carriers from the reaction solution, which not only saves time and labor, but also favors the recovery and reusability of enzyme. Moreover, different catalytic reaction conditions (such as temperature, pH, residence time, and reaction pressure) can be easily optimized in the microfluidic reactors as compared to the operation in batch systems [14]. Furthermore, the stop of reactions can be easily achieved by pumping the substrate out of the reactors without the need for the addition of acid or base that may affect the detection accuracy or products. Therefore, the microfluidic reactors can be directly incorporated into many instruments for real-time analysis and monitoring. Besides, many natural biocatalytic reactions involve multiple enzymes to catalyze a series of cascaded reactions, in which enzymes are usually assembled in orders [15]. Immobilizing enzymes in the microfluidic reactors make it easy to control the relative position of multiple enzymes, thus mimicking the behavior of enzymes in nature.

This chapter gives a comprehensive discussion on the factors that affect the performance of continuous biocatalysis in the μ-IMERs using a top-down strategy. From the macroscopic point of view, the first things to consider are the materials and the configuration designs of the microfluidic reactors. Various materials have been developed in microfluidics, such as silicon, glass, polymers and paper. The characteristics of fabrication materials are of vital importance to the performance of catalytic reactions. Special biocatalysis can also be achieved with careful design of the configuration of the device. From the microscopic point of view, the capacity of inner structures of microreactors for enzyme loading also plays a significant role in the overall biocatalytic efficiency. In addition, the specific substrate diffusion path induced by different types of microreactors should also be taken into account. Finally, from the nanoscopic point of view, different immobilization techniques, which dominate the performance of enzymes such as their activity, stability and reusability in the nano-environment of biocatalytic reactions, are also thoroughly studied. We hope the discussion in this review can help understand the main characteristics of the rapidly developing μ-IMERs for continuous biocatalysis and can provide a clear guide to the future research.

2.2 Fabrication of microfluidic reactors

2.2.1 Materials for microfluidic reactors

There are many choices of materials that can be used for the fabrication of microfluidic reactors, and the basic characteristics of the materials should be stable and inert [16]. The

materials used in early days were mostly silicon [17, 18] and glass, which directly inherit from the semiconductor industry and the microelectromechanical systems (MEMS) [19]. They usually require the surface salinization and the introduction of some functional groups such as carboxyl groups or amino groups for better enzyme immobilization on the surface [20]. The common problems they have are high cost and complicated fabrication procedures, limiting their applications in microfluidics. Therefore, various polymers have been developed for microfluidics due to easy fabrication and high compatibility with the biocatalysis.

Polydimethylsiloxane (PDMS) is one typical silicon-based organic polymer and is very popular in the biomicrofluidics application because of its excellent biocompatibility, easy fabrication, low cost and optical transparency which is beneficial for the monitor and optical detection of the biocatalytic reaction [21]. The flexible feature also makes PDMS an excellent material to fabricate valves and pumps in microfluidic devices. Nevertheless, there are also some problems to be solved: the swelling in some organic solvents, the change of solution concentration due to the water evaporation and the hydrophobic surface which leads to the non-specific adsorption of biomolecules. Thus, oxygen plasma or surface modification are usually required to change the hydrophobicity and to introduce functional groups for enzyme immobilization.

Some other polymer materials, such as polymethylmethacrylate (PMMA) [22-24], polystyrene (PS) [25], polycarbonate (PC) [26], poly (ethylene terephthalate) (PET) [27]

and polytetrafluoroethylene (PTFE) [28, 29], are also widely used for microfluidics fabrication due to their excellent chemical, electrical, mechanical, optical and thermal properties [30-33]. However, surface modifications are also needed because of the lack of functional groups on their surfaces. Sometimes stainless steel and ceramic are used for the reactor fabrication if the reaction is operated under high temperature and high pressure [34]. But their high fabrication cost largely limits their broad applications. D. Ogończyk's groups firstly used PC microchannels for enzyme immobilization in 2012 [26]. The PC microfluidic chip was able to immobilize different kinds of enzymes like alkaline phosphatase (ALP) and urease by the physical-chemical method described in the paper. And the enzymatic microfluidic chips also present attractive operation reproducibility, storage stability and high conversion rates.

Paper is another material that has recently become a promising microfluidic substrate. It is mainly used for the detection of various type of substances and compounds [35, 36]. The paper-based microfluidics have porous and open channels, which provide larger surface areas for enzyme immobilization as compared to the conventional microfluidics that have only hollow channels.

2.2.2 Configuration design of microfluidic reactors

Various microfluidic chip designs have been constructed by researchers; four representative designs are illustrated in **Figure 2.1**. The single-channel microfluidic chip is the simplest and has only one straight channel for the immobilization of enzyme and

the transferring of substrate. The open-tubular or capillaries can also be classified into this category. Nevertheless, the single-channel microfluidic chip generally has a limited volume for the enzyme loading. Therefore, researchers have come up with an improved design that utilizes a serpentine channel (or curved channel). Here a single microchannel is folded up into a serpentine (curved) shape to increase the effective volume for immobilization. As a more advanced design, the multi-channel microfluidic chip is developed to divide into a channel array on the input side and a similar unit on the output side, which also multiplies the effective immobilization volume [37]. For further improvement, the planar microfluidic chip is presented to increase the immobilization volume by simply enlarging the channel into a planar chamber in the lateral direction.

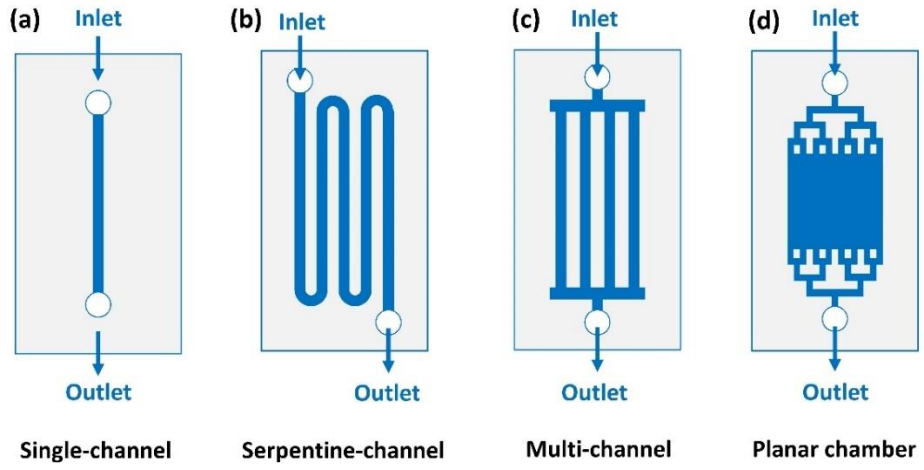

Figure 2.1 Representative configuration designs of microfluidic chips.

The microfluidic reactors should be well designed for their constructions. When the immobilization amount of enzyme and the residence time of the biocatalysis are set the same, the configuration design has an impact mainly on the accessibility of the substrate

to the immobilized enzyme and then affects the overall biocatalytic reaction performance. In microfluidic chip, the reactant fluids can be easily controlled to react with all the enzymes immobilized in the chip. While in the bulk system, the reactant solution may need a longer time to react with all the enzymes by mixing and diffusion. It has also been proved that channel shape has a great impact on the backpressure which further affects the enzyme activity [38, 39]. Nakagawa et al. [38] designed five microreactors with different numbers and lengths of elbow and straight sections. Different reaction yields were obtained in the same resident time. The microreactor with the least number of elbow sections had the smallest backpressure and therefore possessed the highest reaction yield.

2.3 Internal structure designs of microfluidic channel

The biocatalytic reaction rate mainly depends on two factors, the amount and the activity of the immobilized enzyme in the microfluidic chip. And the internal structure of microfluidic channels would strongly affect these two factors by adjusting the surface-area-to-volume (SAV) ratio of the microchannel and the diffusion pressure of the solution passing through it. Generally, the μ-IMERs with different internal structures can be classified into three designs: wall-coated type, monolithic type and packed-bed type (**Figure 2.2**).

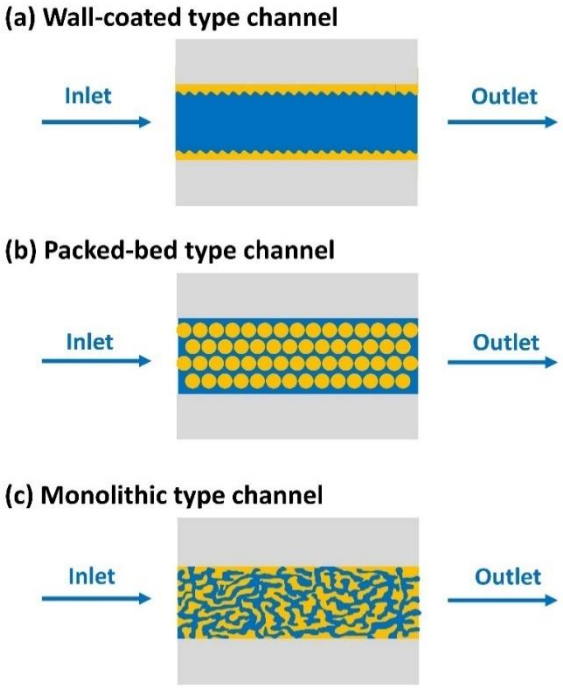

Figure 2.2 Typical designs for the internal structure of microfluidic channels.

2.3.1 Wall-coated type channel

For the wall-coated type μ-IMERs (**Figure 2.2**(a)), the enzyme is directly immobilized onto the inner wall surface of the microchannel [40, 41]. However, the available surface areas of the microfluidic walls are quite limited, resulting in low enzyme loading capacity. In addition, the reactant diffusion path is relatively large in this case and thereby it results in low biocatalytic conversion rate. Researchers are dedicated to increase the SAV ratio of microchannel to improve its enzyme loading capacity [42]. One efficient method is to modify the inner wall with some nanostructured materials like gold nanoparticles [43], graphene [44, 45], graphene oxide [46, 47], or nanosprings [48].

Recently, Nidetzky's group designed a borosilicate microchannel with silica

nanosprings attached on the surface for the immobilization of sucrose phosphorylase [48]. It was demonstrated that the enzyme loading amount was increased by an order of magnitude or more as compared to the enzyme loading on the uncoated microchannel walls. Moreover, the device also showed an enhanced conversion efficiency on the synthesis of α-glucose 1-phosphate and an improved reusability and stability.

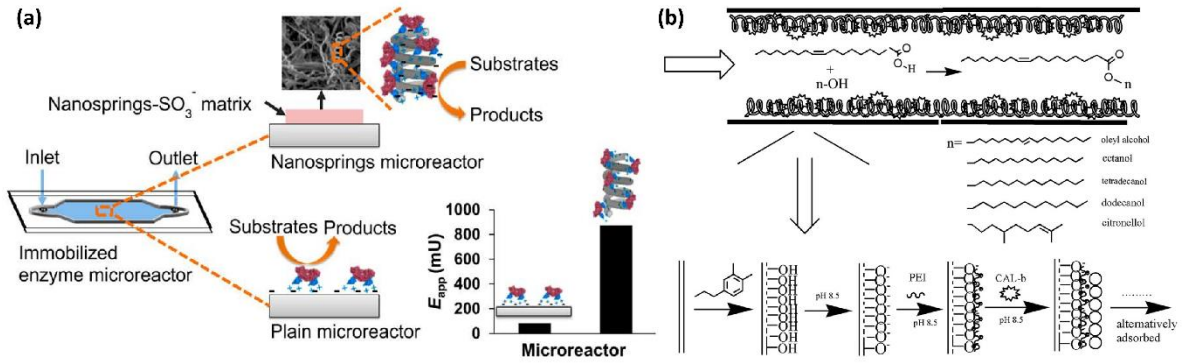

Figure 2.3 Examples of wall-coated microchannels for enzyme immobilization. (a) Schematic of the sucrose phosphorylase immobilized on the nanosprings microreactor with enhanced enzyme activity [48]; (b) Process of immobilization of CAL-b based on self-oxidation of dopamine and LBL method. Long chains with positive charges represents PEI, and the circles represents the lipase [28].

Another feasible solution to increase the active enzyme loading amount is the addition of extra layers of enzyme on the inner wall, which is also defined as the layer-by-layer (LBL) assembly approach [27, 28, 49-51]. A representative work was conducted by Hua Zhou's group [28] who alternatively absorbed polyethyleneimine (PEI) and *Candida antarctica* lipase B (CAL-b) on the microreactor surface. The lipase loading was enlarged as the number of layers was increased. It reached saturation at the 8th layer. The

production of wax ester was also demonstrated to have a high conversion efficiency and an excellent stability.

2.3.2 Packed-bed type channel

Even though many methods have been developed to increase the SAV ratio of the wall-coated type μ-IMERs, there is still very little room for the enhancement. In order to maximize the space utilization of the size-limited channels and therefore to maximize the enzyme loading amount, enzymes are designed to be immobilized on polymeric or inorganic particles, which are then packed into the microchannel of the μ-IMERs (**Figure 2.2** (b)). There are many commercially available polymeric particles for the packing [52-55], and some inorganic materials like glass [56, 57], silica [58], and Fe_2O_3 microparticles [59-61] have also been used for packing. These packed-bed type of μ-IMERs can be easily fabricated and present an extremely high enzyme loading ability.

Gross and Beers' group designed a microreactor packed with commercially available mesoporous PMMA beads where CAL-b was physically immobilized to study the polymerization of ε-caprolactone to polycaprolactone in the continuous mode [52]. It was demonstrated that faster polymerization and higher molecular mass were obtained in the microreactors as compared to that in the batch reactors. Another example is the packing of glucose oxidase modified magnetic nanoparticles in microfluidic channels for the electrochemical detection of glucose [61]. The performance of the microfluidic device could be optimized by changing the packing length of the magnetic nanoparticles, which

was hard to achieve in other types of devices. Moreover, the device also showed good reproducibility and stability and great potential in glucose detection without the need for the pretreatment of serum samples.

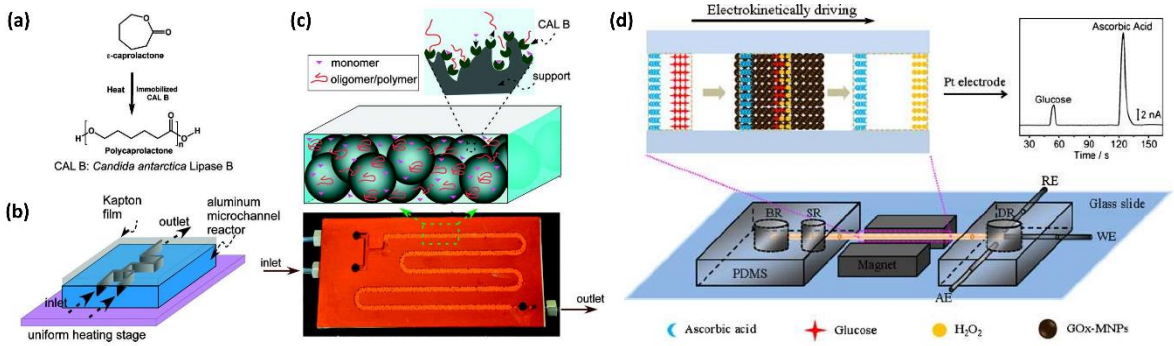

Figure 2.4 Examples of packed-bed microchannels for enzyme immobilization. (a) Reaction scheme for ring-opening polymerization of ε-caprolactone to polycaprolactone. (b) Schematic of the microreactor setup. (c) Image shows the photograph of a typical microreactor used in this study. CAL-b immobilized solid beads (macroporous polymethyl methacrylate) were filled in the channel [52]. (d) Scheme representation of the construction and analytical procedure of GOx–MNPs–MD. BR, buffer reservoir; SR, sample reservoir; DR, detection reservoir; WE, working electrode; RE, reference electrode; AE, auxiliary electrode. [61]

However, due to the densely packed particles, the fluid passing through the channel is hard to control and the heat transfer inside the channel is very limited [62]. Moreover, there may be huge pressure drops when the substrate solution flows along the channel. These may have negative impact on the enzyme activity.

2.3.3 Monolithic type channel

To overcome the drawbacks of the packed-bed type channel, such as high pressure drop

or limited heat transfer, the monolithic type channel (**Figure 2.2** (c)) is developed. In such a case, the channel is filled by the monolithic material with interconnected meso- or micro- porous structures. The porous structure makes it easy for the fluid flowing, and allows for relatively high flow rates, low back pressures, and high productivities as compared to the packed-bed type channel. It also possesses the advantages of high mechanical durability and reduced diffusion path length over the wall-coated type channel. Yi Chen's group immobilized L-asparaginase (L-Asnase) in both the monolithic microreactor and the coating reactor (i. e., the wall-coated type) by the same immobilization method [63]. The monolithic microreactor was demonstrated to have a lower Michaelis constant than the coating microreactor, showing that a better affinity between the substrate and the enzyme can be obtained in the monolithic structures as a result of the lower diffusion path length in monoliths. However, a higher maximal velocity was observed in the coating microreactor due to its relatively lower flow pressure.

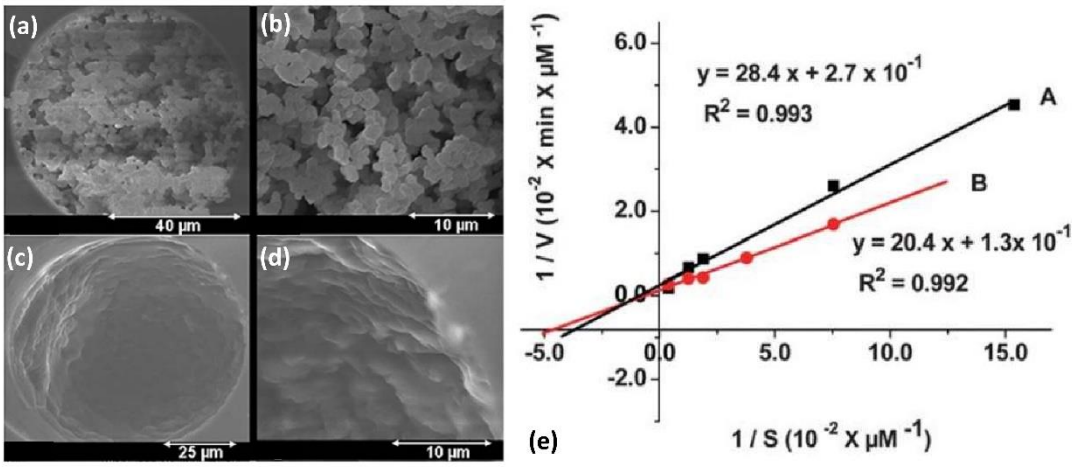

Figure 2.5 SEM of monolithic and coating in capillary: (a, b) monolithic, (c, d) coating. (e) Lineweaver–Burk plots for L-Asnase immobilized in the monolithic (A, ■) and

coating (B, ●) enzymatic microreactors [63].

The monolithic materials can be organic [64-68], inorganic [69-72] or hybrid [43, 73-75], which should be carefully chosen for different enzyme immobilizations and different reaction environments. Generally, the organic monoliths are copolymerized from different monomers and sometimes one of the monomers is the enzyme. They usually have good biocompatibility and pH resistance but may be damaged by some organic solvents. An example is the immobilization of amylase in the PVA foams by mixing the amylase solution with the PVA solution before they were put in a cylindrical sample case for freeze drying [65]. The amylase-immobilized microreactor was demonstrated to successfully conduct continuous starch hydrolysis reactions over 8 days. For the inorganic monoliths, silica-based monoliths are most widely used due to their high binding capacity, great biocompatibility, chemical and thermal stability, and easily functionalization [76]. But compared with the organic polymer monoliths, the preparation of inorganic monoliths is relatively difficult [77]. Therefore, the monoliths used for enzyme immobilization are hybrids of organic and inorganic materials in most of the time. For example, Yukui Zhang's group developed an organic-inorganic hybrid silica monolith with immobilized trypsin and demonstrated its excellent enzymatic activity and long-term stability in proteome analysis [73]. However, there is still the possibility that the pores are blocked, leading to the non-uniform permeability along the channel. And the fabrication of monolithic materials is usually time consuming and poorly reproducible.

2.4 Enzyme immobilization techniques

Since Nillson and Griffin firstly reported that invertase remained its activity after physical adsorption to charcoal in 1916 [78], various enzyme immobilization techniques have been developed and studied. Most of these techniques can be directly used for enzyme immobilizations in microfluidic chips for biocatalysis. The combination of enzyme immobilization and microfluidic chips provides the advantages of high stability and reusability, high enzyme to substrate ratio, and rapid catalytic reactions [79]. Basically, the techniques of enzyme immobilization in microfluidic chips can be classified into two types: surface binding and encapsulation, as shown in **Figure 2.6**. For the surface binding method, it is usually subdivided into non-covalent binding and covalent binding. The non-covalent binding method is defined as that the enzymes are bonded to the surface via non-covalent interactions, such as non-specific physical adsorption, ionic bonding, his-tag/metal binding, and affinity binding [2, 80]. While the covalent binding is to immobilize enzymes on the surface via covalent forces with certain functional groups, like amino, carboxyl, hydroxyl or sulfhydryl groups [81]. Encapsulation immobilization is the confinement of enzymes in small spaces built by polymeric networks, membranes, or nanochannels. Different immobilization methods have different advantages as well as disadvantages. Therefore, careful consideration should be given before one immobilization strategy is adopted. Some representative examples of μ-IMERs for biocatalysis are summarized in **Table 2.1**.

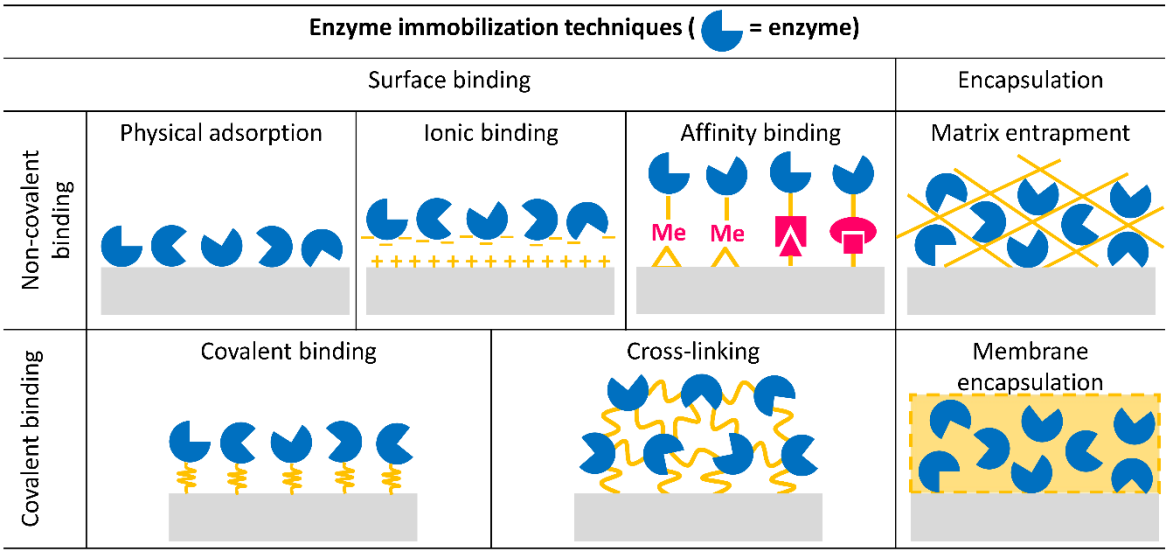

Figure 2.6 Different enzyme immobilization techniques.

Table 2.1 Summary of recent μ-IMERs studies.

Platform	Enzyme	Immobilization techniques	Biocatalysis performance	Refs.
Macroporous PMMA microbeads packed aluminum microreactor	CAL-b	Physcial immobilization	Faster polymerization and higher molecular mass	[52]
Fused silica capillary column	Angiotensin-converting enzyme	Ionic binding	High activity, stability, reusability, renewability and reduced costs.	[82]
Nanosprings-coated Borosilicate glass	Sucrose phosphorylase	Ionic binding	10-fold activity enhancement, 11-fold operational stability increase, 85% conversion rate retaining after 840 reactor cycles	[48]
Wall-coated PET microfluidic chip	Trypsin	Layer-by-layer ionic binding	Short digestion time and small volume of protein	[27]

			samples, a potential solution for low-level protein analysis	
PTFE open-tubular microreactor	CAL-b	Layer-by-layer ionic binding	Production efficiency reached to 95% within 35 mins, 83% initial activity retained after 144 hours usage	[28]
Wall-coated silicon microchannels	Urease	Layer-by-layer ionic binding	Significant activity can be obsereved in the multi-layers microreactors after more than 2 weeks	[18]
Agarose beads packed PDMS microfluidic reactor	PikC hydroxylase	His-tag/Ni-NTA binding	High enzyme loading and conversion rate	[83]
Wall-coated PMMA microfluidic chip	Transketolase	His-tag/Ni-NTA binding	The 1-step-immobilization method without the pre-amination of PMMA surface showed higher specific activity.	[84]
Phospholipid bilayer-coated PDMS microchannels and borosilicate microcapillary tubes	ALP, GOx and HRP	Streptavidin/biotin	The feasibility of using the microchannels to obtain kinetic data and the potential application for multistep chemical synthesis were demonstrated.	[85]

PDMS microchip reactor packed with commercial microbeads	HRP and β-galactosidase	Streptavidin/biotin	Similar kinetic analysis results were obtained in the microfluidic-based assays as that obtained in solution, reduced cost, reagent economy and increased throughput were observed.	[54]
Protein coated PDMS/glass microchannel	ALP, Gox and HRP	Streptavidin or avidin/biotin	Photoimmobilization of multiple, well-defined enzymes were developed for both single-enzyme and multi-enzyme systems.	[86]
Fused silica capillaries with polymer coated	CAL-b and HRP	DNA directed immobilization	High reusability and renewability, the reaction time available for glucose oxidase could be independently and modularly varied by the distance between two enzymes	[87]
Porous polymer monolithic microfluidic capillaries and chips	Trypsin	Covalent binding	Very short digestion time compared to the traditional approach and great potential for broader application in various protein mapping	[68]

Magnetic nanoparticles packed microreactor	GOx	Covalent binding	Low detection limit of glucose, hign reproducibility and storage stability, avaliability of direct detectio of serum samples	[61]
PMMA microchip filled with sol-gel	Trypsin	Encapsulation	Analytic time was shortened and operation stability was increased, digestion of protein with multiple cleavage sits and separation of digest fragments are applicable.	[88]
Titania and alumina sol-gel based PDMS microfluidic reactors	Trypsin	Encapsulation	Short digestion time and increased operation stability	[89]
Wall-coated PTFE microtubes	Aminoacylase	Cross-linking	Higher stability against heat and organic solvents, applicable to various enzymes with low isoelectric points.	[29]
PDMS microfluidic device with PEG-based hydrogel structures	ALP and urease	Cross-linking/encapsulation	enzyme-catalyzed reactions were able to reach 90% conversion within 10min.	[90]
Mesoporous silica coated PDMS/glass microreactor	Lipase	Encapsulation	Higher activity compared to that in batch system	[91]

			5 times	
Au coated PDMS microfluidic chip	β-Gal and GOx	Encapsulation	the reaction yield could be obtained if the gap distance decreased from 100 to 50 μm	[92]

2.4.1 Surface binding

2.4.1.1 Non-specific physical adsorption

The non-specific physical adsorption is the simplest and most convenient approach for enzyme immobilization. The interactions between enzyme and support are non-specific forces such as van der Waals forces, hydrogen bonds and hydrophobic interactions [20]. Compared with other immobilization methods, the conditions for physical adsorption are very mild and no chemical modification is needed during the procedures. Therefore, the chances of conformational change caused by the immobilization are very little. In addition, the reversible physical adsorption makes it possible for the same device to be reused by washing and reloading new enzymes, indicating a relatively low fabrication cost [2].

However, the interactions between enzyme and surface are generally very weak and highly dependent on environmental and surface conditions. As a result, the enzymes are easy to fall off from the surface especially in fluidic systems or high ionic and pH solutions, which causes to the contamination of reaction systems or the reduction of enzyme activity. In addition, since the enzymes adsorbed on the support are randomly oriented, the activity of enzyme can be affected due to the hindering of active sites.

Moreover, some other problems, like diffusion resistance, denaturation of enzyme, and overloading, could also cause a loss of the enzyme activity when this method is adopted [93]. Therefore, the combination of other immobilization methods with the adsorption method is usually applied to overcome these shortcomings and to enhance the enzyme activity, the stability and the overall efficiency.

2.4.1.2 Ionic binding

The ionic binding is achieved by the electrostatic interactions between the positively and negatively charged functional groups of the enzymes and the supports. The amount of immobilized enzyme can be well manipulated if the pH of solution is controlled below the isoelectric point of the enzyme and above that of the support material [76].

Generally, the ionic binding is stronger than non-specific physical adsorption and subsequently guarantees a higher enzyme stability and reusability. But the ionic binding is highly dependent on the environmental pH and ionic strength, which in turn affect the enzyme loading amount and the pH stability of enzymes. Therefore, attentions are mainly paid to search for suitable chemicals to form an electrostatic layer with appropriate isoelectric point on the support surface. In biochemistry, the typical positively charged functional groups are protonated amine (NH_3^+) and quaternary ammonium cations (NR_4^+) and the negatively charged functional groups are usually carboxylic acid ($-COO^-$) and sulfonic acid ($-RSO_3^-$) [20]. PEI is one popular polycation which has multiple cation groups with strong anion exchange capacity for enzyme immobilization by ionic binding

[28, 94-97]. Some other polycations have also been used for the ionic binding, such as hexadimethrine bromide (HDB) [82, 98], poly (diallyl dimethylammonium chloride) (PDDA) [99, 100] and chitosan [27, 49]. Sometimes, polyanions like alginate [94, 95], hyaluronic acid (HA) [27, 49], poly(Lys) [29], and functionalized graphene oxide [47] are also employed to form multi-layers for the stabilization of the ionic binding.

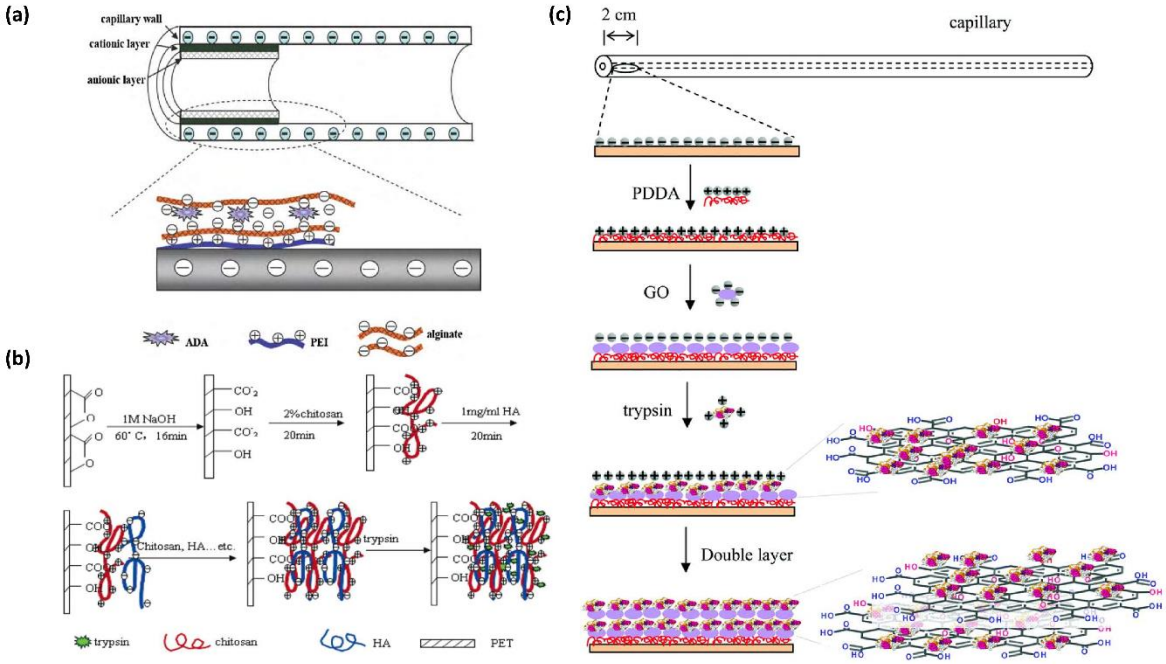

Figure 2.7 Schematic representations of enzyme immobilization by ionic binding via different polycations and polyanions. (a) Adenosine deaminase (ADA) immobilization of by PEI and alginate [94]. (b) Trypsin immobilization by HA and chitosan [27]. (c) Trypsin immobilization by PDDA and negatively charged graphene oxide [47].

The schematic representations of enzyme immobilization by ionic binding via different polycations and polyanions are shown in **Figure 2.7**. The reversibility of the enzyme immobilization by ionic binding is also an important advantage over other immobilization methods. The support surface can be washed without damages by simply

changing the ionic strength of the environment and then be immobilized with new enzymes. In this way, the microfluidic chip can be reused for several times to save the assay cost.

2.4.1.3 Affinity binding

The affinity binding enables to immobilize enzyme on the support via some specific ligands, such as his-tag/metal binding, avidin/biotin binding, DNA-directed immobilization and antigen/antibody binding. Sometimes, more than one affinity binding methods are adopted into one device to improve the binding efficiency and the loading amount. In non-specific enzyme immobilization methods like physical adsorption or covalent binding, the orientation of enzymes is hard to control, and the activities of enzyme are likely to lose due to the block of active sites and the conformation change. In the affinity binding, the original orientation of enzymes can be maintained, and the enzyme activity can be maximized by exposure of the active sites to the reaction solution. In addition, enzymes can get a high specific binding to the support, resulting in a high enzyme loading amount and a high enzyme stability. Moreover, the affinity binding can also be reversed by pH or temperature change or some special chemical treatments. However, before the immobilization, the enzymes often need to be decorated by some tags genetically or chemically, which is complicated and costly as compared to the other methods.

A) His-tag/metal binding

To immobilize enzymes on the supports by metal binding, enzymes and supports are bonded together by the coordination with metals in between of them. Generally, this method can obtain highly active, stable and specific immobilized enzymes [101-103]. And the enzyme loading amount by this method can also be higher than that by other methods [83, 102]. In such case, polyhistidine linkers are genetically tagged to the enzyme and then connected to the nitrilotriacetic acid (NTA) attached on the support for the enzyme immobilization. Recently, Baganz's group immobilized transketolase (TK) in PMMA microfluidic devices by two methods of the his-tag/Nickel-NTA interactions, the 1-step-immobilization method (see **Figure 2.8** (a)) and the 3-step-immobilization method [84]. The device fabricated by the 1-step-immobilization method presented higher specific activity and reusability than the 3-step method. The 1-step method also required fewer chemicals and less time. Moreover, it was also demonstrated that the his-tag/Ni binding had high reversibility, making it possible for the microreactor to detach the denatured enzyme and to attach a new one [104].

However, this method also suffers many intrinsic drawbacks. Sometimes this enzyme immobilization method is not easily reproducible due to the nonuniform adsorption sites and the metal ion leakage [105]. Therefore, it is usually combined with covalent bonding or cross-linking to get a more stable formation of adsorption sites and chelation.

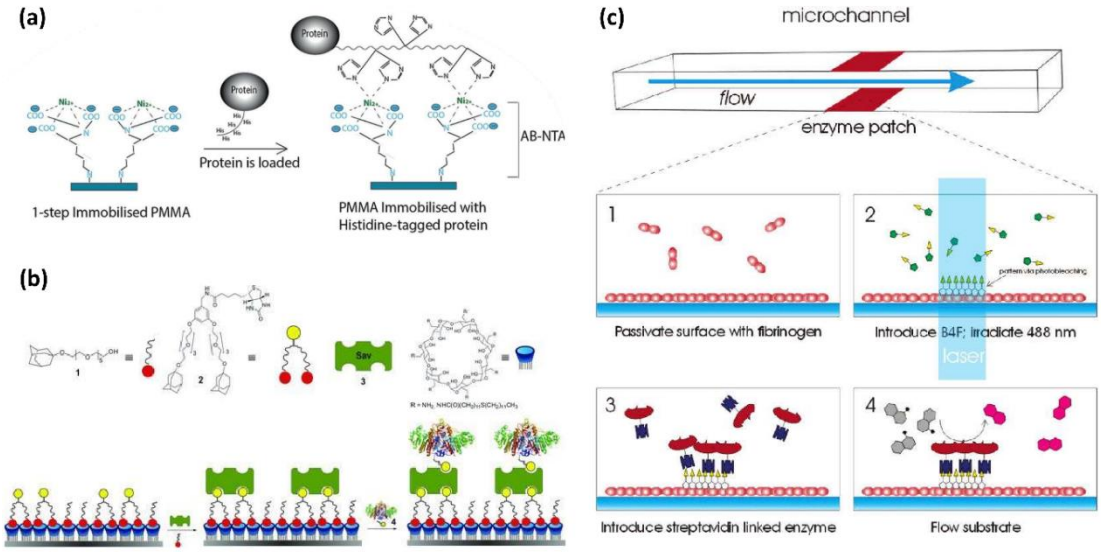

Figure 2.8 Schematic representations of enzyme immobilization by His-tag/metal binding (a) Diagram of enzyme immobilized by the His-tag/Ni-NTA binding [84]; (b) Chemical structures of the building blocks and scheme for the step-wise assembly process. Ethylene glycol-based mono-adamantyl linker (1) for minimizing the non-specific protein adsorption, biotinylated bisadamantyl linker (2) for the first assembly step and streptavidin (3) as the second assembly step. Biotinylated ALP (bt-ALP, 4) is immobilized onto these streptavidin-biotin surfaces [86]; (c) Schematic diagram of the photo-immobilization process. (Top) Enzyme patches are formed on the top and bottom of a microchannel using the following procedure: (i) Passivation of the surface with a fibrinogen monolayer is followed by (ii) biotin-4-fluorescein surface attachment. This is accomplished by photobleaching with a 488-nm laser line. (iii) Next, the binding of streptavidin-linked enzymes that can be exploited to immobilize catalysts and (iv) to monitor reaction processes on-chip [106].

B) Avidin/biotin binding

The avidin/biotin binding is one of the most popular affinity binding with high affinity and specificity. The interaction is regarded as the strongest non-covalent interaction [107] having the advantages of rapid fabrication and insensitivity to pH, temperature,

proteolysis and denaturing agents [59, 85, 108]. Moreover, the avidin or biotin can be easily modified by other chemicals, enabling more effective enzyme immobilization or some interesting functions [86, 106].

Huskens and Jonkheijm developed a supramolecular platform with combination of orthogonal supramolecular interactions of host (β-cyclodextrin)–guest (adamantane) and biotin–Streptavidin interactions for site-selectively immobilization of enzyme in microchannel [106]. The microfluidic chip with supramolecular platform was demonstrated to present great reproducibility and reusability in enzymatic reactions when calfintestine alkaline phosphatase (ALP) was used as the model enzyme and the site-selectively immobilized ALP was able to maintain the comparable activity in other environments (free in solution or immobilization by other methods). In Cremer's work, biotin-linked dye solution was used for the site-specific immobilization of streptavidin linked enzyme on the selected photopatterning positions [86]. The pattern enzymes inside multiple locations inside microfluidic channel were achieved without valves, and this method was easily broadened to immobilize two enzymes into one microfluidic chip.

C) DNA-directed immobilization

The DNA-directed immobilization (DDI) is based on the Waston-Crick paring mechanism between the single-strand DNA (ssDNA) attached on enzymes and the complementary DNA (cDNA) attached on the supports. The attachment of ssDNA to enzyme is usually accomplished by covalent binding or avidin/biotin binding [87, 109,

110]. Generally, the attachment of cDNA to the supports is more stable and robust than the other chemical attachments and the DDI can present high immobilization efficiency and site-specificity. An important aspect of DDI superior to the other methods lies in the aspect that it enables to precisely control the relative positions of different enzymes [15], which is quite important for the cascaded enzymatic reactions.

2.4.1.4 Covalent binding

In this method, the covalent binding between the enzyme and the support is formed by the chemical reaction between functional groups on the surface of support and the amino acid residues of the enzyme. The most commonly used covalent bonds are based on the Schiff or carbodiimide chemistries as shown in **Figure 2.9** [9]. Since the covalent binding always offers the strongest bond between the enzyme and the support, the enzyme usually has higher stability and reusability. In addition, the enzyme immobilized by covalent binding is usually more stable under extreme environment. However, conformation change and activity reduction may sometimes occur due to the modification or activation for enzyme immobilization. Moreover, the orientation of enzyme is not easy to control as compared to the specific immobilization, resulting in the activity loss. Nevertheless, this can be overcome by blocking the active sites of enzyme with a competitive inhibitor or substrate before immobilization.

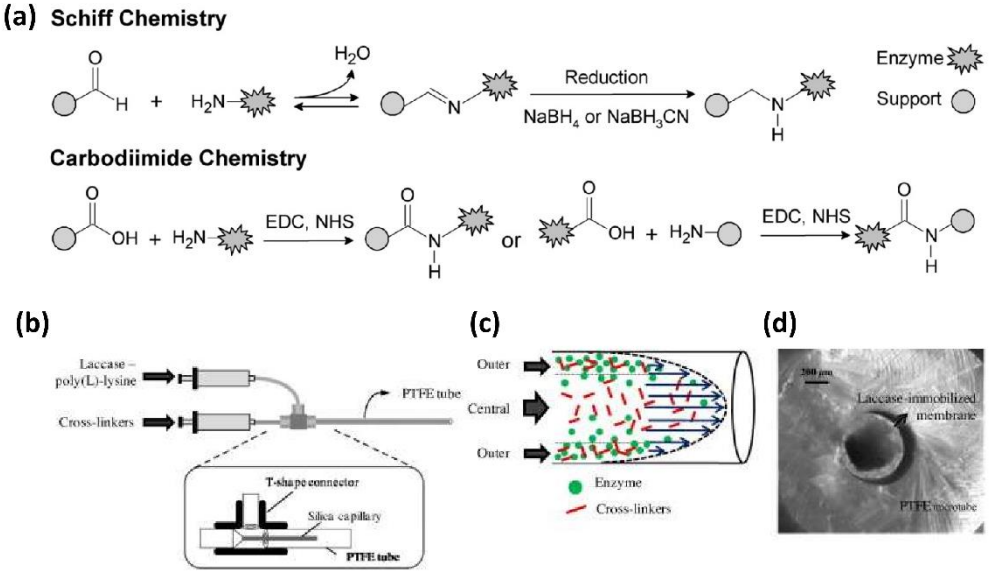

Figure 2.9 Covalent binding for enzyme immobilization. (a) Commonly used covalent bonds: mechanisms of the Schiff chemistry and the Carbodiimide chemistry [9]; (b) Preparation of laccase-immobilized membrane on the inner wall of a PTFE microtube; (c) Parabolic velocity profile characteristic of the laminar flow inside the microtube, and (d) confocal acquisition of the sectional view of the laccase-immobilized microreactor (dry state) [111].

Generally, the covalently immobilized enzyme can only form one layer on the surface of support with a limited amount. Therefore, a cross-linker can be used to form an enzyme polymerization on the support surface for the significant enlargement of the enzyme loading amount. Miyazaki's groups prepared a laccase-immobilized microreactor by the formation of an enzyme-polymeric membrane on the inner wall of microtubes [111]. The membrane was formed by the cross-linking polymerization reaction between laccase and the cross-linkers (paraformaldehyde and glutaraldehyde). The microreactor with cross-linked laccase not only presented important biotransformation efficiency

compared with conventional bioreactors, but also exhibited excellent pH, temperature, inactivating agent, storage and long-term stabilities.

2.4.2 Encapsulation

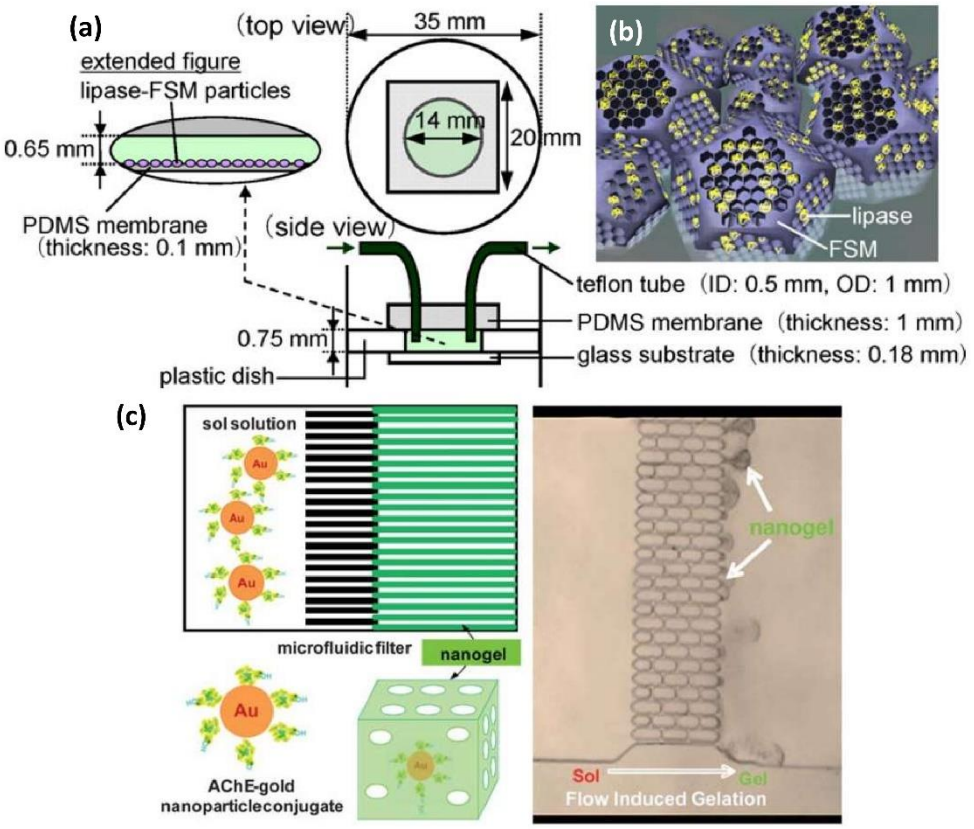

Figure 2.10 Examples of enzyme immobilization by encapsulation. (a) Schematic illustrations of the microreactor with immobilized lipase–nanoporous material (FSM) composite particles; (b) Lipase molecules encapsulated in the FSM pores [91]; (c) Schematic diagram of the flow-induced gelation in a microfluidic filter device (left) and a typical microscope image showing the nanogel production at a flow rate of 10 ml h^{-1} (right) [112].

The encapsulation of enzyme is defined as enzyme being entrapped inside a nanoporous matrix that allows the substrates and products to pass through but retains the enzyme. The

matrix can be a particle, a membrane, or a fiber. Compared with the physical adsorption, the entrapment method is more stable and can a immobilize larger amount of enzyme. In addition, the entrapment does not need the chemical modification of enzyme, which not only saves time but also avoids the conformation changes of enzyme. But the slow diffusion in this case may severely limit the biocatalytic production as compared to the other immobilization methods. Moreover, there are also the possibilities of enzyme leakage and contamination of the matrix. Besides, the microenvironments of the matrix are hard to control, which may lead to the reduction of enzyme activity and stability. However, the impact of all these shortcomings can be reduced by carefully choosing the polymer materials with proper modification and by adjusting the pore size or capsule size.

The matrix used for entrapment can be polymers (like alginate [94, 95], PEG hydrogels [90]) and some inorganic materials (like Titania [89] and silica [69, 88, 113] sol-gels). The pore size of the matrix should be adjusted to prevent the enzyme leakage while allowing the solution to pass. Different matrix materials can form different pore sizes, which can be further adjusted by the concentration of the polymer. Mizukami developed a microreactor containing lipase encapsulated in folded-sheet mesoporous (FSM) silicas with two different pore diameters [91]. The FSM with larger diameter (~7 nm) indicated a higher enzyme loading amount than the FSM with a smaller diameter (~4 nm). The two types of lipase-FSMs were loaded in the microreactors for the hydrolysis of a triglyceride, both presented a higher enzyme activity than the batch reaction.

In Yuehe Lin's work, acetylcholinesterase (AChE) attached to gold nanoparticles were entrapped into a gel matrix for the monitoring of organophosphorus compounds [112]. The synthesis of gel scaffolds was facilitated and controlled by the fluid mechanics without the chemical and thermal treatments. High sensitivity and reactivation efficiency were observed due to the retaining of the AChE's native stability and bioactivity as a result of the same local microenvironments provided by the gel matrix as those in biological media. Moreover, the gel matrix also prevented the enzymes from self-aggregation and leaching by isolating them from each other.

2.5 Multi-enzymes systems

Most biocatalytic reactions are catalyzed by more than one enzyme. Many efforts have also been devoted to immobilizing multiple enzymes in one microfluidic reactor to artificially construct a variety of biocatalytic reactions in nature [55, 92, 109, 114, 115]. The methods for multi-enzymes immobilization are based on those of single enzyme immobilization, while careful considerations should be taken to maintain the activities and catalytic efficiencies of all enzymes according to the enzymes' different structures and different optimal environments. One major issue for multi-enzymes immobilization is the control of relative spatial positions of multiple enzymes in one reactor. The relative spatial control is much easier when microfluidic reactors are used for enzyme immobilization as compared to the batch reactors. Once the relative spatial positions are well controlled, there would be a great possibility to increase the reaction rate and to avoid

the unwanted side reactions and the accumulation of inhibitors or reactive intermediates [116-118]. Multiple enzymes can be immobilized in one pot [115], sequentially [87, 92, 109] or layer by layer [119]. For different systems, the optimal catalytic efficiency can be obtained by immobilizing the enzymes in different spatial positions.

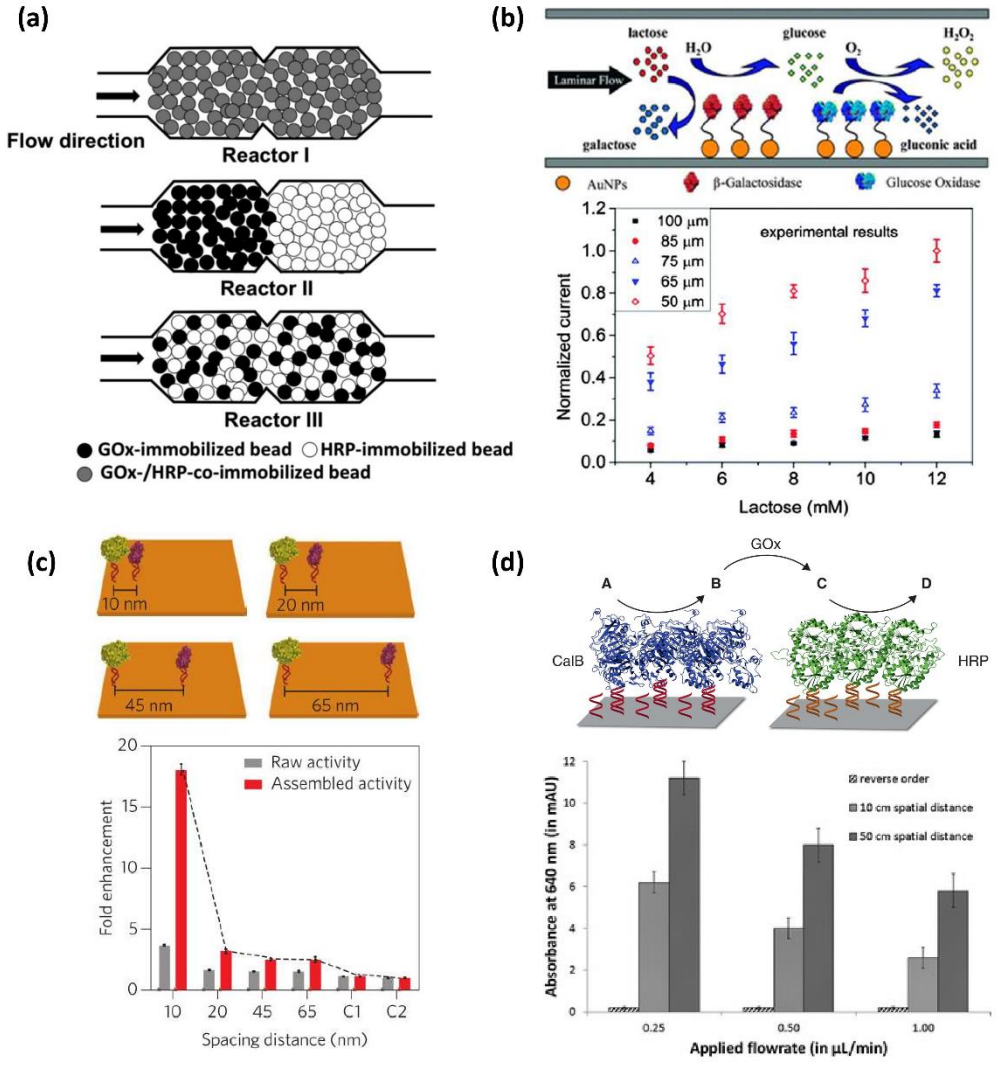

Figure 2.11 Examples of enzyme immobilization in multi-enzyme systems. (a) Diagrams of three different configurations of microfluidic reactors. In reactor I, GOx and HRP were co-immobilized on a single set of beads. In reactor II, GOx-immobilized beads and HRP immobilized beads were loading sequentially. In reactor III, the two beads were mixed in the reactor; [120] (b) Schematic of enzyme cascade reaction confined in a microchannel.

β-galactosidase and glucose oxidase were assembled on the Au-films with controllable distances (up). Graph of the normalized response currents of H_2O_2 as a function of the concentration of lactose with different gap distances in the experiment (down). [92] (c) Localization of GOx (yellow) and HRP (purple) at defined distances on the surface of DNA origami tiles (up). An increased catalytic activity was observed when the inter-enzyme distance was decreased to 10 nm, as analyzed with d-glucose, $ABTS_2$–(2,2'-azinobis(3-ethylbenzothiazoline-6-sulfonate)) and O_2 as substrates at pH 7.2 (down). C_1 and C_2 refer to the tiles without nucleic acid and free enzymes, respectively. [118] (d) A three-enzyme cascade was performed in a microchannel using the two immobilized enzymes Cal-b and HRP in combination with GOx, which was added in solution together with the substrates (up). [121] The graph plotted the measured product absorbances of a three-enzyme cascade reaction at different flow rates and different distances between the immobilized enzyme Cal-b and HRP. [87]

Jinseok Heo's group packed glucose oxidase (GOx) and horseradish peroxidase (HRP) bearing microbeads into microfluidic reactors with different spatial distances as shown in **Figure 2.11** (a) [120]. It was demonstrated that a better overall reaction efficiency was obtained in the microreactor packed with the co-immobilized GOx and HRP microbeads than the other two reactors in which two enzymes were immobilized on different beads and then loaded at different distances. The increased efficiency due to the decreased enzyme distance can be attributed to the reduced diffusional loss of intermediate product (H_2O_2) and the prevention of the accumulation of inhibitor. Another work presented by Xinghua Xia's group investigated the distance for multi-enzyme immobilization in micrometers and arrived at a similar result [92]. β-galactosidase and

glucose oxidase were immobilized on two separated gold films patterned in one microfluidic channel, as shown in **Figure 2.11** (b). The highest conversion efficiency of the cascaded reaction was obtained when the two enzymes were in minimum distance (50 μm). Even though the spatial positions of enzymes are easy to control by the separating microchannels into multiple areas, the different enzymes are still not very close to each other like the case in the natural cascaded systems [121]. Researcher paid their attentions to the combination of microfluidic reactors and DDI, by which more precise spatial control can be obtained for the reaction efficiency enhancement. It has been demonstrated that when the enzymes GOx and HRP were immobilized via DNA origami tiles at 10 nm from each other, an increase of more than 15-fold in the overall cascade activity was observed as compared to the free enzymes [122]. The reason of the activity increase was suggested to be the efficient transport of the reaction intermediate (H_2O_2) between the two enzymes.

However, the multi-enzyme cascade reactions are also highly dependent on other factors like the reaction time, the initial reactant concentration and the enzyme concentration. In Zuilhof and Hest's work, lipase Cal-b and HRP were sequentially immobilized into the microchannel by DDI, and GOx was dissolved in solution due to its lowest turnover speed as compared to CalB and HRP [87]. The product formation was increased with the increasing distance of CalB and HRP. In this case, the increased production may be due to the increase of reaction time or the diffusion time.

2.6 Summary and outlooks

Biocatalytic reaction plays an important role in the study of bio-chemistry thanks to its merits of environmental-friendliness, high efficiency and strong selectivity. However, the most popular biocatalyst, enzymes, often fail to retain the activity and stability in practical applications. The μ-IMERs for the continuous biocatalysis can draw on the benefits of both the microfluidic reactors and the enzyme immobilization techniques for highly efficient, stable, reproducible and continuous biocatalytic reactions. In this chapter, different factors that affect the production efficiency, stability and reusability in the μ-IMERs are summarized following a top-down strategy.

From the macroscopic aspect, the materials used for microfluidic reactors should be temperature and chemical stable, biocompatible with enzymes, and easy to fabricate. Among all the organic and inorganic materials (glass, silicon, PDMS, PMMA, PC, paper, etc.), PDMS is most popular. It not only meets all the requirements mentioned above, but also has the advantages of optical transparency, great flexibility, and easy surface modification. Once the fabrication material is chosen, the configuration of microfluidic reactors should also be well designed to make full use of the space for the enzyme loading and the substrates accessing.

From the microscopic aspect, the internal structures of microfluidic reactors should provide a large specific area for the enzyme loading and a short diffusion path to facilitate the affinity of substrate to enzyme. There are three main types of microfluidic channels:

wall-coated, packed-bed and monolithic. Generally, the wall-coated channels have the least effects of diffusion resistance on the enzyme activity. However, they usually possess a low specific area and a long diffusion path. Nevertheless, the packed-bed channels have the shortcomings of huge pressure drops and little control of the fluids and the heat transfer inside the channels. The monolithic channels also have some problems of such as non-uniform permeability, poor reproducibility and time-consuming fabrication. Overall, each of them has its own different strengths and weaknesses, and it is hard to say which one is the best. The design of internal structures should balance these advantages and disadvantages and take into account the choice of enzyme immobilization techniques.

From the nanoscopic aspect, the enzyme immobilization is the most important factor that affects the overall biocatalysis efficiency of μ-IMERs. The enzyme immobilization techniques have been extensively investigated by many researchers. For most non-covalent binding methods like physical adsorption and ionic binding, they have the advantages of simple fabrication, mild condition for immobilization, low chance of conformational change and great reversibility. However, the bonds are generally weak and dependent on pH or ionic strength. To overcome these problems, covalent binding is usually employed to provide a stronger and more stable interactions for the enzyme and the support. In the enzyme immobilization by covalent binding, the conformation would be changed, which to some extent may reduce enzyme activity. Additionally, these non-specific methods cause the block of active sites as a result of the random orientation of

enzymes. This problem may be solved by the site-specific affinity binding, which has three distinctive merits: (1) a precise control of the orientation of enzymes; (2) an exposure of the active center of enzymes to the reaction solutions; (3) a fine positioning of different enzymes in confined spaces. The third one is also noted to play a key role in the multi-enzyme systems. As another technique, the encapsulation offers a three-dimensional matrix for enzyme immobilization, by which the enzyme loading amount is relatively larger than that by those surface binding methods. Nevertheless, there are also some drawbacks like the slow diffusion, enzyme leakage and contamination from the encapsulation materials. In general, there is no perfect method to avoid all the problems that may be induced by the immobilization procedures. Different strategies are often combined to optimize the activity, stability and reusability of enzymes.

Although the idea of μ-IMERs for continuous biocatalysis is not new, challenges remain in the optimization of simple and cheap microfluidic reactors design, and the choice of enzyme immobilization methods. Some new nanomaterials or nanostructures with high SAV ratios have already been developed as the enzyme immobilization carriers, like molybdenum disulfide [123, 124], halloysite nanotube [125-127], metal-organic frameworks [128-130], and so on. But there is still a lack of research in the integration of enzyme-loaded new nanomaterials with the microfluidic reactors for biocatalysis. Moreover, new enzyme immobilization methods still need further exploration. And more types of enzymes should be developed for the μ-IMERs since most of previous studies

focus on common model enzymes like trypsin, lipase, GOx and HRP. It is expected that μ-IMERs with new configuration design and new enzyme immobilization method could be applied to a variety of biocatalyses for both experimental research and industrial production.

The literature review in this chapter provides a technical guide to this PhD research to be discussed in the next four chapters.

2.7 References

[1] A. Schmid, J. Dordick, B. Hauer, A. Kiener, M. Wubbolts, and B. Witholt, "Industrial Biocatalysis Today and Tomorrow," *Nature,* vol. 409, p. 258, 2001.

[2] X. Zhao, F. Qi, C. Yuan, W. Du, and D. Liu, "Lipase-Catalyzed Process for Biodiesel Production: Enzyme Immobilization, Process Simulation and Optimization," *Renewable and Sustainable Energy Reviews,* vol. 44, pp. 182-197, 2015.

[3] D.-M. Liu, J. Chen, and Y.-P. Shi, "Advances on Methods and Easy Separated Support Materials for Enzymes Immobilization," *TrAC Trends in Analytical Chemistry,* 2018.

[4] C. Mateo, J. M. Palomo, G. Fernandez-Lorente, J. M. Guisan, and R. Fernandez-Lafuente, "Improvement of Enzyme Activity, Stability and Selectivity Via Immobilization Techniques," *Enzyme and Microbial Technology,* vol. 40, pp. 1451-1463, 2007.

[5] S. Cantone, V. Ferrario, L. Corici, C. Ebert, D. Fattor, P. Spizzo*, et al.*, "Efficient Immobilisation of Industrial Biocatalysts: Criteria and Constraints for the Selection of Organic Polymeric Carriers and Immobilisation Methods," *Chemical Society Reviews,* vol. 42, pp. 6262-6276, 2013.

[6] A. Liese and L. Hilterhaus, "Evaluation of Immobilized Enzymes for Industrial Applications," *Chemical Society Reviews,* vol. 42, pp. 6236-6249, 2013.

[7] N. R. Mohamad, N. H. C. Marzuki, N. A. Buang, F. Huyop, and R. A. Wahab, "An Overview of Technologies for Immobilization of Enzymes and Surface Analysis Techniques for Immobilized Enzymes," *Biotechnology & Biotechnological Equipment,* vol. 29, pp. 205-220, 2015.

[8] R. A. Sheldon and S. van Pelt, "Enzyme Immobilisation in Biocatalysis: Why, What and How," *Chemical Society Reviews,* vol. 42, pp. 6223-6235, 2013.

[9] K. Meller, M. Szumski, and B. Buszewski, "Microfluidic Reactors with Immobilized Enzymes− Characterization, Dividing, Perspectives," *Sensors and Actuators B: Chemical,* 2016.

[10] E. Wolfgang, H. Volker, and L. Holger, "Microreactors: New Technology for Modern Chemistry," *Wiley/VCH, Weinheim,* pp. 41-84, 2000.

[11] V. Hessel, S. Hardt, and H. Löwe, *A Multi‐Faceted, Hierarchic Analysis of Chemical Micro Process Technology: Sections 1.1–1.5*: Wiley Online Library, 2004.

[12] N. Wang, X. Zhang, Y. Wang, W. Yu, and H. L. Chan, "Microfluidic Reactors for Photocatalytic Water Purification," *Lab on a Chip,* vol. 14, pp. 1074-1082, 2014.

[13] Y. Liu and X. Jiang, "Why Microfluidics? Merits and Trends in Chemical Synthesis," *Lab on a Chip,* vol. 17, pp. 3960-3978, 2017.

[14] K. S. Elvira, X. C. i Solvas, and R. C. Wootton, "The Past, Present and Potential for Microfluidic Reactor Technology in Chemical Synthesis," *Nature Chemistry,* vol. 5, p. 905, 2013.

[15] F. Jia, B. Narasimhan, and S. Mallapragada, "Materials - Based Strategies for Multi - Enzyme Immobilization and Co - Localization: A Review," *Biotechnology and Bioengineering,* vol. 111, pp. 209-222, 2014.

[16] E. Laurenti and A. dos Santos Vianna Jr, "Enzymatic Microreactors in Biocatalysis: History, Features, and Future Perspectives," *Biocatalysis,* vol. 1, pp. 148-165, 2016.

[17] S. R. Forrest, B. B. Elmore, and J. D. Palmer, "Activity and Lifetime of Organophosphorous Hydrolase (Oph) Immobilized Using Layer-by-Layer Nano Self-Assembly on Silicon Microchannels," *Catalysis Today,* vol. 120, pp. 30-34, 2007.

[18] S. R. Forrest, B. B. Elmore, and J. D. Palmer, "Activity and Lifetime of Urease Immobilized Using Layer-by-Layer Nano Self-Assembly on Silicon Microchannels," in *Twenty-Sixth Symposium on Biotechnology for Fuels and Chemicals*, 2005, pp. 85-91.

[19] P. Abgrall and A. Gue, "Lab-on-Chip Technologies: Making a Microfluidic Network and Coupling It into a Complete Microsystem—a Review," *Journal of Micromechanics and Microengineering,* vol. 17, p. R15, 2007.

[20] D. Kim and A. E. Herr, "Protein Immobilization Techniques for Microfluidic Assays," *Biomicrofluidics,* vol. 7, p. 041501, 2013.

[21] K. F. Lei, "Materials and Fabrication Techniques for Nano-and Microfluidic Devices," in *Microfluidics in Detection Science*, ed, 2014, pp. 1-28.

[22] L. M. C. Ferreira, E. T. Da Costa, C. L. Do Lago, and L. Angnes, "Miniaturized Flow System Based on Enzyme Modified Pmma Microreactor for Amperometric Determination of Glucose," *Biosensors and Bioelectronics,* vol. 47, pp. 539-544, 2013.

[23] M. R. F. Cerqueira, D. Grasseschi, R. C. Matos, and L. Angnes, "A Novel Functionalisation Process for Glucose Oxidase Immobilisation in Poly (Methyl Methacrylate) Microchannels in a Flow System for Amperometric

Determinations," *Talanta,* vol. 126, pp. 20-26, 2014.

[24] M. R. F. Cerqueira, M. S. F. Santos, R. C. Matos, I. G. R. Gutz, and L. Angnes, "Use of Poly (Methyl Methacrylate)/Polyethyleneimine Flow Microreactors for Enzyme Immobilization," *Microchemical Journal,* vol. 118, pp. 231-237, 2015.

[25] X. Hu, Y. Dong, Q. He, H. Chen, and Z. Zhu, "Fabrication of a Polystyrene Microfluidic Chip Coupled to Electrospray Ionization Mass Spectrometry for Protein Analysis," *Journal of Chromatography B,* vol. 990, pp. 96-103, 2015.

[26] D. Ogończyk, P. Jankowski, and P. Garstecki, "Functionalization of Polycarbonate with Proteins; Open-Tubular Enzymatic Microreactors," *Lab on a Chip,* vol. 12, pp. 2743-2748, 2012.

[27] Y. Liu, H. Lu, W. Zhong, P. Song, J. Kong, P. Yang*, et al.*, "Multilayer-Assembled Microchip for Enzyme Immobilization as Reactor toward Low-Level Protein Identification," *Analytical Chemistry,* vol. 78, pp. 801-808, 2006.

[28] Y. Bi, H. Zhou, H. Jia, and P. Wei, "Polydopamine-Mediated Preparation of an Enzyme-Immobilized Microreactor for the Rapid Production of Wax Ester," *RSC Advances,* vol. 7, pp. 12283-12291, 2017.

[29] T. Honda, M. Miyazaki, H. Nakamura, and H. Maeda, "Facile Preparation of an Enzyme‐Immobilized Microreactor Using a Cross‐Linking Enzyme Membrane on a Microchannel Surface," *Advanced Synthesis & Catalysis,* vol. 348, pp. 2163-2171, 2006.

[30] H. Becker and C. Gärtner, "Polymer Microfabrication Methods for Microfluidic Analytical Applications," *Electrophoresis,* vol. 21, pp. 12-26, 2000.

[31] H. Becker and L. E. Locascio, "Polymer Microfluidic Devices," *Talanta,* vol. 56, pp. 267-287, 2002.

[32] A. Alrifaiy, O. A. Lindahl, and K. Ramser, "Polymer-Based Microfluidic Devices for Pharmacy, Biology and Tissue Engineering," *Polymers,* vol. 4, pp. 1349-1398, 2012.

[33] E. Roy, A. Pallandre, B. Zribi, M. C. Horny, F. D. Delapierre, A. Cattoni*, et al.*, "Overview of Materials for Microfluidic Applications," in *Advances in Microfluidics-New Applications in Biology, Energy, and Materials Sciences*, ed: InTech, 2016.

[34] J. P. McMullen and K. F. Jensen, "Integrated Microreactors for Reaction Automation: New Approaches to Reaction Development," *Annual Review of Analytical Chemistry,* vol. 3, pp. 19-42, 2010.

[35] P. Lisowski and P. K. Zarzycki, "Microfluidic Paper-Based Analytical Devices

(Mpads) and Micro Total Analysis Systems (Mtas): Development, Applications and Future Trends," *Chromatographia,* vol. 76, pp. 1201-1214, 2013.

[36] F. Figueredo, P. T. Garcia, E. Cortón, and W. K. Coltro, "Enhanced Analytical Performance of Paper Microfluidic Devices by Using Fe3o4 Nanoparticles, Mwcnt, and Graphene Oxide," *ACS Applied Materials & Interfaces,* vol. 8, pp. 11-15, 2015.

[37] K. Szymańska, M. Pietrowska, J. Kocurek, K. Maresz, A. Koreniuk, J. Mrowiec-Białoń, *et al.*, "Low Back-Pressure Hierarchically Structured Multichannel Microfluidic Bioreactors for Rapid Protein Digestion–Proof of Concept," *Chemical Engineering Journal,* vol. 287, pp. 148-154, 2016.

[38] K. Nakagawa, A. Tamura, and C. Chaiya, "Preparation of Proteolytic Microreactors by Freeze-Drying Immobilization," *Chemical Engineering Science,* vol. 119, pp. 22-29, 2014.

[39] M. Petro, F. Svec, and J. M. Fréchet, "Immobilization of Trypsin onto "Molded" Macroporous Poly (Glycidyl Methacrylate - Co - Ethylene Dimethacrylate) Rods and Use of the Conjugates as Bioreactors and for Affinity Chromatography," *Biotechnology and Bioengineering,* vol. 49, pp. 355-363, 1996.

[40] J. S. Lee, S. H. Lee, J. H. Kim, and C. B. Park, "Artificial Photosynthesis on a Chip: Microfluidic Cofactor Regeneration and Photoenzymatic Synthesis under Visible Light," *Lab on a Chip,* vol. 11, pp. 2309-2311, 2011.

[41] A. Küchler, J. N. Bleich, B. Sebastian, P. S. Dittrich, and P. Walde, "Stable and Simple Immobilization of Proteinase K inside Glass Tubes and Microfluidic Channels," *ACS Applied Materials & Interfaces,* vol. 7, pp. 25970-25980, 2015.

[42] H. Jang, P. Lee, S. Kim, S. M. Kim, and T.-J. Jeon, "An Antibacterial Microfluidic System with Fish Gill Structure for the Detection of Staphylococcus Via Enzymatic Reaction on a Chromatic Polydiacetylene Material Caused by Lysostaphin," *Microchimica Acta,* vol. 184, pp. 4563-4569, 2017.

[43] Y. Lv, Z. Lin, T. Tan, and F. Svec, "Preparation of Reusable Bioreactors Using Reversible Immobilization of Enzyme on Monolithic Porous Polymer Support with Attached Gold Nanoparticles," *Biotechnology and Bioengineering,* vol. 111, pp. 50-58, 2014.

[44] F. Liu, Y. Piao, J. S. Choi, and T. S. Seo, "Three-Dimensional Graphene Micropillar Based Electrochemical Sensor for Phenol Detection," *Biosensors and Bioelectronics,* vol. 50, pp. 387-392, 2013.

[45] A. Gong, C.-T. Zhu, Y. Xu, F.-Q. Wang, F.-A. Wu, and J. Wang, "Moving and Unsinkable Graphene Sheets Immobilized Enzyme for Microfluidic

Biocatalysis," *Scientific Reports,* vol. 7, p. 4309, 2017.

[46] N. Singh, M. A. Ali, P. Rai, A. Sharma, B. D. Malhotra, and R. John, "Microporous Nanocomposite Enabled Microfluidic Biochip for Cardiac Biomarker Detection," *ACS Applied Materials & Interfaces,* vol. 9, pp. 33576-33588, 2017.

[47] Z. Yin, W. Zhao, M. Tian, Q. Zhang, L. Guo, and L. Yang, "A Capillary Electrophoresis-Based Immobilized Enzyme Reactor Using Graphene Oxide as a Support Via Layer by Layer Electrostatic Assembly," *Analyst,* vol. 139, pp. 1973-1979, 2014.

[48] D. Valikhani, J. M. Bolivar, M. Viefhues, D. N. McIlroy, E. X. Vrouwe, and B. Nidetzky, "A Spring in Performance: Silica Nanosprings Boost Enzyme Immobilization in Microfluidic Channels," *ACS applied materials & interfaces,* vol. 9, pp. 34641-34649, 2017.

[49] Y. Liu, W. Zhong, S. Meng, J. Kong, H. Lu, P. Yang*, et al.*, "Assembly‐Controlled Biocompatible Interface on a Microchip: Strategy to Highly Efficient Proteolysis," *Chemistry-a European Journal,* vol. 12, pp. 6585-6591, 2006.

[50] H. Bao, Q. Chen, L. Zhang, and G. Chen, "Immobilization of Trypsin in the Layer-by-Layer Coating of Graphene Oxide and Chitosan on in-Channel Glass Fiber for Microfluidic Proteolysis," *Analyst,* vol. 136, pp. 5190-5196, 2011.

[51] Y. Bi, H. Zhou, H. Jia, and P. Wei, "A Flow-through Enzymatic Microreactor Immobilizing Lipase Based on Layer-by-Layer Method for Biosynthetic Process: Catalyzing the Transesterification of Soybean Oil for Fatty Acid Methyl Ester Production," *Process Biochemistry,* vol. 54, pp. 73-80, 2017.

[52] S. Kundu, A. S. Bhangale, W. E. Wallace, K. M. Flynn, C. M. Guttman, R. A. Gross*, et al.*, "Continuous Flow Enzyme-Catalyzed Polymerization in a Microreactor," *Journal of the American Chemical Society,* vol. 133, pp. 6006-6011, 2011.

[53] J. Wang, X. Liu, X.-D. Wang, T. Dong, X.-Y. Zhao, D. Zhu*, et al.*, "Selective Synthesis of Human Milk Fat-Style Structured Triglycerides from Microalgal Oil in a Microfluidic Reactor Packed with Immobilized Lipase," *Bioresource Technology,* vol. 220, pp. 132-141, 2016.

[54] G. H. Seong, J. Heo, and R. M. Crooks, "Measurement of Enzyme Kinetics Using a Continuous-Flow Microfluidic System," *Analytical Chemistry,* vol. 75, pp. 3161-3167, 2003.

[55] C. R. Boehm, P. S. Freemont, and O. Ces, "Design of a Prototype Flow Microreactor for Synthetic Biology in Vitro," *Lab on a Chip,* vol. 13, pp. 3426-3432, 2013.

[56] L. C. Lasave, S. M. Borisov, J. Ehgartner, and T. Mayr, "Quick and Simple Integration of Optical Oxygen Sensors into Glass-Based Microfluidic Devices," *RSC Advances,* vol. 5, pp. 70808-70816, 2015.

[57] D. N. Kim, Y. Lee, and W.-G. Koh, "Fabrication of Microfluidic Devices Incorporating Bead-Based Reaction and Microarray-Based Detection System for Enzymatic Assay," *Sensors and Actuators B: Chemical,* vol. 137, pp. 305-312, 2009.

[58] A. Kecskemeti and A. Gaspar, "Preparation and Characterization of a Packed Bead Immobilized Trypsin Reactor Integrated into a Pdms Microfluidic Chip for Rapid Protein Digestion," *Talanta,* vol. 166, pp. 275-283, 2017.

[59] T. Peschke, M. Skoupi, T. Burgahn, S. Gallus, I. Ahmed, K. S. Rabe*, et al.*, "Self-Immobilizing Fusion Enzymes for Compartmentalized Biocatalysis," *ACS Catalysis,* vol. 7, pp. 7866-7872, 2017.

[60] R.-P. Liang, X.-N. Wang, C.-M. Liu, X.-Y. Meng, and J.-D. Qiu, "Construction of Graphene Oxide Magnetic Nanocomposites-Based on-Chip Enzymatic Microreactor for Ultrasensitive Pesticide Detection," *Journal of Chromatography A,* vol. 1315, pp. 28-35, 2013.

[61] J. Sheng, L. Zhang, J. Lei, and H. Ju, "Fabrication of Tunable Microreactor with Enzyme Modified Magnetic Nanoparticles for Microfluidic Electrochemical Detection of Glucose," *Analytica Chimica Acta,* vol. 709, pp. 41-46, 2012.

[62] A. Karim, J. Bravo, D. Gorm, T. Conant, and A. Datye, "Comparison of Wall-Coated and Packed-Bed Reactors for Steam Reforming of Methanol," *Catalysis Today,* vol. 110, pp. 86-91, 2005.

[63] J. Qiao, L. Qi, X. Mu, and Y. Chen, "Monolith and Coating Enzymatic Microreactors of L-Asparaginase: Kinetics Study by Mce–Lif for Potential Application in Acute Lymphoblastic Leukemia (All) Treatment," *Analyst,* vol. 136, pp. 2077-2083, 2011.

[64] A. S. de León, N. Vargas-Alfredo, A. Gallardo, A. Fernández-Mayoralas, A. Bastida, A. Muñoz-Bonilla*, et al.*, "Microfluidic Reactors Based on Rechargeable Catalytic Porous Supports: Heterogeneous Enzymatic Catalysis Via Reversible Host–Guest Interactions," *ACS Applied Materials & Interfaces,* vol. 9, pp. 4184-4191, 2017.

[65] K. Nakagawa and Y. Goto, "Preparation of A-Amylase-Immobilized Freeze-Dried Poly (Vinyl Alcohol) Foam and Its Application to Microfluidic Enzymatic Reactor," *Chemical Engineering and Processing: Process Intensification,* vol. 91, pp. 35-42, 2015.

[66] J. P. Lafleur, S. Senkbeil, J. Novotny, G. Nys, N. Bøgelund, K. D. Rand, *et al.*, "Rapid and Simple Preparation of Thiol–Ene Emulsion-Templated Monoliths and Their Application as Enzymatic Microreactors," *Lab on a Chip,* vol. 15, pp. 2162-2172, 2015.

[67] T. C. Logan, D. S. Clark, T. B. Stachowiak, F. Svec, and J. M. Frechet, "Photopatterning Enzymes on Polymer Monoliths in Microfluidic Devices for Steady-State Kinetic Analysis and Spatially Separated Multi-Enzyme Reactions," *Analytical Chemistry,* vol. 79, pp. 6592-6598, 2007.

[68] D. S. Peterson, T. Rohr, F. Svec, and J. M. Fréchet, "Enzymatic Microreactor-on-a-Chip: Protein Mapping Using Trypsin Immobilized on Porous Polymer Monoliths Molded in Channels of Microfluidic Devices," *Analytical Chemistry,* vol. 74, pp. 4081-4088, 2002.

[69] O. Yesil-Celiktas, S. Cumana, and I. Smirnova, "Silica-Based Monoliths for Enzyme Catalyzed Reactions in Microfluidic Systems with an Emphasis on Glucose 6-Phosphate Dehydrogenase and Cellulase," *Chemical Engineering Journal,* vol. 234, pp. 166-172, 2013.

[70] M. Alotaibi, J. Manayil, G. M. Greenway, S. J. Haswell, S. M. Kelly, A. F. Lee, *et al.*, "Lipase Immobilised Silica Monoliths as Continuous-Flow Microreactors for Triglyceride Transesterification," *Reaction Chemistry & Engineering,* 2017.

[71] P. He, B. P. Burke, G. S. Clemente, N. Brown, N. Pamme, and S. J. Archibald, "Monolith-Based 68 Ga Processing: A New Strategy for Purification to Facilitate Direct Radiolabelling Methods," *Reaction Chemistry & Engineering,* vol. 1, pp. 361-365, 2016.

[72] Y. Yi, Y. Chen, M. A. Brook, and J. D. Brennan, "Development of Macroporous Titania Monoliths by a Biocompatible Method. Part 2: Enzyme Entrapment Studies," *Chemistry of Materials,* vol. 18, pp. 5336-5342, 2006.

[73] J. Ma, Z. Liang, X. Qiao, Q. Deng, D. Tao, L. Zhang, *et al.*, "Organic− Inorganic Hybrid Silica Monolith Based Immobilized Trypsin Reactor with High Enzymatic Activity," *Analytical chemistry,* vol. 80, pp. 2949-2956, 2008.

[74] P. Liang, H. Bao, J. Yang, L. Zhang, and G. Chen, "Preparation of Porous Graphene Oxide–Poly (Urea–Formaldehyde) Hybrid Monolith for Trypsin Immobilization and Efficient Proteolysis," *Carbon,* vol. 97, pp. 25-34, 2016.

[75] D. Pirozzi, M. Abagnale, L. Minieri, P. Pernice, and A. Aronne, "In-Situ Sol-Gel Modification Strategies to Develop a Monolith Continuous Microreactor for Enzymatic Green Reactions," *Chemical Engineering Journal,* vol. 306, pp. 1010-1016, 2016.

[76] D. N. Tran and K. J. Balkus Jr, "Perspective of Recent Progress in Immobilization of Enzymes," *ACS Catalysis,* vol. 1, pp. 956-968, 2011.

[77] J. Ma, L. Zhang, Z. Liang, W. Zhang, and Y. Zhang, "Monolith - Based Immobilized Enzyme Reactors: Recent Developments and Applications for Proteome Analysis," *Journal of Separation Science,* vol. 30, pp. 3050-3059, 2007.

[78] J. Nelson and E. G. Griffin, "Adsorption of Invertase," *Journal of the American Chemical Society,* vol. 38, pp. 1109-1115, 1916.

[79] T. Honda, H. Yamaguchi, and M. Miyazaki, "Development of Enzymatic Reactions in Miniaturized Reactors," *Applied Bioengineering: Innovations and Future Directions,* vol. 5, 2017.

[80] L. Cao, "Adsorption-Based Immobilization," in *Carrier-Bound Immobilized Enzymes*, ed: Wiley-VCH Verlag GmbH & Co. KGaA, 2006, pp. 53-168.

[81] M. L. Shuler, F. Kargi, and F. Kargi, *Bioprocess Engineering: Basic Concepts* vol. 2: Prentice Hall Upper Saddle River, NJ, 2002.

[82] Z.-m. Tang and J.-w. Kang, "Enzyme Inhibitor Screening by Capillary Electrophoresis with an on-Column Immobilized Enzyme Microreactor Created by an Ionic Binding Technique," *Analytical Chemistry,* vol. 78, pp. 2514-2520, 2006.

[83] A. Srinivasan, H. Bach, D. H. Sherman, and J. S. Dordick, "Bacterial P450 - Catalyzed Polyketide Hydroxylation on a Microfluidic Platform," *Biotechnology and Bioengineering,* vol. 88, pp. 528-535, 2004.

[84] G. Kulsharova, N. Dimov, M. P. Marques, N. Szita, and F. Baganz, "Simplified Immobilisation Method for Histidine-Tagged Enzymes in Poly (Methyl Methacrylate) Microfluidic Devices," *New Biotechnology,* 2017.

[85] H. Mao, T. Yang, and P. S. Cremer, "Design and Characterization of Immobilized Enzymes in Microfluidic Systems," *Analytical Chemistry,* vol. 74, pp. 379-385, 2002.

[86] M. A. Holden, S.-Y. Jung, and P. S. Cremer, "Patterning Enzymes inside Microfluidic Channels Via Photoattachment Chemistry," *Analytical Chemistry,* vol. 76, pp. 1838-1843, 2004.

[87] T. Vong, S. Schoffelen, S. F. van Dongen, T. A. van Beek, H. Zuilhof, and J. C. van Hest, "A DNA-Based Strategy for Dynamic Positional Enzyme Immobilization inside Fused Silica Microchannels," *Chemical Science,* vol. 2, pp. 1278-1285, 2011.

[88] K. Sakai-Kato, M. Kato, and T. Toyo'oka, "Creation of an on-Chip Enzyme

Reactor by Encapsulating Trypsin in Sol− Gel on a Plastic Microchip," *Analytical Chemistry,* vol. 75, pp. 388-393, 2003.

[89] H. Wu, Y. Tian, B. Liu, H. Lu, X. Wang, J. Zhai*, et al.*, "Titania and Alumina Sol−Gel-Derived Microfluidics Enzymatic-Reactors for Peptide Mapping: Design, Characterization, and Performance," *Journal of Proteome Research,* vol. 3, pp. 1201-1209, 2004.

[90] W.-G. Koh and M. Pishko, "Immobilization of Multi-Enzyme Microreactors inside Microfluidic Devices," *Sensors and Actuators B: Chemical,* vol. 106, pp. 335-342, 2005.

[91] S.-i. Matsuura, R. Ishii, T. Itoh, S. Hamakawa, T. Tsunoda, T. Hanaoka*, et al.*, "Immobilization of Enzyme-Encapsulated Nanoporous Material in a Microreactor and Reaction Analysis," *Chemical Engineering Journal,* vol. 167, pp. 744-749, 2011.

[92] Z.-Q. Wu, Z.-Q. Li, J.-Y. Li, J. Gu, and X.-H. Xia, "Contribution of Convection and Diffusion to the Cascade Reaction Kinetics of B-Galactosidase/Glucose Oxidase Confined in a Microchannel," *Physical Chemistry Chemical Physics,* vol. 18, pp. 14460-14465, 2016.

[93] A. A. Homaei, R. Sariri, F. Vianello, and R. Stevanato, "Enzyme Immobilization: An Update," *Journal of Chemical Biology,* vol. 6, pp. 185-205, 2013.

[94] X. Ji, F. Ye, P. Lin, and S. Zhao, "Immobilized Capillary Adenosine Deaminase Microreactor for Inhibitor Screening in Natural Extracts by Capillary Electrophoresis," *Talanta,* vol. 82, pp. 1170-1174, 2010.

[95] W. Min, W. Wang, J. Chen, A. Wang, and Z. Hu, "On-Line Immobilized Acetylcholinesterase Microreactor for Screening of Inhibitors from Natural Extracts by Capillary Electrophoresis," *Analytical and Bioanalytical Chemistry,* vol. 404, pp. 2397-2405, 2012.

[96] J. J. Virgen-Ortíz, J. C. dos Santos, Á. Berenguer-Murcia, O. Barbosa, R. C. Rodrigues, and R. Fernandez-Lafuente, "Polyethylenimine: A Very Useful Ionic Polymer in the Design of Immobilized Enzyme Biocatalysts," *Journal of Materials Chemistry B,* vol. 5, pp. 7461-7490, 2017.

[97] S. Zhao, X. Ji, P. Lin, and Y.-M. Liu, "A Gold Nanoparticle-Mediated Enzyme Bioreactor for Inhibitor Screening by Capillary Electrophoresis," *Analytical Biochemistry,* vol. 411, pp. 88-93, 2011.

[98] T.-F. Jiang, T.-T. Liang, Y.-H. Wang, W.-H. Zhang, and Z.-H. Lv, "Immobilized Capillary Tyrosinase Microreactor for Inhibitor Screening in Natural Extracts by Capillary Electrophoresis," *Journal of Pharmaceutical and Biomedical Analysis,*

vol. 84, pp. 36-40, 2013.

[99] M. A. Camara, M. Tian, L. Guo, and L. Yang, "Application of Capillary Enzyme Micro-Reactor in Enzyme Activity and Inhibitors Studies of Glucose-6-Phosphate Dehydrogenase," *Journal of Chromatography B,* vol. 990, pp. 174-180, 2015.

[100] Z. Tang, T. Wang, and J. Kang, "Immobilized Capillary Enzyme Reactor Based on Layer‐by‐Layer Assembling Acetylcholinesterase for Inhibitor Screening by Ce," *Electrophoresis,* vol. 28, pp. 2981-2987, 2007.

[101] F. Wang, C. Guo, H.-Z. Liu, and C.-Z. Liu, "Reversible Immobilization of Glucoamylase by Metal Affinity Adsorption on Magnetic Chelator Particles," *Journal of Molecular Catalysis B: Enzymatic,* vol. 48, pp. 1-7, 2007.

[102] D. Kirstein, "Chelate Mediated Immobilization of Proteins," *Advances in Molecular and Cell Biology,* vol. 15, pp. 247-256, 1996.

[103] Q.-H. Shi, Y. Tian, X.-Y. Dong, S. Bai, and Y. Sun, "Chitosan-Coated Silica Beads as Immobilized Metal Affinity Support for Protein Adsorption," *Biochemical Engineering Journal,* vol. 16, pp. 317-322, 2003.

[104] M. Miyazaki, J. Kaneno, R. Kohama, M. Uehara, K. Kanno, M. Fujii, *et al.*, "Preparation of Functionalized Nanostructures on Microchannel Surface and Their Use for Enzyme Microreactors," *Chemical Engineering Journal,* vol. 101, pp. 277-284, 2004.

[105] B. Brena, P. González-Pombo, and F. Batista-Viera, "Immobilization of Enzymes: A Literature Survey," *Immobilization of Enzymes and Cells: Third Edition,* pp. 15-31, 2013.

[106] A. González‐Campo, B. Eker, H. J. Gardeniers, J. Huskens, and P. Jonkheijm, "A Supramolecular Approach to Enzyme Immobilization in Micro‐Channels," *Small,* vol. 8, pp. 3531-3537, 2012.

[107] P. C. Weber, D. Ohlendorf, J. Wendoloski, and F. Salemme, "Structural Origins of High-Affinity Biotin Binding to Streptavidin," *Science,* vol. 243, pp. 85-88, 1989.

[108] F. Rusmini, Z. Zhong, and J. Feijen, "Protein Immobilization Strategies for Protein Biochips," *Biomacromolecules,* vol. 8, pp. 1775-1789, 2007.

[109] H. Schröder, L. Hoffmann, J. Müller, P. Alhorn, M. Fleger, A. Neyer, *et al.*, "Addressable Microfluidic Polymer Chip for DNA‐Directed Immobilization of Oligonucleotide‐Tagged Compounds," *Small,* vol. 5, pp. 1547-1552, 2009.

[110] D. Liu, R. K. Perdue, L. Sun, and R. M. Crooks, "Immobilization of DNA onto Poly (Dimethylsiloxane) Surfaces and Application to a Microelectrochemical Enzyme-Amplified DNA Hybridization Assay," *Langmuir,* vol. 20, pp. 5905-5910,

2004.

[111] L. Lloret, G. Eibes, M. Moreira, G. Feijoo, J. Lema, and M. Miyazaki, "Improving the Catalytic Performance of Laccase Using a Novel Continuous-Flow Microreactor," *Chemical Engineering Journal,* vol. 223, pp. 497-506, 2013.

[112] D. Lu, G. Shao, D. Du, J. Wang, L. Wang, W. Wang, *et al.*, "Enzyme Entrapped Nanoporous Scaffolds Formed through Flow-Induced Gelation in a Microfluidic Filter Device for Sensitive Biosensing of Organophosphorus Compounds," *Lab on a Chip,* vol. 11, pp. 381-384, 2011.

[113] S. Cumana, J. Simons, A. Liese, L. Hilterhaus, and I. Smirnova, "Immobilization of Glucose 6-Phosphate Dehydrogenase in Silica-Based Hydrogels: A Comparative Study," *Journal of Molecular Catalysis B: Enzymatic,* vol. 85, pp. 220-228, 2013.

[114] S. Fornera, P. Kuhn, D. Lombardi, A. D. Schlüter, P. S. Dittrich, and P. Walde, "Sequential Immobilization of Enzymes in Microfluidic Channels for Cascade Reactions," *ChemPlusChem,* vol. 77, pp. 98-101, 2012.

[115] F. Costantini, R. Tiggelaar, S. Sennato, F. Mura, S. Schlautmann, F. Bordi, *et al.*, "Glucose Level Determination with a Multi-Enzymatic Cascade Reaction in a Functionalized Glass Chip," *Analyst,* vol. 138, pp. 5019-5024, 2013.

[116] R. J. Conrado, J. D. Varner, and M. P. DeLisa, "Engineering the Spatial Organization of Metabolic Enzymes: Mimicking Nature's Synergy," *Current Opinion in Biotechnology,* vol. 19, pp. 492-499, 2008.

[117] Y.-H. P. Zhang, "Substrate Channeling and Enzyme Complexes for Biotechnological Applications," *Biotechnology Advances,* vol. 29, pp. 715-725, 2011.

[118] A. Küchler, M. Yoshimoto, S. Luginbühl, F. Mavelli, and P. Walde, "Enzymatic Reactions in Confined Environments," *Nature Nanotechnology,* vol. 11, pp. 409-420, 2016.

[119] G. Palazzo, G. Colafemmina, C. G. Iudice, and A. Mallardi, "Three Immobilized Enzymes Acting in Series in Layer by Layer Assemblies: Exploiting the Trehalase-Glucose Oxidase-Horseradish Peroxidase Cascade Reactions for the Optical Determination of Trehalose," *Sensors and Actuators B: Chemical,* vol. 202, pp. 217-223, 2014.

[120] J. Heo, "Spatial Distance Effect of Bienzymes on the Efficiency of Sequential Reactions in a Microfluidic Reactor Packed with Enzyme-Immobilized Microbeads," *Analytical Sciences,* vol. 30, pp. 991-997, 2014.

[121] S. Schoffelen and J. C. van Hest, "Chemical Approaches for the Construction of Multi-Enzyme Reaction Systems," *Current Opinion in Structural Biology,* vol. 23, pp. 613-621, 2013.

[122] J. Fu, M. Liu, Y. Liu, N. W. Woodbury, and H. Yan, "Interenzyme Substrate Diffusion for an Enzyme Cascade Organized on Spatially Addressable DNA Nanostructures," *Journal of the American Chemical Society,* vol. 134, pp. 5516-5519, 2012.

[123] R. Das, H. Mishra, A. Srivastava, and A. M. Kayastha, "Covalent Immobilization of B-Amylase onto Functionalized Molybdenum Sulfide Nanosheets, Its Kinetics and Stability Studies: A Gateway to Boost Enzyme Application," *Chemical Engineering Journal,* vol. 328, pp. 215-227, 2017.

[124] H.-L. Shuai, K.-J. Huang, Y.-X. Chen, L.-X. Fang, and M.-P. Jia, "Au Nanoparticles/Hollow Molybdenum Disulfide Microcubes Based Biosensor for Microrna-21 Detection Coupled with Duplex-Specific Nuclease and Enzyme Signal Amplification," *Biosensors and Bioelectronics,* vol. 89, pp. 989-997, 2017.

[125] J. Sun, R. Yendluri, K. Liu, Y. Guo, Y. Lvov, and X. Yan, "Enzyme-Immobilized Clay Nanotube–Chitosan Membranes with Sustainable Biocatalytic Activities," *Physical Chemistry Chemical Physics,* vol. 19, pp. 562-567, 2017.

[126] A. A. Kadam, J. Jang, and D. S. Lee, "Supermagnetically Tuned Halloysite Nanotubes Functionalized with Aminosilane for Covalent Laccase Immobilization," *ACS Applied Materials & Interfaces,* vol. 9, pp. 15492-15501, 2017.

[127] M. Z. Anwar, D. J. Kim, A. Kumar, S. K. Patel, S. Otari, P. Mardina*, et al.*, "Sno 2 Hollow Nanotubes: A Novel and Efficient Support Matrix for Enzyme Immobilization," *Scientific Reports,* vol. 7, p. 15333, 2017.

[128] X. Lian, Y. Fang, E. Joseph, Q. Wang, J. Li, S. Banerjee*, et al.*, "Enzyme–Mof (Metal–Organic Framework) Composites," *Chemical Society Reviews,* 2017.

[129] P. Li, J. A. Modica, A. J. Howarth, E. Vargas, P. Z. Moghadam, R. Q. Snurr*, et al.*, "Toward Design Rules for Enzyme Immobilization in Hierarchical Mesoporous Metal-Organic Frameworks," *Chem,* vol. 1, pp. 154-169, 2016.

[130] Z. Li, H. Xia, S. Li, J. Pang, W. Zhu, and Y. Jiang, "In Situ Hybridization of Enzymes and Their Metal–Organic Framework Analogues with Enhanced Activity and Stability by Biomimetic Mineralisation," *Nanoscale,* vol. 9, pp. 15298-15302, 2017.

CHAPTER 3
MATERIALS AND METHODOLOGY

This chapter will focus on presenting the common materials, and the general methods to be used for the fabrication, test and analysis of the three microfluidic reactors in the next three chapters.

3.1 Chemicals and reagents

The reaction buffer (pH 8.0) used for enzyme assay consisted of 0.1 M Tris(hydroxymethyl)aminomethane buffer (Tris-HCl, pH 8.0, Beijing Solarbio Technology Co., Ltd., Beijing), 5 mM magnesium chloride hexahydrate ($MgCl_2 \cdot 6H_2O$, AR, Sinopharm Chemical Reagent Co., Ltd, Shanghai), 66 mM potassium bicarbonate ($KHCO_3$, AR, Sinopharm Chemical Reagent Co., Ltd, Shanghai), and 5 mM DL-Dithiothreitol (DTT, 99%, Aladdin Industrial Corporation, Shanghai). Dopamine hydrochloride (98%, J&K Scientific Ltd., Beijing) was used as 1 $mg \cdot mL^{-1}$ solution in 10 mM Tris-HCl buffer (pH=8.8, Beijing Solarbio Technology Co., Ltd., Beijing). Reduced nicotinamide adenine dinucleotide disodium salt (NADH Na_2, ≥98.0), adenosine-5'-triphosphate, disodium salt, trihydrate (ATP Na_2, ≥98.0) and fluorescein isothiocyanate isomer I (FITC, ≥90%, HPLC) were purchased from Beijing Solarbio Technology Co., Ltd. D-ribulose 1,5-bisphosphate sodium salt hydrate (RuBP, ~90%), D-ribulose 1,5-diphosphate carboxylase (RuBisCO, from spinach partially purified powder, 0.01-0.1

unit/mg solid), D-(−)-3-Phosphoglyceric acid disodium salt, ⩾ 93% (3-PGA), glyceraldehyde 3-phosphate dehydrogenase (GAPDH, from rabbit muscle lyophilized powder), 3-phosphoglyceric phosphokinase (PGK, from baker's yeast (S. cerevisiae), ammonium sulfate suspension, ≥1000 units/mg protein), Glycerol 3-phosphate Oxidase (G3POX, from Pediococcus sp. lyophilized powder), α-glycerophosphate dehydrogenase (G3PDH, from rabbit muscle, type I, ammonium sulfate suspension), triosephosphate isomerase (TPI, from baker's yeast (S. cerevisiae), ammonium sulfate suspension) and Catalase (from bovine liver powder) were provided by Sigma-Aldrich.

3.2 Instruments

3.2.1 Ultraviolet-visible spectrophotometer

Spectrophotometer is a double beam photometer system of which a monochromatic light is split into two beams; one transmits through the object, while the other beam transmits through a standard specimen. The intensity of the two beams is recorded and calculated to obtain the resultant spectrum. When the spectrophotometer is designed for ultraviolet-visible spectral detection, it is so called an ultraviolet-visible spectrophotometer (UV-Vis or UV/Vis). The scheme of an UV-Vis is shown in **Figure 3.1 (a)**.

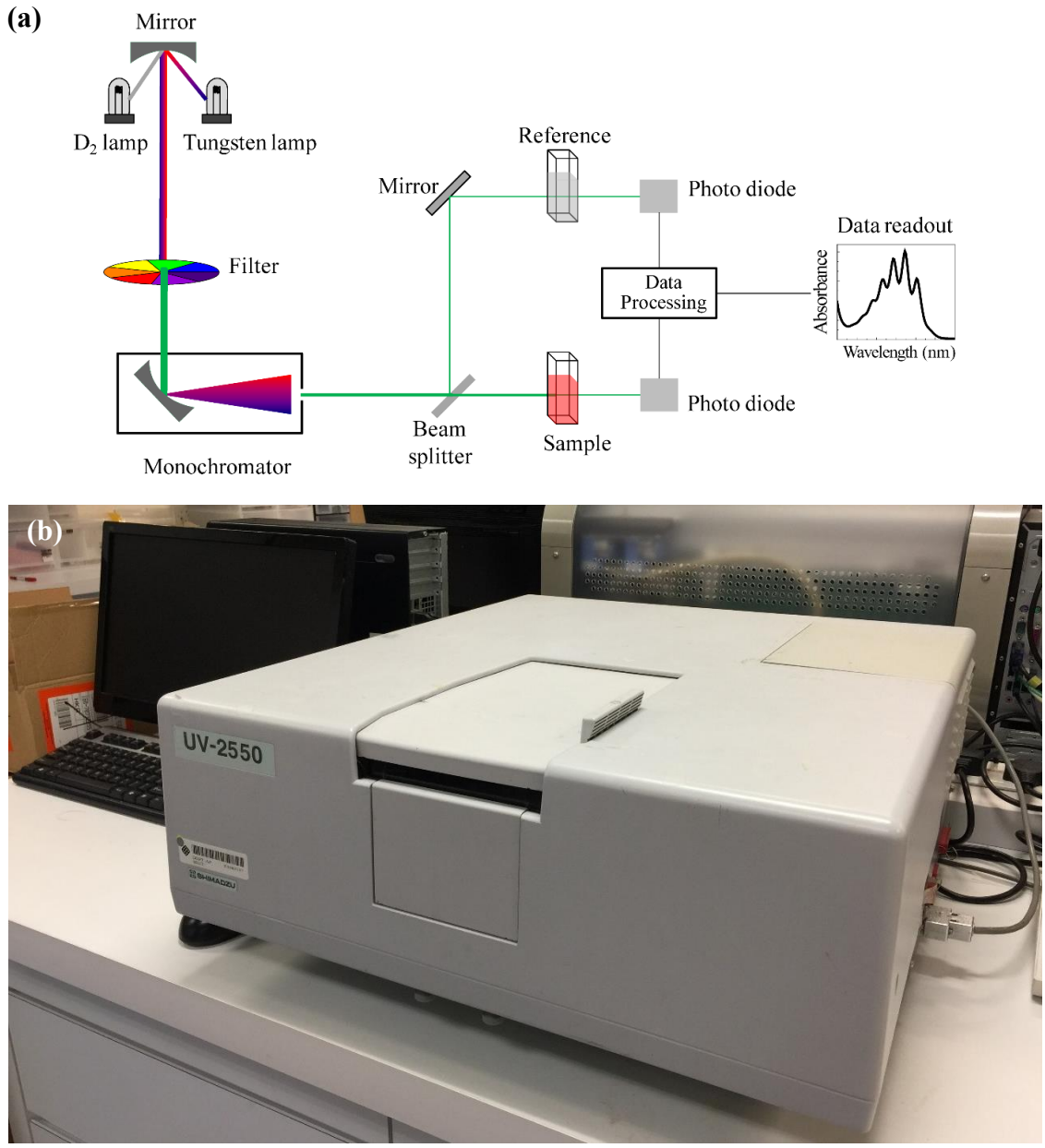

Figure 3.1 Schematic (a) and photograph (b) for an ultraviolet-visible spectrophotometer.

When a monochromatic light beam passes through a sample which is not opaque in the UV-visible region, a quantitative relationship called the Beer's law can be applied to describe the thickness dependence of the intensity of transmitted light. If T is the transmittance, then

$$T = \frac{I}{I_0} = e^{-kd} \tag{3.1}$$

where I_0 and I are the intensity of the incident light and the transmitted light respectively, d is the thickness of the sample and k is absorption coefficient of the sample material. The absorbance A is based on the transmittance:

$$A = -\log(T) \tag{3.2}$$

When solutions are analyzed by the UV-Vis, the principle is described as the Beer-Lambert Law, which states that the absorbance of a solution is proportional to the concentration of the absorbing species in solution and the path length. The Beer-Lambert Law can be expressed as follows when it is used to determine the concentration of the absorbing species:

$$A = \varepsilon cL \tag{3.3}$$

where A is the measured absorbance, in Absorbance Units (AU), L is the path length through the sample, and c is the concentration of the absorbing species. ε is a constant called the extinction coefficient of the specific absorbing species at the specific wavelength. It is related to the intrinsic molecular property of the absorbing species in a given solvent at a particular temperature and pressure. The unit is 1/(M·cm) or often AU/(M·cm). In our experiments, UV-Vis (Shimadzu UV-2450, **Figure 3.1 (b)**) is used to analyze the reaction solutions. The absorbance change at 340 nm of the reaction solutions is monitored for the products amount due to the oxidation of NADH by GAPDH in

solution. 6220 $M^{-1} \cdot cm^{-1}$ was used as the extinction coefficient of NADH at the absorbance of 340 nm.

3.2.2 Scanning electron microscopy

A scanning electron microscope (SEM) is a type of electron microscope that produces images of a sample by scanning it with a focused beam of electrons. Using SEM, samples can be observed for their topography, morphology, chemistry, crystallography, orientation of grains, reactions with atmosphere, and effects of temperature. Here, field emission scanning electron microscopy (FESEM, JEOL JSM-6335F, **Figure 3.2**) was used to characterize the surface morphology of the prepared microfluidic reactors. The accelerating voltage used was 5 kV.

Figure 3.2 Photography of JEOL field emission scanning electron microscopy.

During the operation, the incident electron beam is emitted from the field emission

guns using tungsten single crystal emitters and is then scattered in the sample, which gives rise to various signals for the detection (secondary electrons, backscattered electrons, Auger electrons, X-rays and cathodoluminescence). Compared with the optical microscopy, an SEM typically has the depth of focus orders of magnitude better than an optical microscope, making the SEM suitable for studying rough surfaces. The higher the magnification, the lower depth of focus it has. Conductive materials can directly be observed by SEM; however, low-contrast images may be obtained when non-conductive materials are analyzed by SEM directly due to the uneven aggregation of negative charges that are bombarded by the high-energy electron beam. In order to eliminate the charging effect, and to increase the secondary electrons and backscattered electrons for high-quality images, a thin film gold layer can be deposited on the samples before analyzed by SEM.

3.2.3 Attenuated total reflection-Fourier transform infrared spectroscopy

Fourier transform infrared spectroscopy (FTIR) is a spectroscopy mainly used for infrared (IR) radiation. In the FTIR, when the IR radiation goes through a sample, some of the IR radiation may be absorbed by the sample due to the vibrations between the bonds of the atoms. Different materials are composed of different atoms; therefore, one compound would have its unique infrared spectrum. The resulted spectrum with absorption peaks can be used to identify or qualitatively analyze different functional groups of materials.

The most notable feature of FTIR is the use of the interferometer to measure all the infrared frequencies simultaneously, making it very fast. Hence, the detectors used in the FTIR need to be designed specifically for the measurement of the interferogram signal. Then, the measured signal goes for the Fourier transformation in a computer for further analysis.

(a)

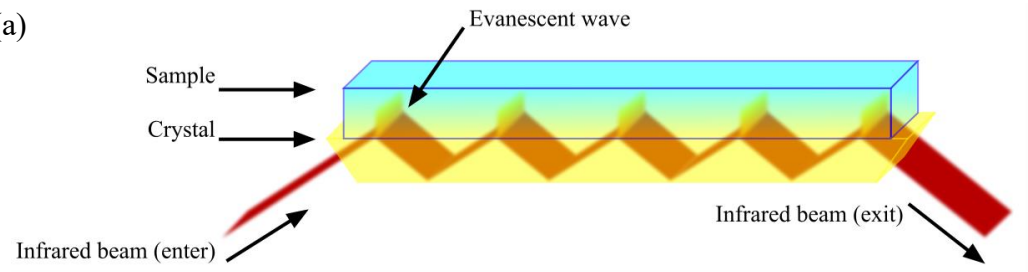

(b)

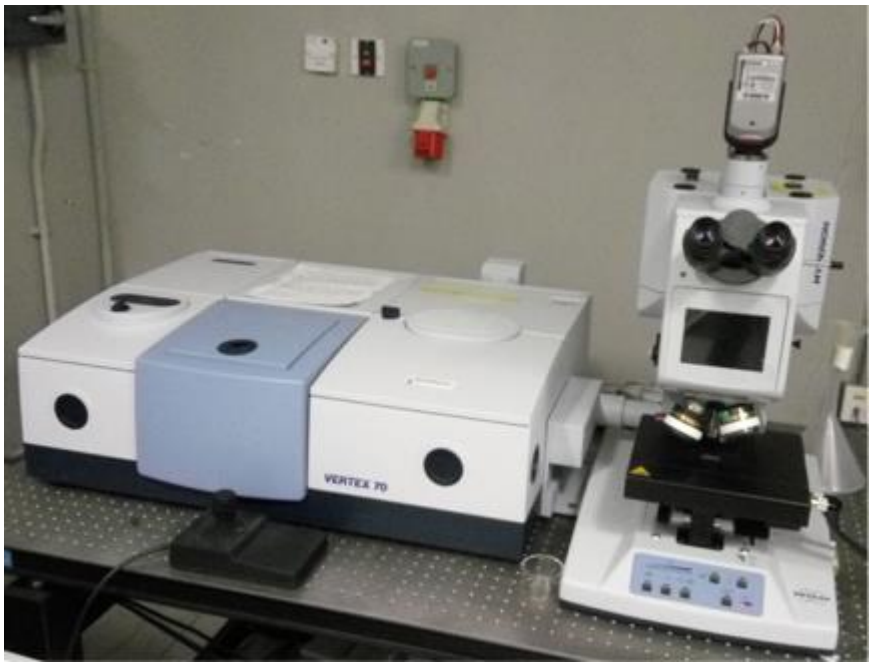

Figure 3.3 Mechanism of the ATR accessory (a) and photography of the Bruker Vertex-70 FTIR (b).

Attenuated total reflection (ATR) is a sampling technique used in conjunction with

the FTIR, which enables to directly examine the samples in the solid or liquid state without the need for further preparation. The ATR makes use of the evanescent wave of total internal reflection. More specifically, a beam of infrared light is passed through the ATR crystal in such a way that it reflects at least once off the internal surface in contact with the sample. This reflection forms the evanescent wave that extends into the sample, as shown in **Figure 3.3**(a). The penetration depth into the sample is typically between 0.5 and 2 μm, the exact value is determined by the wavelength of light, the angle of incidence and the indices of refraction of the ATR crystal and the medium to be probed [1].

In our work, Bruker Vertex-70 FTIR with ATR accessory as shown in **Figure 3.3**(b) was used to characterize the surface modification of PDMS slides.

3.2.4 Raman spectroscopy

Raman spectroscopy is another spectroscopy to identify and quantitatively analyze materials. It provides the molecular vibration information of materials. In the Raman spectroscopy, a monochromatic light (for example, laser) is irradiated on the sample and the scattered light is detected by the detector. If the frequency of most light is the same as that of the excitation light, this phenomenon is called Rayleigh or elastic scattering. However, the frequency of a small portion of the scattered light may be different from that of the excitation light as a result of the interaction between the incident electromagnetic waves and the molecular vibrations of the sample. Therefore, the band positions of Raman spectrum can be corresponded to the energy levels of the vibrations

of each functional group in the sample.

Compared with the FTIR spectrum, the Raman spectrum is sharper than their infrared spectrum. The more isolated bands of Raman spectrum make it more straightforward for quantitative analysis. Moreover, the bands of symmetric linkages, which are weak in FTIR spectrum, are relatively strong. In our work, the surface modification of the PDMS films were also characterized by the LabRAM HR 800 Raman Spectroscopy (**Figure 3.4**).

Figure 3.4 Photograph of the LabRAM HR 800 Raman Spectrometer.

3.2.5 Fluorescence microscopy

Fluorescence microscopy is a kind of optical microscopy to study the fluorescence characteristics of substances. In the fluorescence microscopy, the samples are irradiated by the light of a particular wavelength that is absorbed by the fluorophore groups of the samples, leading to the release of the light at a different wavelength (the fluorescence

light). Most fluorescence microscopes are epifluorescence microscopes, in which the excitation light and the much weaker emitted light both pass through the same objective and the excitation light should be separated by a specific filter. In our experiments, Olympus BX41 (**Figure 3.5**) was used to confirm the enzyme immobilization.

Figure 3.5 Photograph of the Olympus BX41 fluorescence microscope.

3.2.6 Ultra-high-performance liquid chromatography-electrospray ionization triple quadrupole mass spectrometer

Liquid chromatography (LC, Agilent 1290 UHPLC) is a physical separation process in which the components of a liquid mixture are distributed between two immiscible phases, a stationary phase and a mobile phase [2]. Typically, the mobile phase is a mixture of water and other polar solvents such as methanol, isopropanol, and acetonitrile. And the stationary phase is prepared by attaching some special groups (e.g., n-octadecyl, C18 or amino) to the irregularly or spherically silica particles and then embedding these silica

particles into a column. During the process, the sample of interest is injected into the mobile phase stream delivered by a high-pressure pump. The mobile phase containing the analytes permeates through the column in a definite direction. Then, depending on the chemical affinity to the mobile and stationary phase, the components in the sample would be separated and flowed out of the column at different times.

(a)

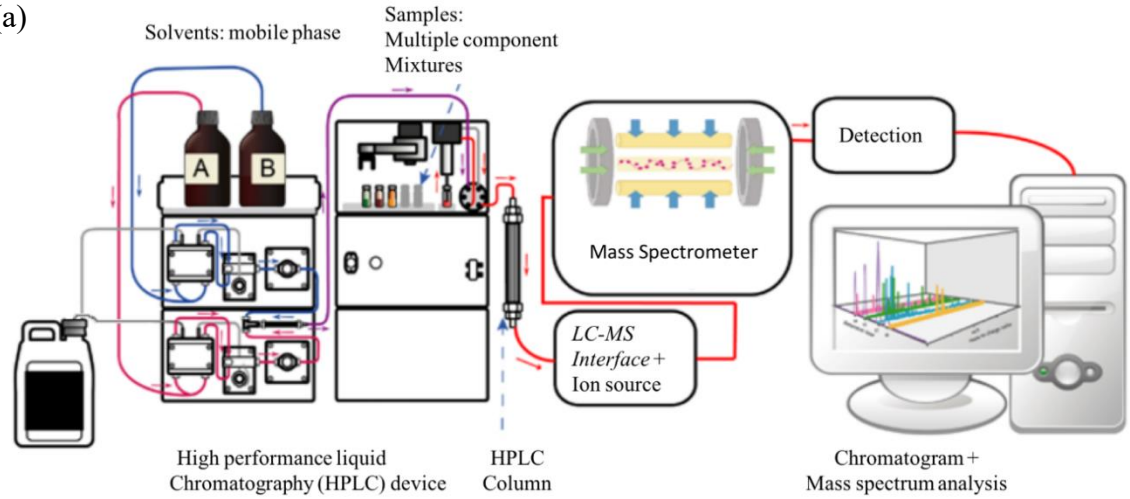

(b)

Figure 3.6 Diagram (a) and photography (b) of the LC-MS system.

Mass spectrometry (MS, Agilent 6460) is an analytical technique that measures the

mass-to-charge ratio (*m/z*) of charged particles (ions) [3]. It uses electric or magnetic fields to control the motion of ions produced from an analyte of interest and to determine the value of *m/z*. It consists of an ion source, a mass analyzer, a detector, and a vacuum system. When a sample is introduced into an MS system from the LC system, the neutral molecules of the sample would be converted and fragmented into gas-phase ions by electron beams, photon beams (UV lights), laser beams or corona discharge in the ion source. The gas-phase ions are then sent to a mass analyzer, which applies the electric and magnetic fields to sort the ions by their masses. The detector measures and amplifies the ion current to calculate the abundances of each mass-resolved ion and then sends the information to the data systems (MassHunter Quantitative Analysis software) to generate a mass spectrum.

The interface between the LC and MS systems is commonly electrospray ionization (ESI) [4]. The liquid eluate from the LC column is pumped through a metal capillary held at 3 to 5 kV. The liquid is nebulized at the tip of the capillary and forms a fine spray of charged droplets. The droplets are then evaporated in an atmosphere of dry nitrogen by the heat created by the electric potential. Later, the ionized analytes are transferred into the high vacuum chamber of the MS as the charged ions flow through a series of small apertures with the aid of focusing voltages. Positively and negatively charged ions can be detected by switching of the operation modes.

3.3 Determination of reaction time

The reaction time t_r is regarded as the residence time of the reaction mixture flowing through the microfluidic reactors, which is calculated by the equation of $t_r = V_r/Q$, where V_r is the volume of the microfluidic reactors and Q is the flow rate of the injected RuBP solution passing through the reactor controlled by the syringe pump.

3.4 Determination of protein concentration

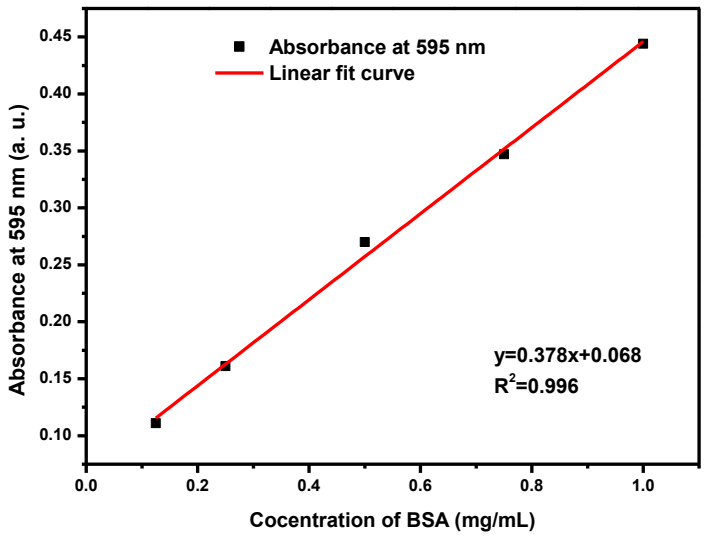

Figure 3.7 Calibration curve of protein amount determined from BSA solutions by the Bradford method.

The protein concentration was qualified by the Bradford method [5] using the Quick Start Bradford Protein Assay kit (Bio-Rad Pacific Limited.). Briefly, 20 μL of RuBisCO solution were diluted by 980 μL water. Then 1 mL 1x dye reagent, which was warmed to ambient temperature before the test, was added into the diluted RuBisCO solution with vortex. The mixture was incubated at room temperature for 5 min before measuring the

absorbance at 595 nm using a UV-Visible spectrometer (UV-2450, Shimadzu). The instrument was firstly zeroed with the blank samples, which were the 20-μL reaction buffer diluted by 980-μL water. BSA solutions (0.125-1 $mg \cdot mL^{-1}$) were selected as the standards to plot the calibration curve (**Figure 3.7**). The protein concentration of samples then can be determined by the absorbance at 595 nm using the calibration curve.

The protein loading amount of the reactor was calculated by

$$\text{protein loading amount } (\mu g \cdot cm^{-2}) = (C_0 V_i - C_1 V_w)/A_r \quad (3.4),$$

where C_0 is the protein concentration of the initially injected RuBisCO solution ($\mu g \cdot \mu L^{-1}$), C_1 is the protein concentration of the rinsed-out RuBisCO solution ($\mu g \cdot \mu L^{-1}$), V_i is the volume of initially injected RuBisCO solution (μL), V_w is the volume of washing solution collected from the outlet of the reactor (μL), and A_r is the surface area of the reactor. The maximum protein loading amount was then regarded as the protein loading capacity of the microfluidic reactor. The protein loading efficiency was also obtained by

$$\text{protein loading efficiency } (\%) = \left(C_0 V_i - C_1 V_w\right)/C_0 V_i \quad (3.5).$$

Then, the optimal RuBisCO concentration for further research can be determined by referring to the protein loading capacity and the protein loading efficiency. All the error bars represent the standard deviations of three repeated experiments.

3.5 Determination of RuBisCO activity

3.5.1 RuBisCO activity determination by NADH decreasing

In the past, the activity of RuBisCO was determined by the radioisotope assay based on $^{14}CO_2$ fixation into phosphoglycerate (acid-stable ^{14}C activity) [6]. This method gives a high sensitivity and a continuous measurement of the reaction. But it has the disadvantage of time-lag [7] and radioactivity constraints. The activity can also be determined using the first two phases reactions of Calvin cycle in the presence of 3-phosphoglycerate kinase (PGK), adenosine triphosphate (ATP), glyceraldehyde-3-phosphate dehydrogenase (GAPDH), and reduced form of nicotinamide adenine dinucleotide (NADH) by following the rate of NADH oxidation spectrophotometrically. 3-PGA was generated from RuBP and then transferred to G3P by two enzymatic reactions as shown in **Figure 3.8**.

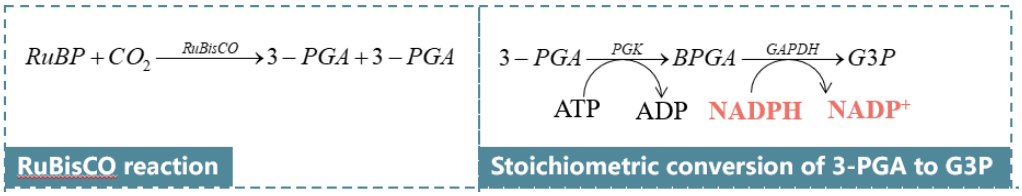

Figure 3.8 Principle of the stoichiometric determination of 3-PGA by the spectrophotometer.

The final assay mixture contained 625 μg of RuBisCO, 5 units of GAPDH, 10 units of PGK, 250 nmol of NADH, 375 nmol of RuBP, and 750 nmol of ATP in a volume of 750 μL of reaction buffer (pH 7.8) containing 0.1 M Tris-HCl, 5 mM $MgCl_2$, 66 mM $KHCO_3$, and 5 mM DTT. The assay was then allowed to react for 20 minutes at room

temperature with the absorbance being measured at 10 second intervals. The change in absorbance at 340 nm due to the oxidation of NADH was monitored using the UV-Vis spectrophotometer. The 3-PGA production was calculated using the extinction coefficient of 6220 $M^{-1} \cdot cm^{-1}$ for NADH concentration. The concentration of NADH was calculated by:

$$c = A/(e \cdot b) \tag{3.6}$$

where c is the concentration of the solution, A is the absorbance of the absorption peak, e is the extinction coefficient of the solution and b is the length of the optical path. Accordingly, the decreasing amount of NADH would reflect the produced amount of 3-PGA. As show in **Figure 3.9** (b), about 40 nmol of 3-PGA was produced from RuBP and CO_2 in 20 mins.

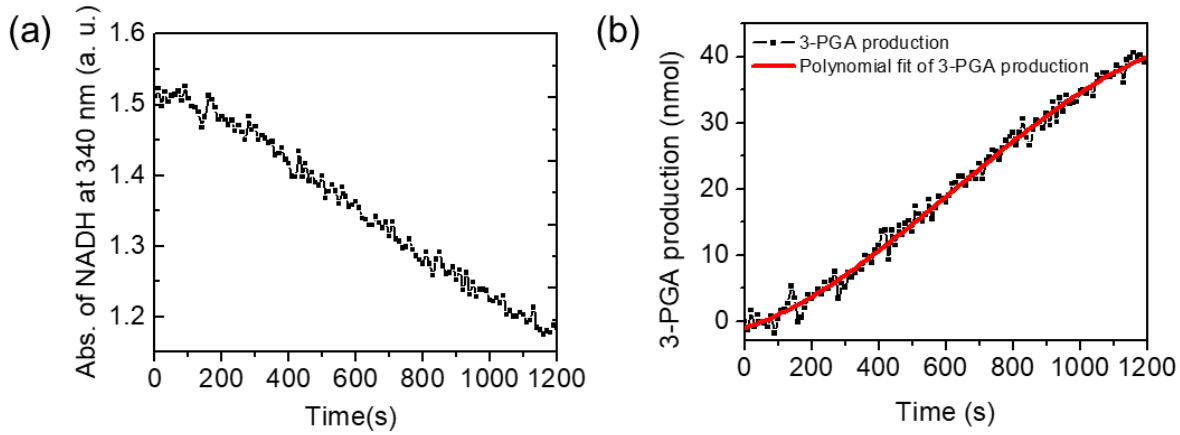

Figure 3.9 (a) UV-Vis spectral absorbance of NADH over time during the reaction; (b) 3-PGA production and polynomial fit of the produced 3-PGA.

3.5.2 RuBisCO activity determination by NADH decreasing with amplification method

The spectrophotometric assay using the NADH oxidation is usually very slow, insensitive and time consuming. It is noticed that the production amount of 3-PGA is very small under current experimental conditions. When the immobilized amount of RuBisCO is very small, the decreasing signal in absorbance may be weak, making it difficult to measure the produced amount of 3-PGA in the microfluidic reactor (see **Figure 3.10**).

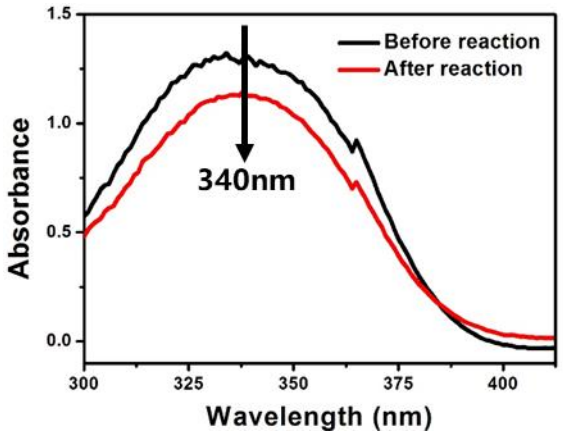

Figure 3.10 Decrease of the NADH absorbance at 340 nm after the assay mixture except for RuBisCO is flowed through the RuBisCO-immobilized microreactor.

Therefore, a rapid and sensitive non-radioactive assay was adopted here for the RuBisCO activity assay with the amplified NADH decreasing signal. **Figure 3.11** depicts the principle of the amplification signal assay. During the reaction, the product 3-PGA was first converted into dihydroxyacetone-phosphate (DAP) with PGK, GAPDH, ATP and NADH. Catalase was also added here to prevent the inhibition of GAPDH. Then DAP was transformed into the cycle of mutual conversion with glycerol-3 phosphate (G3P). It can be monitored as the cumulative oxidation of NADH, whose amount is much larger

than the original amount of 3-PGA, therefore providing strong amplification of signal for 3-PGA monitoring (**Figure 3.12** (a)). The signal of production solutions can be linked to the specific amount of 3-PGA by using a standard curve that is generated by adding different amounts of standard 3-PGA to the assay mixture as shown in **Figure 3.12** (b). Therefore, the RuBisCO activity can be determined by the produced 3-PGA amount.

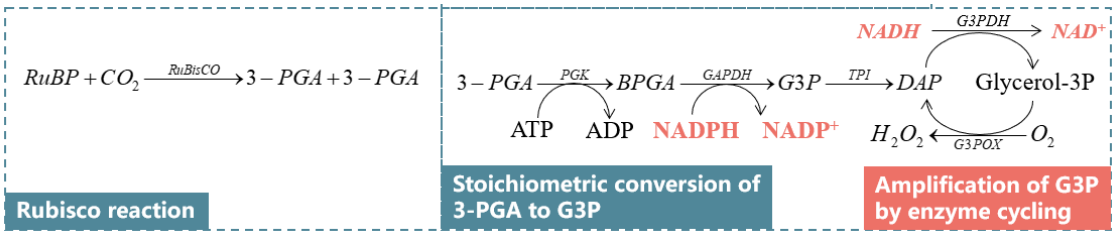

Figure 3.11 Principle of the amplification signal assay for RuBisCO activity.

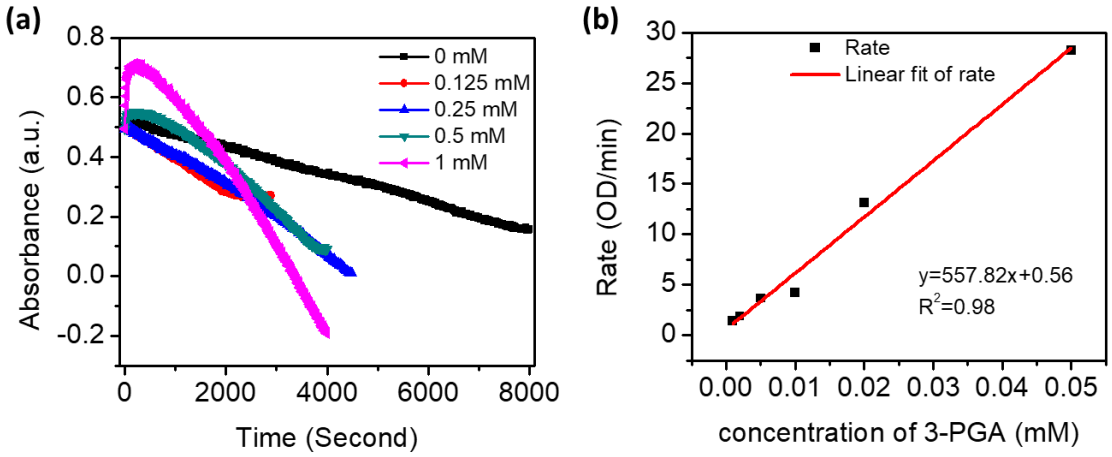

Figure 3.12 Calibration for the determination of 3-PGA amount by UV-Vis spectrophotometer. (a) The absorbance decreasing at 340 nm at different concentrations of 3-PGA. (b) Calibration curve for the 3-PGA determination by the decreasing rate of absorbance at 340 nm.

For the free RuBisCO activity assay, RuBisCO was incubated with RuBP in the reaction buffer for 1 min before the reaction was stopped by using the same volume of

80% ethanol. The production solution I (RuBisCO, RuBP, HCO_3^-, products and ethanol) was kept for further assay. The amount of RuBisCO used here was the same as that was immobilized into the microfluidic reactors. And in the immobilized RuBisCO activity assay, RuBP in the reaction buffer was passed through the microfluidic reactors and the production solution II (RuBisCO, RuBP, HCO_3^- and 3-PGA) was collected from the outlet of the reactors for further assay. 20 μL of the production solutions (production solution I for free RuBisCO assay and production solution II for the immobilized RuBisCO assay) were added with 80 μL of assay mixture (final concentrations were 5 unit·mL^{-1} PGK, 0.5 unit·mL^{-1} GAPDH, 0.5 unit·mL^{-1} TPI, 0.5 unit·mL^{-1} G3PDH, 1 unit·mL^{-1} G3POX, 1000 unit·mL^{-1} catalase, 0.5 mM ATP, 1 mM NADH, 1.5 mM $MgCl_2$ and 100 mM Tricine/KOH pH 8.0). The reaction was immediately and continuously monitored by measuring absorbance change at 340 nm by the UV-Visible spectrometer.

3.5.3 RuBisCO activity determination by HPLC-MS/MS

The monitoring of the reaction was also performed using a liquid chromatography-tandem mass spectrometer (LC-MS/MS) system consisting of an Agilent 1290 Infinity LC and 6460 Electrospray Ionization Triple Quadrupole Mass Spectrometer (Agilent Technologies, Palo Alto, CA, USA) to check the RuBP and 3-PGA ingredients. LC-MS/MS was only applied in the enzyme immobilized experiments. A Luna NH_2 column (Phenomenex, 2mm×250mm, 5μm) was used for the chromatography separation. The mobile phases consisted of (A) water: acetonitrile (ACN) (95:5, v/v, pH 9.45) with

addition of 20 mM ammonium acetate and 20 mM ammonium hydroxide in H_2O, (B) ACN. The LC separation was carried out at 35°C with a linear gradient elution condition at a flow rate of 0.3 mL/min with an injection volume of 10 μL. The LC conditions are as follows: gradient elution was varied from 85 to 0% ACN in 15 min (held for 23 min), then went back to 85% ACN in 2 minutes and held for 10 min until the column reached equilibrium.

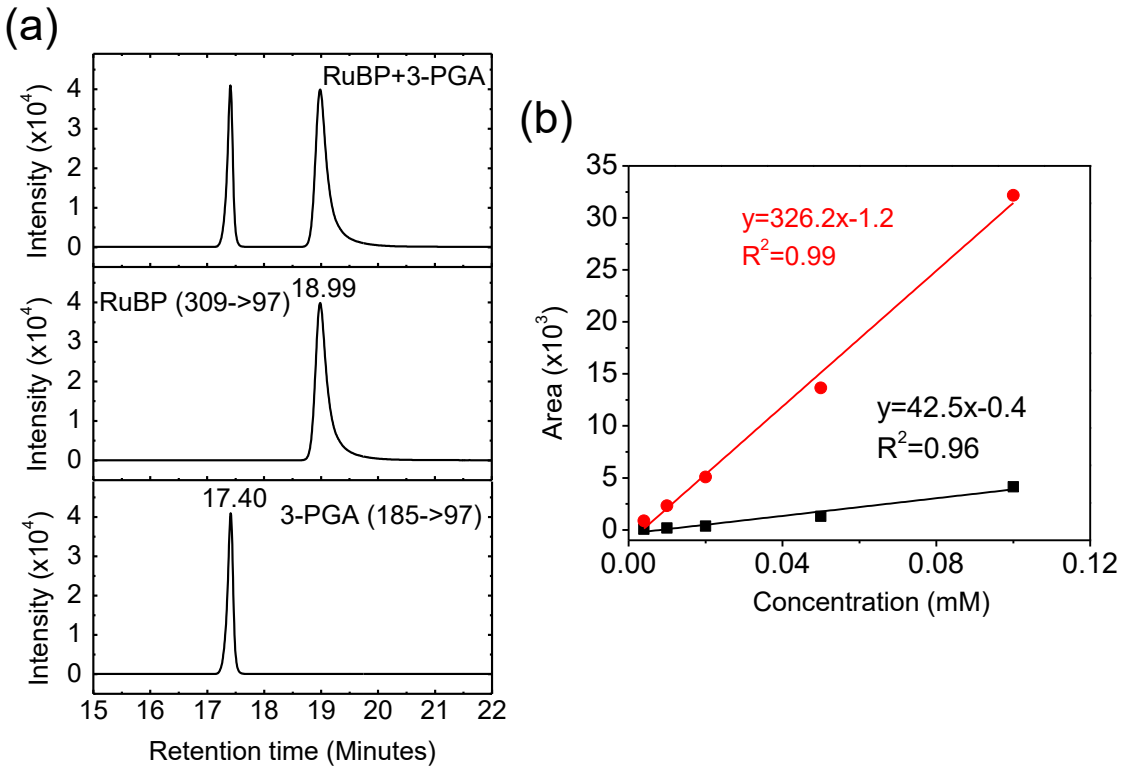

Figure 3.13 Calibration for the determination of 3-PGA amount by HPLC-MS/MS. (a) HPLC-MS/MS chromatography of the standard RuBP and 3-PGA. (b) Calibration curves of the RuBP (red circle) and 3-PGA (black square) signals by the areas of the peaks.

The MS/MS system was equipped with the electrospray ionization source operated under the negative mode. The multi-reaction monitoring (MRM) was used in the MS

detection with the transition (309→97) and (185→97) for RuBP and 3-PGA, respectively. The retention times of standard RuBP and 3-PGA were observed at 18.99 min and 17.40 min, respectively (**Figure 3.13** (a)). As seen from **Figure 3.13 (b)**, the area of the peak has a linear relationship with the concentration for both RuBP and 3-PGA. Therefore, the peak area can be used to determine the concentration of produced 3-PGA. However, it was found that the 3-PGA production amount by the microreactor was usually too small to detect. In the following experiments, the HPLC-MS/MS method would only be used to determine the exist of produced 3-PGA.

3.6 Summary

This chapter has discussed the common materials, the typical instruments and the standard measurement procedures, which are key to the fabrication and characterization of the three types of RuBisCO-immobilized microfluidic reactors to be presented in the next three chapters.

3.7 References

[1] F. Mirabella, "Principles, Theory, and Practice of Internal Reflection Spectroscopy," *Internal Reflection Spectroscopy: Theory and Applications,* pp. 17-52, 1993.

[2] C. Dass, *Fundamentals of Contemporary Mass Spectrometry* vol. 16: John Wiley & Sons, 2007.

[3] J. J. Pitt, "Principles and Applications of Liquid Chromatography-Mass Spectrometry in Clinical Biochemistry," *The Clinical Biochemist Reviews,* vol. 30, p. 19, 2009.

[4] J. B. Fenn, M. Mann, C. K. Meng, S. F. Wong, and C. M. Whitehouse, "Electrospray Ionization for Mass Spectrometry of Large Biomolecules," *Science,* vol. 246, pp. 64-71, 1989.

[5] M. M. Bradford, "A Rapid and Sensitive Method for the Quantitation of Microgram Quantities of Protein Utilizing the Principle of Protein-Dye Binding," *Analytical Biochemistry,* vol. 72, pp. 248-254, 1976.

[6] M. Wishnick and M. D. Lane, "Ribulose Diphosphate Carboxylase from Spinach Leaves," in *Methods in Enzymology*. vol. 23, ed: Elsevier, 1971, pp. 570-577.

[7] L. E. Anderson and R. Fuller, "Photosynthesis in Rhodospirillum Rubrum Iv. Isolation and Characterization of Ribulose 1, 5-Diphosphate Carboxylase," *Journal of Biological Chemistry,* vol. 244, pp. 3105-3109, 1969.

CHAPTER 4
PDMS MICROFLUIDIC REACTORS FOR 3-PGA PRODUCTION

This chapter will present the first and the simplest design of microfluidic reactor for the enzymatic generation of 3-PGA. Here the enzyme RuBisCO is immobilized onto the PDMS surface by the physical adsorption.

4.1 Brief

The polymer materials that have been developed for microfluidic reactors include polymethylmethacrylate (PMMA), polystyrene (PS), polycarbonate (PC), and polydimethylsiloxane (PDMS). Here, PDMS is chosen as our fabrication material due to the advantages of easy fabrication, optical transparency, biocompatibility, and favorable thermal and electrical properties. These are very important characteristics for developing microfluidic devices in biological applications [1]. One of the most notable features of PDMS is its hydrophobicity (contact angle <110^{o}) and porosity, allowing non-specific adsorption of various molecules [2]. Physical adsorption is a mild method for enzyme immobilization on supports as compared to chemical immobilization. Compared with the hydrophilic materials, hydrophobic materials can immobilize a large amount of enzyme due to the hydrophobic interaction [3-5]. The immobilized enzyme on hydrophobic materials also presents higher activity and excellent activity retention [6, 7]. PDMS can

also exhibit hydrophilicity as long as some special strategies are applied, such as plasma treatment, UV oxidation, chemical modification and dynamic coating [8, 9]. The plasma treatment is the most commonly used method for hydrophilic improvement without introducing additional chemical bonds [10-12]. In this chapter, the pristine PDMS and plasma-treated PDMS are both used to fabricate the PDMS-based microfluidic reactors (PMRs) to immobilize RuBisCO. Their performances are compared in term of the protein loading capacity and the 3-PGA production.

Generally, the PMRs consist of a molded layer with a microchannel pattern and a flat layer which is bonded to the molded layer. The most commonly used method to fabricate microfluidic reactor using PDMS is the soft-photolithography, which includes design of microfluidic channels (mask design), fabrication of microfluidic mold by photolithography, molding of microfluidic chips and bonding of microfluidic chip [13]. RuBisCO is then immobilized onto the inner surface of the pristine and plasma-treated PMRs. Optimal conditions are investigated in terms of RuBisCO concentration, immobilization flow rate and immobilization time for the RuBisCO-immobilized PDMS-based microfluidic reactors (RI-PMRs) fabrication. The feasibility and reusability are also tested to check the performance of RI-PMRs under optimal conditions.

4.2 Experimental methods

4.2.1 Fabrication of PMRs

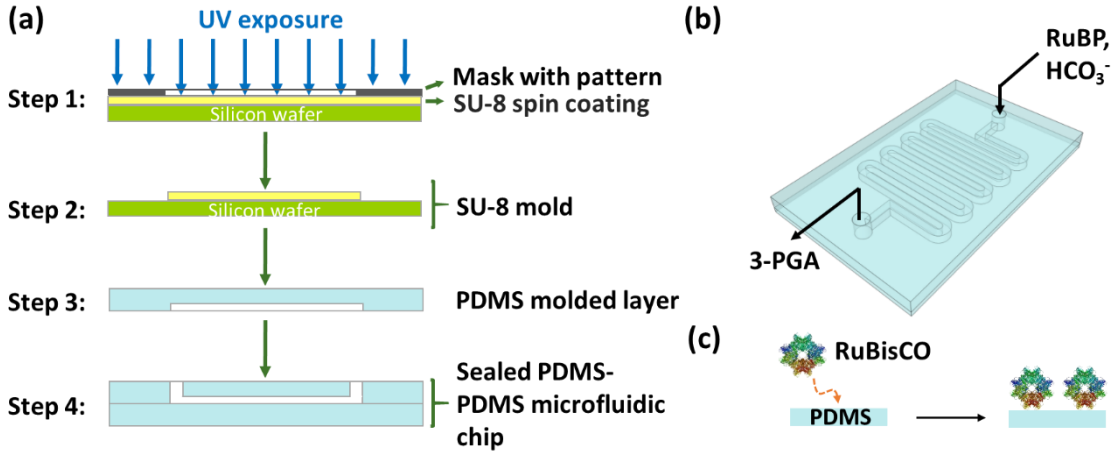

Figure 4.1 Schematics for the fabrication of RI-PMRs. (a) Process flow of the fabrication of the PMRs using soft lithography. (b) Three-dimensional diagram of the RI-PMRs. (c) Illustration of the procedures for RuBisCO immobilization by physical adsorption.

The PMRs were fabricated by sealing one molded PDMS layer against another flat PDMS layer on top. The molded layer was made by using the standard soft-lithography technique (**Figure 4.1** (a)) [14] using the Sylgard 184 elastomer kit (Dow Corning Corporation) and SU-8 mold (SU-8 50, MicroChem Crop.). Briefly, a 4'' silicon wafer was first cleaned by acetone, ethanol and deionized water (DIW), followed by drying in an oven to remove any contamination. Then, the SU-8 was spin-coated to a thickness of 40 μm (at 500 rpm for 15 s followed by 2500 rpm for 60 s) on the cleaned wafer and then soft-baked at 65 ^{o}C for 5 min and another baking step at 95 ^{o}C for 15 min. The soft-baked SU-8 was then exposed to UV light for 45 s (with exposure energy of 180 mJ/cm^2), followed by a post-

baking process at 65 ºC for 5 min and at 95 ºC for 15 min. Afterward, the SU-8 was developed in SU-8 developer for 3 min and then washed with isopropyl alcohol (IPA) for 10 seconds, followed by air dry using compressed nitrogen. Finally, the mold was hard-baked at 150 ºC for 5 min. The SU-8 mold was ready for further use. Next, the PDMS compound that is formed by mixing PDMS and its curing agent at a weight ratio of 10:1 was poured into the SU-8 mold and put on a hot plate at 80 ºC for 30 min.

Two methods were applied to seal the PMRs with two types of inner surfaces, the hydrophilic and the hydrophobic. The hydrophilic microfluidic reactors were made by the traditional plasma bonding method. Oxygen plasma (PVA TePla America - IoN Radical Plasma Cleaner, 50 W) was used to treat the cured molded PDMS slice and another flat PDMS slice for 5 min, which were then immediately bonded together. The reactors with hydrophobic inner surfaces were fabricated by direct bonding. The cured molded PDMS was directly placed onto another half-cured flat PDMS layer (7 min baking) and then baked for another 30 min. The two layers were finally bonded with each other after the curing.

4.2.2 Immobilization of RuBisCO

RuBisCO in the reaction buffer were injected into PRMs at the flow rate of 2.5 μL·min^{-1} for a specific time. Then, 100 μL reaction buffer was used to rinse the microreactors at the same flow rate. The RI-PMRs were ready for use as the diagram shown in **Figure 4.1** (b). RuBisCO was immobilized on the PDMS surface by physical adsorption (see **Figure**

4.1 (c)).The rinsed-out RuBisCO solutions were carefully collected to determine the protein loading amount by calculating the protein concentration difference between the initially injected and the rinsed-out RuBisCO solutions as discussed in chapter 3.

4.2.3 Comparison between pristine and plasma-treated PMRs for RuBisCO immobilization

RuBisCO in the reaction buffer (1 $\mu g \cdot \mu L^{-1}$) were injected into the pristine and plasma-treated PMRs for 4 hours. The two types PMRs before and after RuBisCO immobilization were characterized by the SEM and the standard Contact Angle Goniometer (Model 200, Ramé-Hart Instrument Co.) to confirm the enzyme immobilization and to compare the protein loading abilities. The RuBisCO activities which is regarded as the production rate of 3-PGA ($nmol \cdot min^{-1}$) of the two types of RI-PMRs were also examined.

4.2.4 Optimal condition investigation

Increased concentrations of RuBisCO in the reaction buffer (0.5 $\mu g \cdot \mu L^{-1}$ to 4 $\mu g \cdot \mu L^{-1}$) were injected into the PMRs at the flow rate of 2.5 $\mu L \cdot min^{-1}$ for different immobilization times (2h, 3h, and 4h). The protein loading efficiencies were recorded to find the optimal fabrication condition. The RuBisCO activities of RI-PMRs fabricated in different conditions were also studied at the same time.

4.2.5 Feasibility of 3-PGA generation with RI-PMRs

The feasibility of producing 3-PGA with RI-PMRs was tested by injecting 0.5 mM RuBP

in the reaction buffer into the as-prepared RI-PMRs using a syringe pump at different flow rates (from 7 μL·min^{-1} to 0.35 μL·min^{-1}). The production solution II was collected from the outlet for the determination of the 3-PGA amount (nmol) by the amplification signal assay.

4.2.6 Reusability of RI-PMRs for 3-PGA production

The reusability of the RI-PMRs meant the capability of the RI-PMRs being used repeatedly. It was evaluated by conducting the 3-PGA production reaction with one reactor for several cycles of reuse. Here, one cycle of reuse refers to the test that 21 μL of reactant mixture solution was flowed through the RI-PMRs for the 3-PGA production. RuBisCO activity was measured from the collected production solution II for each cycle of reuse. The relative RuBisCO activities were calculated as a percentage of the initial RuBisCO activity in the first cycle.

4.3 Results and discussions

4.3.1 Comparison between pristine and plasma-treated PMRs for RuBisCO immobilization

Surface characterization was first conducted to check the difference between the pristine and plasma-treated PMRs for RuBisCO immobilization. As shown by the water contact angle results in **Figure 4.2**, the pristine PDMS is highly hydrophobic (water contact angle is 103.8 º ± 1.1 º) and the plasma treatment changes it to super hydrophilic PDMS (water

contact angle is 4.0 º ± 0.6 º).

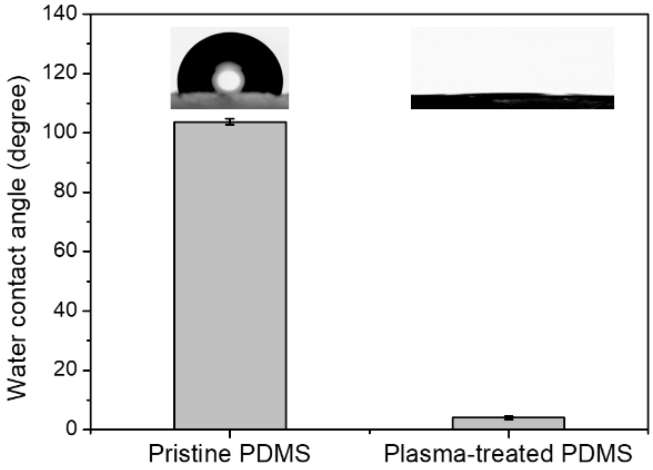

Figure 4.2 Water contact angle measurement of pristine/plasma-treated PDMS surfaces. All data are presented as mean ± s.d. (n = 3).

As shown by the SEM images of PDMS surface before the RuBisCO immobilization, the inner surfaces of both the pristine PMRs (**Figure 4.3** (a)) and plasma-treated PMRs (**Figure 4.3** (c)) are smooth and flat. It is noticed that some cracks are found on the plasma-treated PDMS, which may be due to the prolonged plasma treatment. After the RuBisCO immobilization, some RuBisCO particles are observed from the two surfaces (**Figure 4.3** (b) and (d)). Notably, much denser RuBisCO particles are immobilized on the pristine PDMS surface than on the plasma-treated PDMS surface, which proves a much stronger adsorption of RuBisCO on the hydrophobic surface than that on the hydrophilic surface.

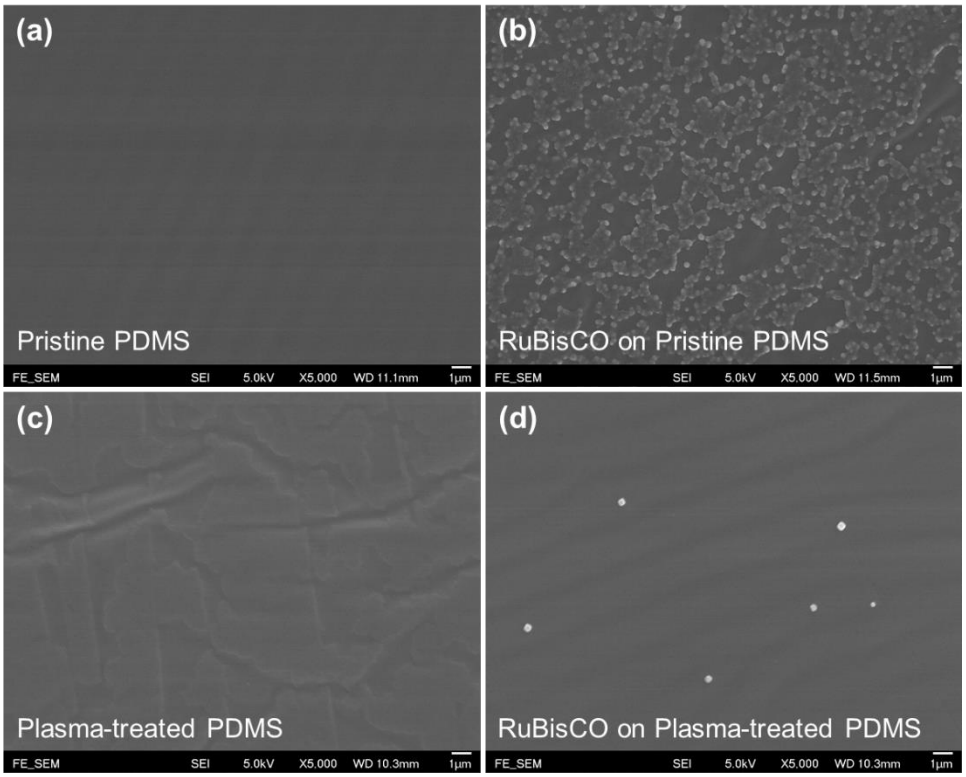

Figure 4.3 SEM images of the surfaces of (a) pristine PDMS, (b) RuBisCO-immobilized pristine PDMS, (c) plasma-treated PDMS and (d) RuBisCO-immobilized plasma-treated PDMS.

Figure 4.4 also shows that the hydrophobic PDMS has a higher protein loading efficiency (~ 23.4%) than the hydrophilic PDMS has (~ 8.6%). The immobilized RuBisCO activity on the hydrophobic PDMS (0.037 nmol·min^{-1}) is 3 folds of that on the hydrophilic PDMS (0.012 nmol·min^{-1}). It has been reported that enzymes in aqueous solutions are more likely to be adsorbed on the hydrophobic surfaces [15]. The interaction forces between enzyme and PDMS are mainly physical forces including van der Waals electrostatic interactions, hydrophobic interactions, Coulombic forces, hydrogen bonds and so on [4, 16]. The experimental results here are consistent with the findings of the

previous research that the hydrophobicity plays a very important role in enzyme immobilization and the hydrophobic interaction would increase the amount of enzyme immobilization [6]. Therefore, in the following experiments, the pristine PDMS (hydrophobic PDMS) was used for the RI-PMRs fabrication.

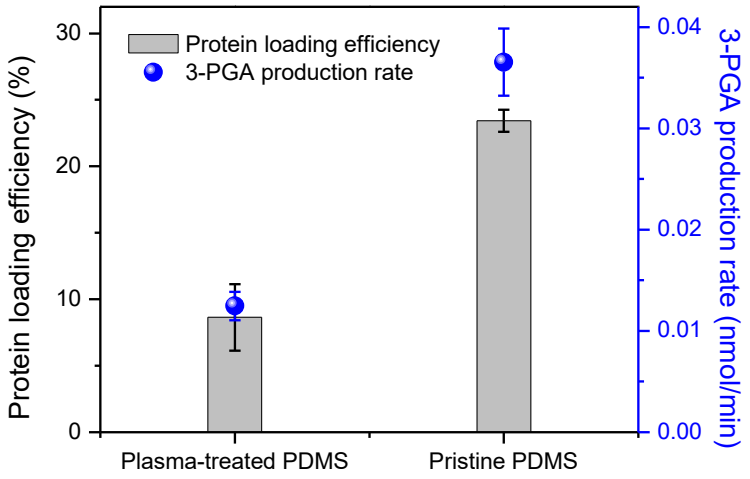

Figure 4.4 Comparisons of the protein loading efficiency and the RuBisCO activity between the pristine and plasma-treated PDMS microfluidic reactors. RuBisCO concentration is 1 $\mu g \cdot \mu L^{-1}$ with the immobilization time of 4 h. 0.5 mM RuBP is injected at the flow rate of 7 $\mu L \cdot min^{-1}$.

4.3.2 Optimal condition investigation for RI-PMRs fabrication

When 1 $\mu g \cdot \mu L^{-1}$ of RuBisCO solution was injected into the PMRs at 2.5 $\mu L \cdot min^{-1}$ for an increased time (from 2 h to 4 h), the protein loading efficiency of PMRs was increased by 5.7 folds (from 4.10% to 23.43%) (**Figure 4.5**). The immobilized RuBisCO activity also increased from 0.019 $nmol \cdot min^{-1}$ to 0.037 $nmol \cdot min^{-1}$ with longer immobilization time. Generally, longer immobilization time results in a larger amount of RuBisCO immobilized onto the PMRs inner surface, therefore ensuring a higher RuBisCO activity

and a larger 3-PGA production.

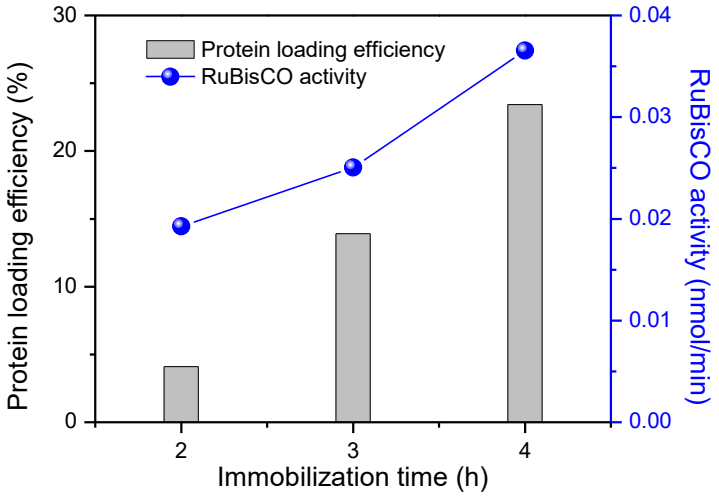

Figure 4.5 Protein loading efficiencies and RuBisCO activities as a function of the immobilization time. RuBisCO concentration is 1 $\mu g \cdot \mu L^{-1}$. 0.5 mM RuBP is injected at the flow rate of 7 $\mu L \cdot min^{-1}$.

When the immobilization time was set as 4 h, an increase of RuBisCO concentration would result in a larger amount of immobilized RuBisCO. However, the protein loading efficiency decreased with the increase of RuBisCO concentration (black squares in **Figure 4.6**). It is because of that the PMRs had a fixed space for the RuBisCO immobilization and the immobilized RuBisCO amount reached saturation as the amount of RuBisCO went up to 4 $\mu g \cdot \mu L^{-1}$. At the same time, the RuBisCO activity was also increased with the higher RuBisCO concentration. But it tended to decrease if the RuBisCO concentration went higher than 2 $\mu g \cdot \mu L^{-1}$. The largest RuBisCO activity appeared at the RuBisCO concentration of 2 $\mu g \cdot \mu L^{-1}$. Since RuBisCO was immobilized on the PDMS surface by the physical adsorption, when one layer of RuBisCO was

deposited on the PDMS surface, additional RuBisCO would aggregate into multiple layers. The active sites of RuBisCO may be covered by the additional layers and the supports, leading to the steric hinderance. The additional RuBisCO may also be rinsed out when the reactant ran through the reactor. Therefore, 2 $\mu g \cdot \mu L^{-1}$ was chosen as the optimal RuBisCO concentration for the following RI-PMRs experiments in order to maximize the protein loading efficiency and the RuBisCO activity at the same time.

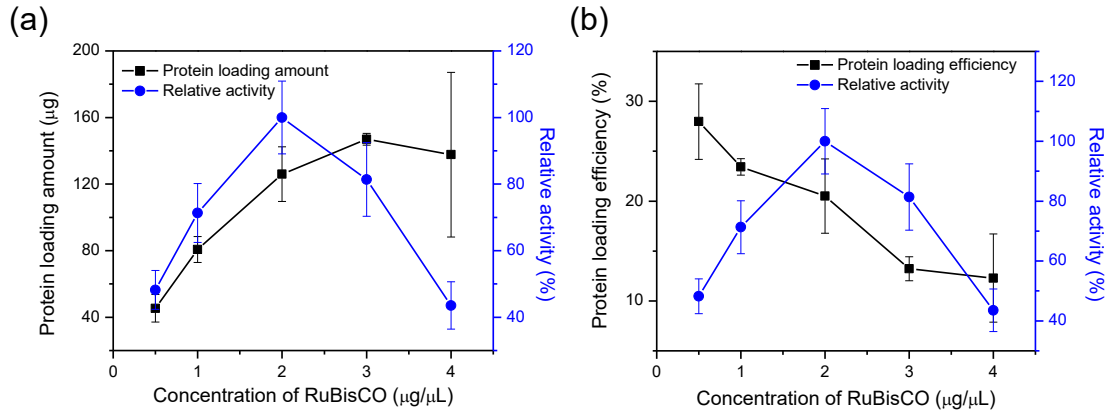

Figure 4.6 Protein loading amount (a) and loading efficiencies (c) and RuBisCO activities as a function of the concentration of injected RuBisCO. The immobilization time is 4 h. 0.5 mM RuBP is injected at the flow rate of 7 $\mu L \cdot min^{-1}$.

4.3.3 Feasibility of RI-PMRs for 3-PGA production

After the optimal conditions (2 $\mu g \cdot \mu L^{-1}$ of RuBisCO solution injected at 2.5 $\mu L \cdot min^{-1}$ for 4 h) were found out, they were used to produce 3-PGA from RuBP and CO_2 for the feasibility tests for different reaction times. The RI-PMRs demonstrated the production of 3-PGA at 0.0111 ± 0.0003 $nmol \cdot min^{-1}$ when the reaction time was less than 10 min (**Figure 4.7**). Noteworthy, the 3-PGA amount produced at 20 min was only a little larger

than that at 10 min. The production rate decreased after 10 min reaction. The continuously increased reaction time (more than 10 min) caused the feedback inhibition of the production (3-PGA) to the reactant (RuBP) and RuBisCO, leading to the decreased production rate. It was well proved that 3-PGA was synthesized successfully from the RI-PMRs by implementing the light-independent reactions pathway. Moreover, the manipulation of the reaction time can be achieved straightforwardly by controlling the flow rate of the reactant mixture. In addition, the production could be easily separated from the reactant by pumping out from the reactor to avoid the feedback inhibition [17].

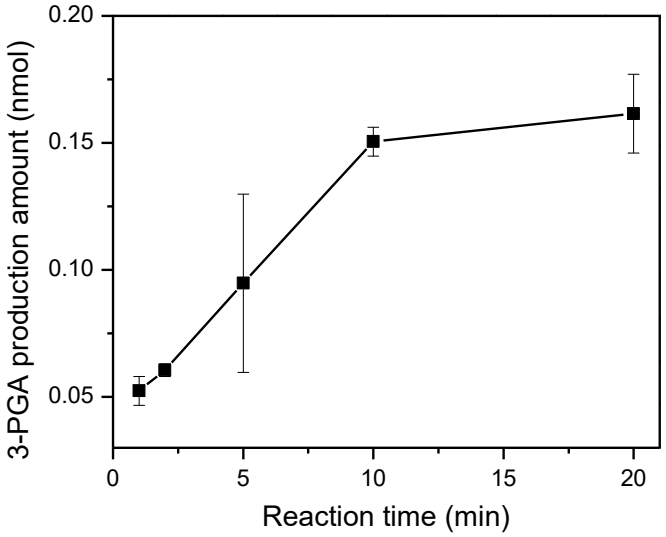

Figure 4.7 Feasibility of RI-PMRs: 3-PGA production amount as a function of the reaction time. The error bars represent the standard deviations of three repeated experiments. RuBisCO concentration is 2 $\mu g \cdot \mu L^{-1}$ with the immobilization time of 4 h.

4.3.4 Reusability of RI-PMRs for 3-PGA production

Excellent reusability of enzyme is essential for industrial applications. As shown in **Figure 4.8**, only 20.3% of initial activity was maintained after five cycles of reuse when

the reaction time was 1 min (flow rate 7 μL·min^{-1}). The enzyme deactivation after the repeated uses and the enzyme detachment owing to the flush of the reactant mixture were responsible for the activity loss [18]. In this case, the physical adsorption was not strong enough to attach the enzyme during flushing. Hence, a stronger enzyme immobilization method should be developed for the RuBisCO immobilization. On the other hand, the product collection and enzyme recycle are quite facile in the RI-PMRs by simultaneously pumping out the production solution and injecting new reactant mixture. Since the bulk reaction generally needs complicated techniques, enzyme immobilization in the microfluidic reactors is favorable.

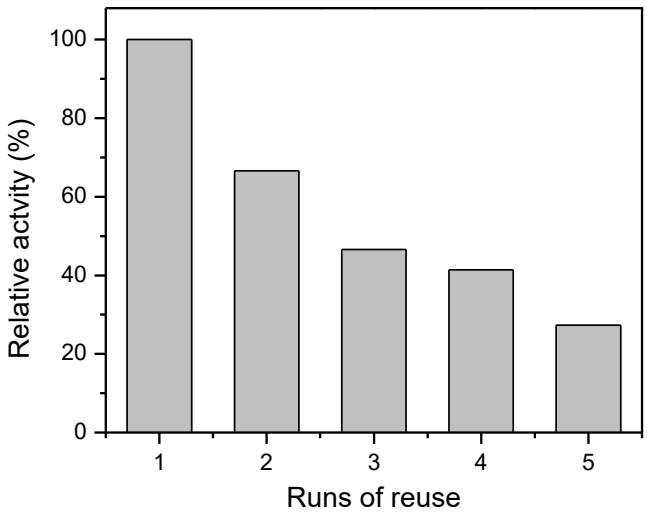

Figure 4.8 Reusability of the RI-PMRs. RuBisCO concentration is 2 μg·μL^{-1} with the immobilization time of 4 h. 0.5 mM RuBP is injected at the flow rate of 7 μL·min^{-1}.

4.4 Summary

In this chapter, RuBisCO has been immobilized into two types of PMRs, the pristine (hydrophobic) and the plasma-treated (hydrophilic). The hydrophobic PMRs showed a

higher protein loading capacity and a larger activity retention compared with the hydrophilic PMRs. Optimal RuBisCO concentration of 2 $\mu g \cdot \mu L^{-1}$ was found to maximize the protein loading efficiency and the RuBisCO activity. The RI-PMRs presented a great feasibility in 3-PGA production but a weak reusability. In conclusion, the glucose precursor production by the RuBisCO-immobilized microfluidic reactors are promising to relieve the food crisis. The future research should be focused on developing stronger enzyme immobilization methods to increase the amount and activity of immobilized RuBisCO, and to eventually enhance the amount of glucose precursor production.

4.5 References

[1] K. F. Lei, "Materials and Fabrication Techniques for Nano-and Microfluidic Devices," in *Microfluidics in Detection Science*, ed, 2014, pp. 1-28.

[2] K. Y. Chumbimuni-Torres, R. E. Coronado, A. M. Mfuh, C. Castro-Guerrero, M. F. Silva, G. R. Negrete*, et al.*, "Adsorption of Proteins to Thin-Films of Pdms and Its Effect on the Adhesion of Human Endothelial Cells," *RSC Advances,* vol. 1, pp. 706-714, 2011.

[3] S. H. Lee and E. Ruckenstein, "Adsorption of Proteins onto Polymeric Surfaces of Different Hydrophilicities—a Case Study with Bovine Serum Albumin," *Journal of Colloid and Interface Science,* vol. 125, pp. 365-379, 1988.

[4] S. Cao and B. Liu, "The Preparation and Enzyme Immobilization of Hydrophobic Polysiloxane Supports," *Macromolecular Bioscience,* vol. 9, pp. 361-368, 2009.

[5] K. D. Caldwell, R. Axén, M. B. Wall, and J. Porath, "Immobilization of Enzymes Based on Hydrophobic Interaction. I. Preparation and Properties of a Β - Amylase Adsorbate," *Biotechnology and Bioengineering,* vol. 18, pp. 1573-1588, 1976.

[6] T. Klotzbach, M. Watt, Y. Ansari, and S. D. Minteer, "Effects of Hydrophobic Modification of Chitosan and Nafion on Transport Properties, Ion-Exchange Capacities, and Enzyme Immobilization," *Journal of Membrane Science,* vol. 282, pp. 276-283, 2006.

[7] P. Kosaka, Y. Kawano, O. El Seoud, and D. Petri, "Catalytic Activity of Lipase Immobilized onto Ultrathin Films of Cellulose Esters," *Langmuir,* vol. 23, pp. 12167-12173, 2007.

[8] J. Zhou, A. V. Ellis, and N. H. Voelcker, "Recent Developments in Pdms Surface Modification for Microfluidic Devices," *Electrophoresis,* vol. 31, pp. 2-16, 2010.

[9] X. Yu, J. Xiao, and F. Dang, "Surface Modification of Poly (Dimethylsiloxane) Using Ionic Complementary Peptides to Minimize Nonspecific Protein Adsorption," *Langmuir,* vol. 31, pp. 5891-5898, 2015.

[10] X. Ren, M. Bachman, C. Sims, G. Li, and N. Allbritton, "Electroosmotic Properties of Microfluidic Channels Composed of Poly (Dimethylsiloxane)," *Journal of Chromatography B: Biomedical Sciences and Applications,* vol. 762, pp. 117-125, 2001.

[11] J. A. Vickers, M. M. Caulum, and C. S. Henry, "Generation of Hydrophilic Poly (Dimethylsiloxane) for High-Performance Microchip Electrophoresis,"

Analytical Chemistry, vol. 78, pp. 7446-7452, 2006.

[12] B. Larson, S. Gillmor, J. Braun, L. Cruz-Barba, D. Savage, F. Denes, *et al.*, "Long-Term Reduction in Poly (Dimethylsiloxane) Surface Hydrophobicity Via Cold-Plasma Treatments," *Langmuir,* vol. 29, pp. 12990-12996, 2013.

[13] Y. Xia and G. M. Whitesides, "Soft Lithography," *Annual Review of Materials Science,* vol. 28, pp. 153-184, 1998.

[14] D. C. Duffy, J. C. McDonald, O. J. Schueller, and G. M. Whitesides, "Rapid Prototyping of Microfluidic Systems in Poly (Dimethylsiloxane)," *Analytical Chemistry,* vol. 70, pp. 4974-4984, 1998.

[15] V. Bartzoka, M. R. McDermott, and M. A. Brook, "Protein - Silicone Interactions," *Advanced Materials,* vol. 11, pp. 257-259, 1999.

[16] S. Koutsopoulos, J. van der Oost, and W. Norde, "Adsorption of an Endoglucanase from the Hyperthermophilic Pyrococcus F Uriosus on Hydrophobic (Polystyrene) and Hydrophilic (Silica) Surfaces Increases Protein Heat Stability," *Langmuir,* vol. 20, pp. 6401-6406, 2004.

[17] E. Magnan, I. Catarino, D. Paolucci-Jeanjean, L. Preziosi-Belloy, and M.-P. Belleville, "Immobilization of Lipase on a Ceramic Membrane: Activity and Stability," *Journal of Membrane Science,* vol. 241, pp. 161-166, 2004.

[18] C. Chao, J. Liu, J. Wang, Y. Zhang, B. Zhang, Y. Zhang, *et al.*, "Surface Modification of Halloysite Nanotubes with Dopamine for Enzyme Immobilization," *ACS Applied Materials & Interfaces,* vol. 5, pp. 10559-10564, 2013.

CHAPTER 5
PDA-PDMS MICROFLUIDIC REACTORS FOR 3-PGA PRODUCTION

This chapter will present the second design of microfluidic reactor for 3-PGA production, which makes use of polydopamine to improve the immobilization of RuBisCO by covalent binding. It would show stronger interaction and increased immobilization amount than the simplest physical adsorption used in the previous chapter.

5.1 Brief

In chapter 4, PDMS has been proved to successfully immobilize RuBisCO simply by physical adsorption. However, the flat PDMS provides a limited surface area for the RuBisCO immobilization, resulting in little amount of immobilized RuBisCO and small amount of produced 3-PGA. In addition, the hydrophobic immobilization and physical adsorption are not strong enough, causing the low reusability. In this chapter, polydopamine will be used to modify the PDMS surface to ameliorate the two shortcomings and improve the reactor performance.

Among the various enzyme immobilization methods, covalent immobilization always offers the strongest bond between enzyme and support [1, 2]. But it usually involves complex linkers and organic solvents. Recently, polydopamine (PDA) becomes rather popular in biomimetic systems for the covalent immobilization of enzymes [3-6].

They possess excellent biocompatibility and high efficiency in imparting biological functionality on inorganic materials. For this reason, this work employs PDA as the linker for RuBisCO immobilization to continuously synthesize 3-PGA. The reaction performance in the RuBisCO-immobilized PDA-PDMS microfluidic reactors (RI-DPMRs) is compared with that in bulk reactors in terms of the stability, reusability and long-term 3-PGA production subsequently. To the best of our knowledge, there is no previous research on the RuBisCO immobilization in the DPMRs. This is also a proof of concept for the NPS pathway configuration using enzyme-immobilized microfluidic reactors for continuous synthesis of glucose precursor.

5.2 Experimental methods

5.2.1 Fabrication of RI-DPMRs

The RI-DPMRs were made in three main steps: (a) preparation of the pristine polydimethylsiloxane (PDMS) microfluidic reactors; (b) modification of PDA; and (c) immobilization of RuBisCO. First, the PDMS microfluidic reactors were fabricated by sealing one molded PDMS layer with another flat PDMS layer on the top. The molded PDMS layer was made by using the standard soft-lithography technique [7] with the Sylgard 184 elastomer kit (Dow Corning Corporation) and a SU-8 mold (SU-8 50, MicroChem) fabricated by the photolithography. Then, the pristine PDMS inner surface of the microfluidic reactors were modified by PDA. The strategy for the PDA modification was adopted from Zheng's group with minor modification [6]. Briefly, the

PDMS microfluidic reactor was first cleaned by 1 M NaOH solution, and then infused with 10% (v/v) (3-Aminopropyl)triethoxysilane (APTES, 99%, Aladdin Industrial Corporation, Shanghai) solution. The reactor was incubated at 50 ºC for 3 hours for amine-functionalization. The APTES-treated microfluidic reactor was further rinsed with ethanol, dried, and baked at 125 ºC for 1 hour. Then, 1.5 mL dopamine solution (1 $mg \cdot mL^{-1}$) was injected into the microfluidic reactor under the flow rate of 2.5 $\mu L \cdot min^{-1}$ on a hot plate at 50 ºC. After being rinsed with 10 mM Tris-HCl buffer (pH 8.8), the microfluidic reactor was successfully modified with PDA and was ready for the enzyme immobilization.

Next, 7 μL of RuBisCO in the reaction buffer was injected into the DPMRs by pipette and kept at room temperature for 6 hours for the RuBisCO immobilization. After that, the reactor was rinsed by the reaction buffer using a syringe pump at a flow rate of 2.5 $\mu L \cdot min^{-1}$ for 40 min. Finally, the RI-DPMRs were ready for use.

5.2.2 Confirmation of RuBisCO immobilization

The surface characterization of the inner surfaces of the microfluidic reactors after each step of RuBisCO immobilization was first conducted for the confirmation of RuBisCO immobilization. An optical microscope (Olympus BX41), a Scanning Electron Microscope (SEM, JEOL JSM-6490), a standard Contact Angle Goniometer (Model 200, ramé-hart instrument co.), a Raman spectrometer (Witec_Confocal Raman system) and an attenuated total reflection Fourier transform infrared spectroscopy (ATR-FTIR,

BRUKER) were used here.

Then, the successful immobilization of RuBisCO in the reactors were also demonstrated by the fluorescence experiments. The RuBisCO-FITC solution was introduced into the PDA-PDMS microfluidic reactor and then kept at room temperature for 6 hours. The reactor was observed under a fluorescence microscope (Olympus BX41) to record the fluorescence phenomenon. Afterwards, it was washed with 0.1 M phosphate-buffered saline (PBS, pH 9.2) thoroughly to check whether the fluorescence phenomenon still existed.

5.2.3 Determination of protein loading capacity

The protein loading capacity of the DPMRs was investigated to select an optimal RuBisCO concentration for the RI-DPMRs fabrication in the following research. Increased concentrations of RuBisCO solutions (1.5625 - 25 $\mu g \cdot \mu L^{-1}$) were injected into the DPMRs for the test. Then, the optimal RuBisCO concentration for further research could be determined to maximize the protein loading capacity and the protein loading efficiency.

5.2.4 Assay of RuBisCO activity

The enzyme activity was defined as the generation rate of 3-PGA ($\mu mol \cdot g^{-1}$ RuBisCO$\cdot min^{-1}$). The activities were then fit to a Michaelis-Menten type model using hyperbola regression to derive V_{max} and K_m parameters of both free and immobilized

RuBisCO.

5.2.5 Feasibility of 3-PGA production with RI-DPMRs

The feasibility of producing 3-PGA with RI-DPMRs was tested by injecting 0.5 mM RuBP in the reaction buffer into the as-prepared RI-DPMRs using a syringe pump at a specific flow rate. The production solution II was collected from the outlet to measure the 3-PGA amount by the amplification signal assay. Different amounts of 3-PGA could be produced when the reactant mixture was injected at different flow rates (from 28 μL·min^{-1} to 1.4 μL·min^{-1}), which directly determined the reaction time of the 3-PGA production reaction. The produced amount of 3-PGA (μmol·g^{-1} RuBisCO) in a specific reaction time could also be determined by the same standard curve obtained from last section. Control experiments were conducted at the same time with the same amount of BSA that was immobilized in microfluidic reactors. HPLC-MS/MS was also applied to detect the produced 3-PGA from the production solution II according to the method tested before [8].

5.2.6 Storage and thermal stability of RI-DPMRs

To test the storage stability of the RI-DPMRs, several prepared RI-DPMRs were incubated at 4 ºC for different days. Then, the immobilized RuBisCO activities of them were measured. The storage stability of free RuBisCO was also tested at the same condition for comparison. The highest RuBisCO activity (A_{hs}) was normalized to 100%

and the relative RuBisCO activities after different storage days were calculated as a percentage of A_{hs}.

Regarding the thermal stability of the RI-DPMRs, several prepared RI-DPMRs were first incubated in the oven at different temperatures (from 20 ºC to 70 ºC) for 10 mins and then the RuBisCO activities of each RI-DPMRs were examined. The thermal stability of free RuBisCO was also tested at the same condition for comparison. A_{ht} was normalized to 100% and the relative RuBisCO activities at different incubation temperatures were calculated as a percentage of A_{ht}.

5.2.7 Reusability of RI-DPMRs

The reusability of the RI-DPMRs means the capability of the RI-DPMRs being used repeatedly. It was evaluated by conducting the 3-PGA production reaction using one reactor for several cycles of reuse. Here, one cycle of reuse refers to the test that 21 μL of reactant mixture solution passes through the RI-DPMRs for 3-PGA production. RuBisCO activity was measured from the collected production solution II for each cycle of reuse. The relative RuBisCO activities were calculated as a percentage of the initial RuBisCO activity in the first cycle.

5.2.8 Continuous production of 3-PGA from RI-DPMRs

Continuous production of 3-PGA was achieved by constantly injecting the reactant mixture into the RI-DPMRs and thus a large amount of 3-PGA can be produced. As a

comparison, 3-PGA production in the bulk reaction with the same amount of free RuBisCO was conducted at the same time. Increasing Q_m (from 21 μL to 1680 μL) was applied to examine the difference of the 3-PGA production ability between the RI-DPMRs reaction and the bulk reaction.

5.3 Results and discussions

5.3.1 Fabrication of RI-DPMRs

Figure 5.1 (a) is the three-dimensional diagram of the RI-DPMRs. It consists of two PDMS layers, and the inner surfaces of microchannels are functionalized by PDA (the dark brown color as presented by the inset of **Figure 5.1** (a)). The abundant catechol groups of PDA layer can react with the amine groups of RuBisCO through the Michael addition or Schiff base reactions [3], facilitating the immobilization of RuBisCO (**Figure 5.1** (b)).

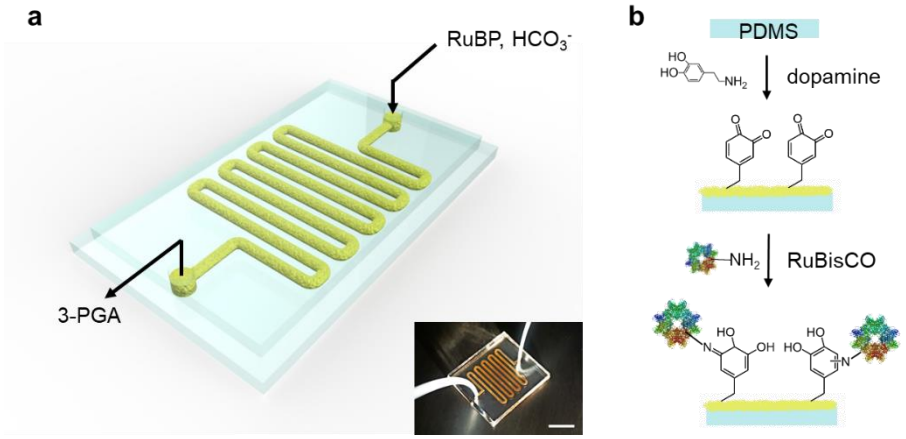

Figure 5.1 Schematics of the fabricated RI-DPMRs. (a) Three-dimensional diagram and the photo (inset) of the RI-DPMRs, the scale bar of the inset is 1 cm. (b) Illustration of

the procedures of RuBisCO immobilization.

5.3.2 Confirmation of RuBisCO immobilization

Figure 5.2 shows the surface characterization of the microchannels' inner surfaces after each step of RuBisCO immobilization. The SEM images of the pristine PDMS surface, PDA-modified PDMS surface, and RuBisCO-immobilized PDA-PDMS surface are presented in **Figure 5.2** (a), (b) and (c), respectively. It is noticed that the pristine PDMS surface is flat and smooth. While after the PDA modification, a rough layer with many nanoparticles is formed (**Figure 5.2** (b) and **Figure 5.3** (a)). This coarse PDA layer can provide a much larger surface area than the smooth PDMS surface, offering more active functional groups to covalently couple with RuBisCO. Then, the immobilization of RuBisCO gives rise to many blocks onto the PDA layer (**Figure 5.2** (c) and **Figure 5.3** (b)). The top right insets in **Figure 5.2** are the optical microscope images of the corresponding microchannels, displaying the surface change of microreactor after each immobilization procedure. After the PDA modification, the transparent PDMS channels become opaque and brown. While the subsequent RuBisCO immobilization makes no big change of the surface roughness. The bottom right insets in **Figure 5.2** show the observed water contact angles. The water contact angle of the inner surface significantly decreases from 103.8^{o} to 25.5^{o} after the PDA modification. This hydrophilicity improvement is resulted from the abundant catechol groups of PDA. In contrast, further immobilization of RuBisCO leads to an increase of water contact angle, which is probably due to the

hydrophobic side chains of amino acids in RuBisCO.

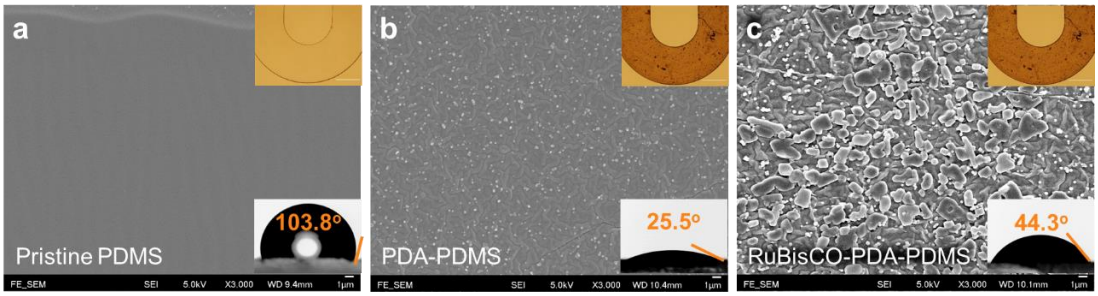

Figure 5.2 Surface characterization of RI-DPMRs inner surfaces. (a), (b) and (c) are the SEM images of the pristine PDMS surface, PDA-modified PDMS surface, and RuBisCO-immobilized PDA-PDMS surface, respectively. The top right insets are the optical microscopic images of the corresponding microfluidic reactors and the bottom right insets are the water contact angle results of the corresponding surfaces.

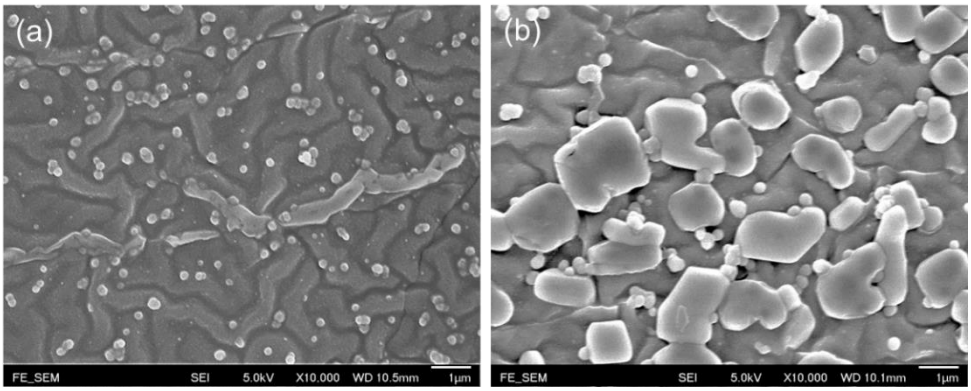

Figure 5.3 SEM images with larger magnification of (a) PDA-modified PDMS surface, and (b) RuBisCO-immobilized PDA-PDMS surface, respectively.

To further confirm the successful immobilization of RuBisCO, the Raman and ATR-FTIR spectra of the microfluidic channels were also obtained (see **Figure 5.4**). New peaks (1368 cm^{-1} and 1564 cm^{-1} in the Raman spectra, and 1400-1800 cm^{-1} and 3000-3750 cm^{-1} in the ATR-FTIR spectra) can be observed after the PDA modification and the RuBisCO

immobilization compared with the pristine PDMS microfluidic channels. These surface characterization results prove the success of the procedures for RuBisCO immobilization.

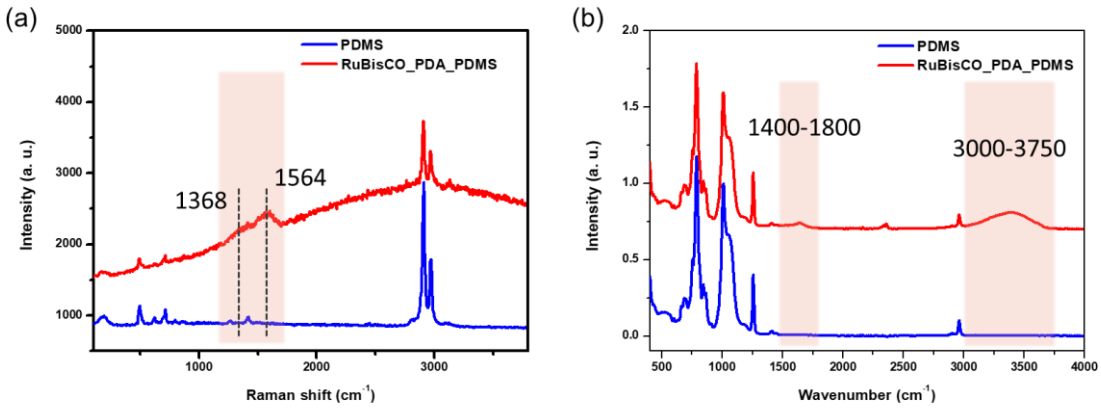

Figure 5.4 Raman spectra (a) and ATR-IR spectra (b) of the PDMS channels before (black line) and after (red line) RuBisCO immobilization.

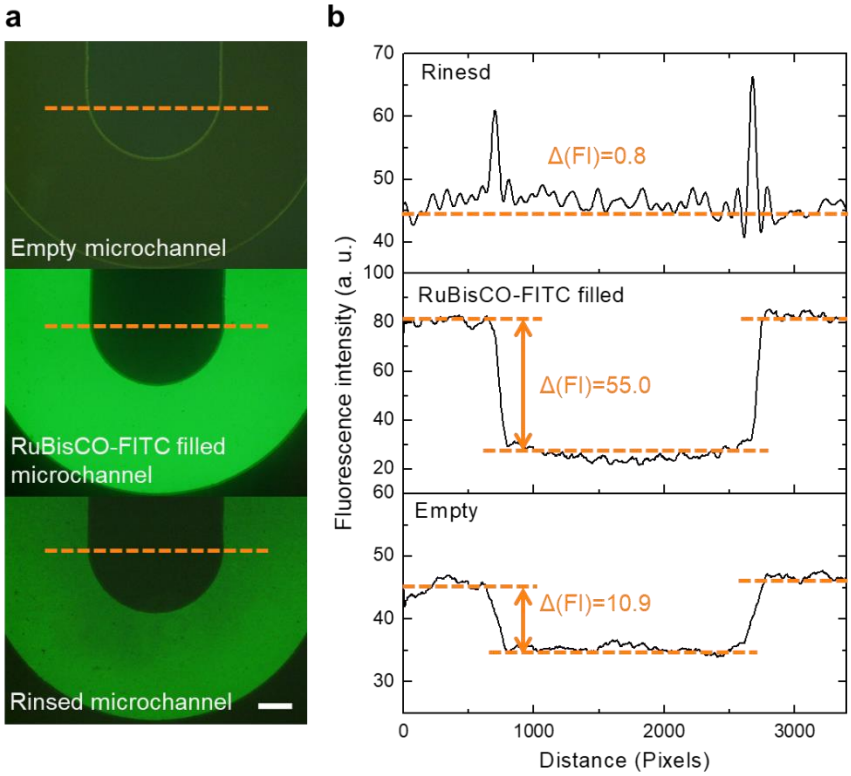

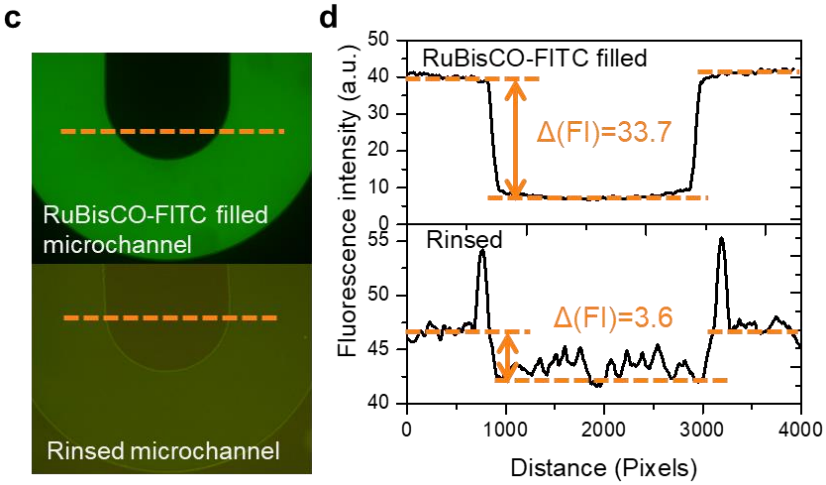

Figure 5.5 Fluorescence experiments for confirming the RuBisCO immobilization. (a) Fluorescence images of the empty microchannel, the RuBisCO-FITC filled microchannel, and the rinsed microchannel. (b) The corresponding fluorescence intensity profiles obtained along the observation lines. (c) Fluorescence images of the the RuBisCO-FITC filled in the pristine PDMS microchannel, and the rinsed pristine PDMS microchannel. (d) The corresponding fluorescence intensity profiles obtained along the observation lines. The scale bar is 500 μm.

The fluorescence experiment was also conducted to verify the RuBisCO immobilization. As shown by the fluorescence images in **Figure 5.5** (a) and the corresponding fluorescence intensity profiles in **Figure 5.5** (b), the fluorescence intensity difference (Δ(FI)) between the microchannel and the microchannel wall is greatly increased after the injection of the RuBisCO-FITC (RuBisCO tagged by fluorescein isothiocyanate) solution. After the thoroughly rinsing by the PBS buffer, Δ(FI) decreases but does not drop to zero. The retained fluorescence is ~ 19.8%. The non-zero Δ(FI) after

the rinsing proves that a portion of RuBisCO is well retained on the microchannel surface and the strategy of RuBisCO immobilization on microfluidic reactor via PDA modification is feasible. As shown in **Figure 5.5** (c) and (d), the retained fluorescence observed by the RuBisCO immobilization on the pristine PDMS by physical adsorption is ~ 10.9%, which is only half of that by PDA immobilization.

5.3.3 Determination of protein loading capacity and kinetic parameters

After the successful immobilization of RuBisCO, the protein loading capacity of the PDA-modified microfluidic reactors should be investigated to determine the optimal RuBisCO concentration for further experiments. As plotted in **Figure 5.6** (black solid squares), the amount of protein loaded in the reactors rises with the increase of the injected RuBisCO concentration. It then saturates to about 2.0 $\mu g \cdot cm^{-2}$ when the RuBisCO concentration reaches about 6.25 $\mu g \cdot \mu L^{-1}$. However, the protein loading efficiency decreases with the increase of RuBisCO concentration (red open triangles in **Figure 5.6**). This shows that RuBisCO can be easily immobilized onto the PDA layer. Once all the functional groups of the PDA are covalently bonded with RuBisCO, any excess RuBisCO would be easily rinsed off from the reactor inner surface. As a consequence, 6.25 $\mu g \cdot \mu L^{-1}$ was chosen as the optimal RuBisCO concentration for the following experiments. The protein loading capacity of the PDA-modified microfluidic reactor is estimated to be 2.029 $\mu g \cdot cm^{-2}$, and the corresponding protein loading efficiency

is about 52%.

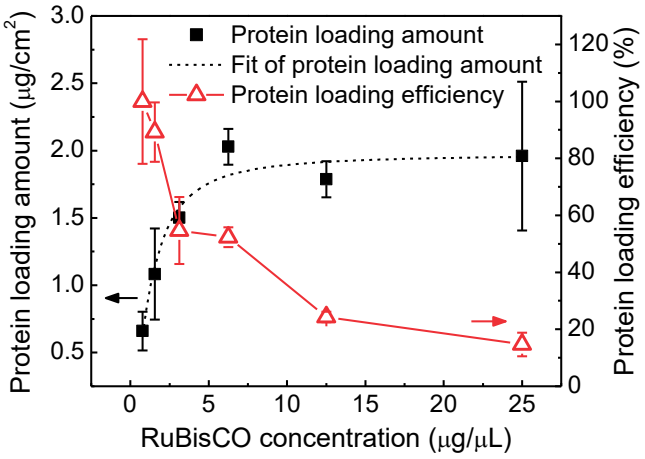

Figure 5.6 Protein loading amount and loading efficiency as a function of the concentration of injected RuBisCO. Immobilization time is 6 h.

After the optimal RuBisCO concentration was selected, the kinetic parameters of the immobilized RuBisCO in the RI-DPMRs and the free RuBisCO in the bulk reactor were determined (see **Table 5.1**). Compared with the kinetic parameters of free RuBisCO, the K_m value (the Michaelis-Menten constant) for the RI-DPMRs is significantly higher (0.52 mM vs. 0.19 mM), which means a lower affinity of the immobilized enzyme for the reactant. This is a common and intrinsic weakness of immobilized enzymes, owing to the steric hindrance introduced by the coverage of some active site by the support [9]. In addition, the immobilized enzyme may lose the flexibility to bind the natural ligands during catalysis and the reactant may have an increased diffusion length to the enzyme [9].

Table 5.1 Summary of different parameters of the RI-DPMRs reaction and bulk reaction.

	V_{max} (mmol·min^{-1}·mg^{-1} RuBisCO)	K_m (RuBP) (mM)	Storage stability [#]	Thermal stability [$]	Reusability [&]	Production of 3-PGA (μmol· g^{-1} RuBisCO)
RI-DPMRs reaction	0.230 ± 0.019	0.083 ± 0.028	30%	65%	90%	∝ Q_m [§]
Bulk reaction	0.357 ± 0.010	0.069 ± 0.008	4%	10%	-	Saturation at 200
Enhancement factor [※]	0.64-fold	1.20-fold	7.5-fold	6.5-fold	-	2.26-fold
Data from ref.	0.08~2.83 [a]	0.0015~0.12 [b]	90% [c]	75% at 55 °C [d]	88% [e]	-

[#] Storage stability is the remaining relative activity after 15 days.

[$] Thermal stability is the remaining relative activity after incubation at 70 °C for 10 min.

[&] Reusability is the remaining relative activity after 5 cycles of reuse at the flow rate of 1.4 μL·min^{-1}.

[§] Q_m is the volume of the reactant mixture (RuBP and HCO_3^- in reaction buffer).

[※] The enhancement factors refer to the factor of the performance in RI-DPMRs reaction as compared to that in bulk reaction.

[a,b] https://www.brenda-enzymes.org/enzyme.php?ecno=4.1.1.39

[c,d,e] Biotechnology and bioengineering 81.6 (2003): 705-711. RuBisCO immobilized on settled beads of protein A Sepharose by the DMP method

From **Table 5.1**, the RI-DPMRs also exhibited a lower V_{max} (the maximal reaction velocity) than that of the free RuBisCO, which may be due to the loss of enzyme activity after the immobilization. According to the previous work, the mechanism of PDA for the enzyme immobilization is to link the amino groups of enzymes to the catechol groups of PDA [3, 6]. It has been reported that the amino groups of lysine residues at the active sites of RuBisCO play a critical role in catalysis [10, 11]. Therefore, the immobilization of RuBisCO by PDA modification may result in the irreversible compromise of the

RuBisCO activity.

5.3.4 Feasibility of the RI-DPMRs

The prepared RI-DPMRs are used to produce the glucose precursor (3-PGA) from RuBP and CO_2 under different reaction times to test the feasibility of the reactors. In the control experiment that albumin from bovine serum (BSA) is immobilized onto the microfluidic reactor, the BSA-immobilized PDA-PDMS microfluidic reactors (BI-DPMRs) produces no obvious amount of 3-PGA (black dash-dotted line in **Figure 5.7** (a)). The production amount does not increase with reaction time either. In contrast, the RI-DPMRs demonstrate the production of 3-PGA at 5.56 $\mu mol \cdot g^{-1}$ RuBisCO$\cdot min^{-1}$(red solid line of **Figure 5.7** (a)). Apart from the UV-Vis spectrometer, a high-performance liquid chromatography-tandem mass spectrometer (HPLC-MS/MS) system is also applied to examine the ingredients of 3-PGA and RuBP in the production solution. The retention times of standard RuBP and 3-PGA are 18.99 and 17.40 min, respectively (see **Figure 3.13**). The peaks with the similar retention times of RuBP and 3-PGA can also be observed from the production solution of the RI-DPMRs (**Figure 5.7** (b)). However, only RuBP can be detected from that of the BIMRs. In consequence, it is well proved that 3-PGA is synthesized successfully from the RI-DPMRs by implementing the light-independent reactions pathway. Moreover, modification of the reaction time can be achieved straightforwardly by controlling the flow rate of the reactant mixture injection.

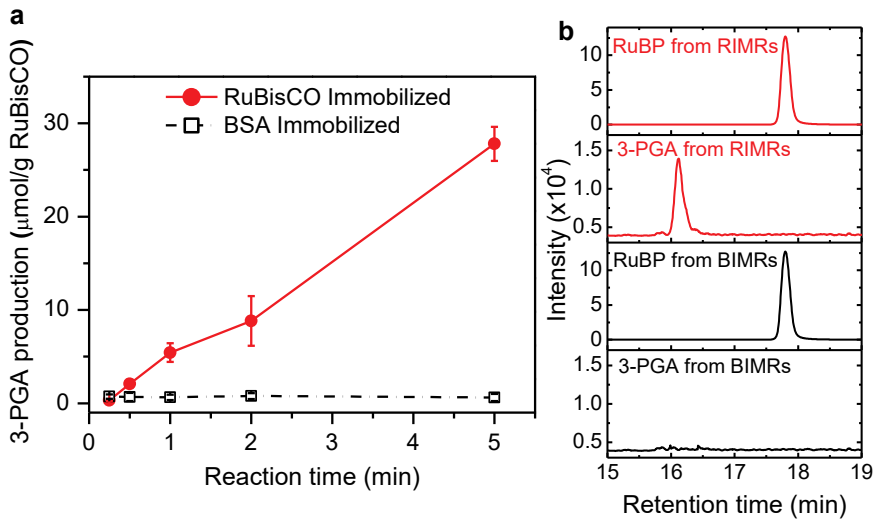

Figure 5.7 Feasibility of the RI-DPMRs for 3-PGA production. (a) Production amount of 3-PGA as a function of the reaction time for the RI-DPMRs (red solid line) and the BI-DPMRs (black dash-dotted line). (b) HPLC-MS/MS chromatography of RuBP and 3-PGA from the production solutions obtained in 5 min.

5.3.5 Storage and thermal stability of the RI-DPMRs

The storage and thermal stabilities of RI-DPMRs are very important properties in practical applications. The storage stability of RI-DPMRs after different days incubation is shown in **Figure 5.8** (a). The half-life (the storage time that 50% of the initial activity can be retained after the 4 ºC incubation) of the free RuBisCO is about 2.5 days. It is doubled (5 days) after the immobilization. In addition, the storage stability of the immobilized RuBisCO is enhanced by 7.5 times compared with the free one (30% vs. 4.2% of the initial activity retention after the incubation for 15 days).

Figure 5.8 (b) shows the influence of temperature on the stability of RuBisCO. The highest enzyme activities (A_{ht}) of immobilized and free RuBisCO both appear at 30 ºC. And the optimal incubation temperature range (the temperature range that over 98% of

maximum enzyme activity could be retained after incubation) of RuBisCO is expanded from 24-34 to 29-40 ºC after the immobilization. It is also worth noting that the immobilized RuBisCO remains 65% of A_{ht} at 70 ºC whereas free RuBisCO retains only 10%. The method of immobilization significantly enhances the resistance of RuBisCO to the thermal inactivation and the immobilized RuBisCO possesses a 6.5-fold relative activity than the free RuBisCO at the elevated temperature.

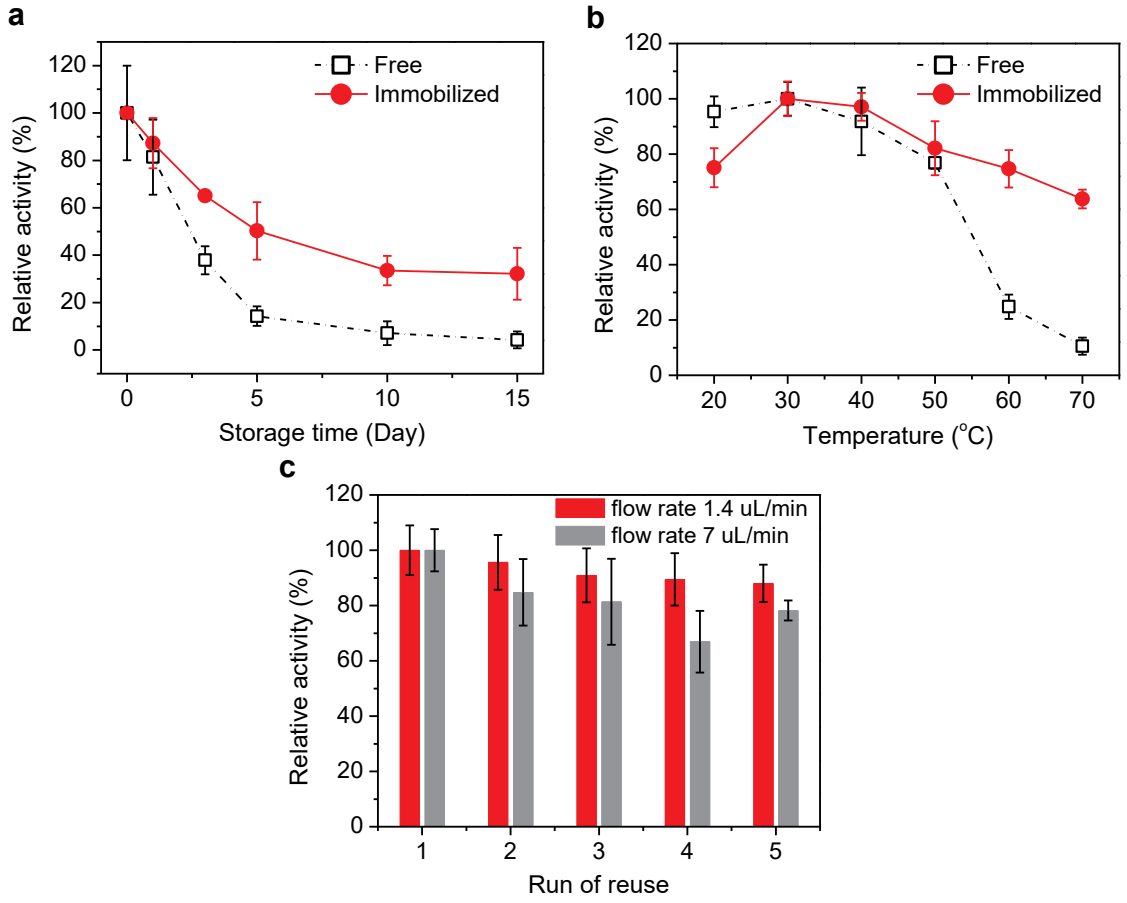

Figure 5.8 Characterizations of the immobilized RuBisCO. (a) Storage stability of immobilized (red line) and free RuBisCO (black line). (b) Thermal stability of immobilized (red line) and free RuBisCO (black line). (c) Reusability of the RI-DPMRs with the flow rates of the injected RuBP at 7 μL/min (grey bar) and 1.4 μL/min (red bar), the reaction times are 1 min and 5 min, respectively.

Both the improved storage and thermal stabilities of RuBisCO can be ascribed to the enhanced stability of the enzyme conformation after the covalent immobilization [12, 13]. Generally, the enzyme activity in solution could be greatly affected by the structure change caused by the unfolding of protein amino acid chains. The elevated temperature or long-time storage would consequently influence the conformation of RuBisCO, leading to the activity reduction. On the other hand, the immobilization technique can offer multipoint anchors of RuBisCO on the support of the microfluidic reactors. As a result, the enzyme structure and the active sites are properly preserved, thus maintaining the activity of immobilized RuBisCO.

5.3.6 Reusability of the RI-DPMRs

In addition to the thermal stability and the storage stability, enzymes are also required to contain an outstanding reusability for industrial usage. As shown by the grey bar in **Figure 5.8** (c), 80% of initial activity can be maintained after five cycles of reuse when the reaction time is 1 min (the flow rate was 7 $\mu L \cdot min^{-1}$). The enzyme deactivation after the repeated uses and the enzyme detachment due to the flush of the reactant mixture are responsible for the activity loss [5]. The enzyme detachment problem can be alleviated when the flow rate is slowed down to 1.4 $\mu L \cdot min^{-1}$. In this case, the reaction time is 5 min and 90% of initial activity can be maintained after five cycles of reuse (the red bars in **Figure 5.8** (c)). The bulk reaction generally needs special techniques to collect the products and recycle the enzyme. But they are quite facile in the RI-DPMRs reaction

through simultaneously pumping out the production solution and the injecting the new reactant mixture.

5.3.7 Continuous production of 3-PGA from RI-DPMRs

When the reactant mixture is pumped constantly into the RI-DPMRs, continuous and massive production of 3-PGA can be achieved with little RuBisCO for maximum efficiency. As shown in **Figure 5.9**, the steric hinderance probably leads to the lower 3-PGA production in RI-DPMRs reaction than that in bulk reaction when Q_m is small. Nevertheless, the 3-PGA production by the RI-DPMRs in the continuous mode (optimal condition, reaction time 1 min) presents an almost linear rate increase at 0.56 $M \cdot g^{-1}$ RuBisCO$\cdot min^{-1}$ over Q_m (red solid circle in **Figure 5.9**). In contrast, the 3-PGA production in the bulk reaction (the black open square in **Figure 5.9**) increases very slowly and tends to saturate when Q_m is larger than 600 μL. The saturation of 3-PGA production in the bulk solution is attributed to the reduced RuBisCO concentration with the increased Q_m. Regarding the RI-DPMRs reaction, the increase of Q_m does not lower the RuBisCO concentration thanks to the pumping out of the production solution instantaneously with the injection of new reactant mixture. Together with the excellent reusability of immobilized RuBisCO, 3-PGA is hence produced at an almost constant rate (0.268 $M \cdot g^{-1}$ RuBisCO). With this, massive production is feasible using little amount of RuBisCO.

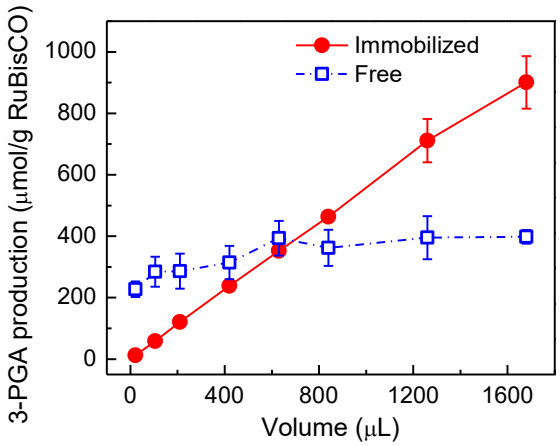

Figure 5.9 Production amount of 3-PGA as a function of the volume of used reactant mixture solution, the black line is the reaction in the bulk reactor with free RuBisCO and the red line is the reaction in the RI-DPMRs with the immobilized RuBisCO.

5.4 Summary

In this work, we have immobilized RuBisCO into the DPMRs for continuous production of glucose precursor. The immobilized RuBisCO showed a 7.5-fold improvement in the storage stability and a 6.5-fold increase in the thermal stability compared with the free RuBisCO. The RI-DPMRs also presented an excellent reusability with 90% of its initial activity retained after 5 cycles. This is the first attempt to build up the NPS pathway in the bio-mimic microfluidic reactors for continuous synthesis of glucose precursor instead of water splitting or microbial growth. Many advantages of microfluidics for enzymatic reactions are perfectly demonstrated here. Compared with the bulk system, the reaction in microfluidic reactor is much easier to control by adjusting the injection of reactant mixture solution. It also enables the continuous 3-PGA production at a constant rate,

enabling the massive production of 3-PGA with very little RuBisCO. The continuous mode maximizes the efficiency of RuBisCO in a low-cost, convenient and durable way to produce basic food.

As compared to the chapter 4 which uses the simple physical adsorption for enzyme immobilization, this chapter introduces the PDA layer to improve the bond strength and amount. To further enhance the 3-PGA production, the surface area of the microfluidic reactor should be further improved. For this reason, a new, monolithic microfluidic reactor will be developed in next chapter using porous PDMS.

5.5 References

[1] L. Cao, *Carrier-Bound Immobilized Enzymes: Principles, Application and Design*: John Wiley & Sons, 2006.

[2] P. Zucca and E. Sanjust, "Inorganic Materials as Supports for Covalent Enzyme Immobilization: Methods and Mechanisms," *Molecules,* vol. 19, pp. 14139-14194, 2014.

[3] H. Lee, S. M. Dellatore, W. M. Miller, and P. B. Messersmith, "Mussel-Inspired Surface Chemistry for Multifunctional Coatings," *Science,* vol. 318, pp. 426-430, 2007.

[4] H. Lee, J. Rho, and P. B. Messersmith, "Facile Conjugation of Biomolecules onto Surfaces Via Mussel Adhesive Protein Inspired Coatings," *Advanced Materials,* vol. 21, pp. 431-434, 2009.

[5] C. Chao, J. Liu, J. Wang, Y. Zhang, B. Zhang, Y. Zhang*, et al.*, "Surface Modification of Halloysite Nanotubes with Dopamine for Enzyme Immobilization," *ACS Applied Materials & Interfaces,* vol. 5, pp. 10559-10564, 2013.

[6] G. Cheng, S.-J. Hao, X. Yu, and S.-Y. Zheng, "Nanostructured Microfluidic Digestion System for Rapid High-Performance Proteolysis," *Lab on a Chip,* vol. 15, pp. 650-654, 2015.

[7] D. C. Duffy, J. C. McDonald, O. J. Schueller, and G. M. Whitesides, "Rapid Prototyping of Microfluidic Systems in Poly (Dimethylsiloxane)," *Analytical Chemistry,* vol. 70, pp. 4974-4984, 1998.

[8] S. U. Bajad, W. Lu, E. H. Kimball, J. Yuan, C. Peterson, and J. D. Rabinowitz, "Separation and Quantitation of Water Soluble Cellular Metabolites by Hydrophilic Interaction Chromatography-Tandem Mass Spectrometry," *Journal of Chromatography A,* vol. 1125, pp. 76-88, 2006.

[9] K. B. de Oliveira, K. L. Mischiatti, J. D. Fontana, and B. H. de Oliveira, "Tyrosinase Immobilized Enzyme Reactor: Development and Evaluation," *Journal of Chromatography B,* vol. 945, pp. 10-16, 2014.

[10] G. H. Lorimer and H. M. Miziorko, "Carbamate Formation on The. Epsilon.-Amino Group of a Lysyl Residue as the Basis for the Activation of Ribulosebisphosphate Carboxylase by Carbon Dioxide and Magnesium (2+)," *Biochemistry,* vol. 19, pp. 5321-5328, 1980.

[11] F. Hartman, C. Stringer, S. Milanez, and E. H. Lee, "The Active Site of Rubisco,"

Philosophical Transactions of the Royal Society of London. B, Biological Sciences, vol. 313, pp. 379-395, 1986.

[12] M. Sarı, S. Akgöl, M. Karataş, and A. Denizli, "Reversible Immobilization of Catalase by Metal Chelate Affinity Interaction on Magnetic Beads," *Industrial & Engineering Chemistry Research,* vol. 45, pp. 3036-3043, 2006.

[13] Y. Zhu, S. Kaskel, J. Shi, T. Wage, and K.-H. van Pée, "Immobilization of Trametes Versicolor Laccase on Magnetically Separable Mesoporous Silica Spheres," *Chemistry of Materials,* vol. 19, pp. 6408-6413, 2007.

CHAPTER 6
SPONGE PDMS EMBEDDED-MICROREACTOR FOR 3-PGA PRODUCTION

This chapter will present a monolithic type microfluidic reactor using sponge PDMS (sp-PDMS). It is different from the two wall-coated type reactors presented in the previous two chapters. Moreover, it presents to have much larger surface area and thus better performance for 3-PGA production.

6.1 Brief

In chapter 4 and chapter 5, the enzyme RuBisCO was immobilized on the inner surfaces of microfluidic reactors, forming the wall-coated type microchannels. However, the low capacity of the wall-coated type microchannels for enzyme immobilization results in limited amounts of immobilized RuBisCO. That brings about the low overall reaction efficiency and the long operation time when the amount of 3-PGA production is large. In order to maximize the space utilization of the size-limited channels and therefore increasing the enzyme loading capacity, monolithic type microfluidic reactors with a high surface area can be used. The monolithic type microchannels also possess the advantages of high mechanical durability and reduced diffusion path length over the wall-coated type channel [1]. Moreover, compared with the packed-bed type channels, the monolithic type channels having interconnected meso- or micro- porous structures make it easy for

the fluid to flow through. Therefore, they allow for relatively higher flow rates, lower back pressures, and higher productivities.

At present, scientists have explored a number of porous solid supports for enzyme immobilization, including porous silicates [2-4], active carbons [5-7], porous polymers [8-10], and metal-organic frameworks (MOFs) [11-13]. Among all the porous polymeric materials, sponge PDMS has received increasing attention due to its outstanding biocompatibility and elasticity [14-16]. For the fabrication of porous PDMS sponges, extensive technologies have been developed, like the template leaching, phase separation, gas foaming, and 3D printing [17]. The sacrificial template method is the most commonly used due to its simple fabrication procedures. Sugar particles [18], salt crystals [19], zinc oxide powders [20], nickel foams [21], and easily dissolved polymer particles [22] are widely used as the sacrificial templates. However, most of the sacrificial templates need a long time to dissolve and sometimes may induce environment-harmful solvents. Recently, Jiang's group [23] used citric acid monohydrate (CAM) particles as the hard template and ethanol as the solvent to fabricate the 3D interconnected porous PDMS. This approach has the advantages of less time-consuming, simpler operation and lower environmental hazard.

Herein, we adopted Jiang's method for the sp-PDMS fabrication. The sp-PDMS was then in-situ embedded into the microreactors for the monolithic sp-PDMS embedded-microreactors (SPMRs) manufacture. Afterwards, RuBisCO was immobilized into the

prepared SPMRs after the surface modification with polydopamine as we did in chapter 5. The feasibility and reusability of the RuBisCO-immobilized SPMRs (RI-SPMRs) were studied. The performance of the RI-SPMRs was also compared with those of the RI-PMRs and RI-DPMRs.

6.2 Experimental methods

6.2.1 Fabrication of SPMRs

The process flow of the SPMRs fabrication is shown in **Figure 6.1**. First, an aluminum mold with a leaf-like pattern fabricated by computer numerical control (CNC) machining was used to prepare the patterned PDMS slice. The dimension of the aluminum mold is shown in **Figure 6.2** and the thickness of the mold is 1 mm. The 10:1 PDMS solution was poured into the aluminum mold and then cured at 85 ºC for 1 h. Then, a hard template method adopted from Jiang's group [23] was used to fabricate the 3D interconnected porous PDMS sponge that was then embedded into the PDMS microreactor. In brief, the grinded citric acid monohydrate (g-CAM) particles were mixed with the prepared PDMS solution (base : cure = 10 : 1) in different mass ratios (1:1, 3:1, 5:1, 7:1) and then filled into the leaf patterned PDMS mold slice. Then the leaf patterned PDMS slice with uncured g-CAM/PDMS composite was degassed for one hour before being cured at 85 ºC for 1 h. After the curing step, the slice was immersed into ethanol with ultrasonic for 2 hours and then kept overnight to remove the g-CAM particles. Next, the patterned PDMS slice with sp-PDMS was sealed with another flat PDMS slice after oxygen plasma

for 5 min. Two PMMA sheets fixed by screws were added outside the SPMRs to reinforce the sealing to avoid the leakage. An aluminon alloy frame having the same leaf pattern was placed onto the surface of the patterned PDMS slice as the mold with increased thickness for thicker (> 1 mm) sp-PDMS preparation. The thicknesses of the frames were made as 1 mm, 2 mm, and 3 mm. Then, four kinds of sp-PDMS slices having different thicknesses (1 mm, 2 mm, 3 mm and 4 mm) were obtained. Thicker sp-PDMS would be compressed to 1 mm height when it was sealed into the microreactor, resulting in multiplied surface area.

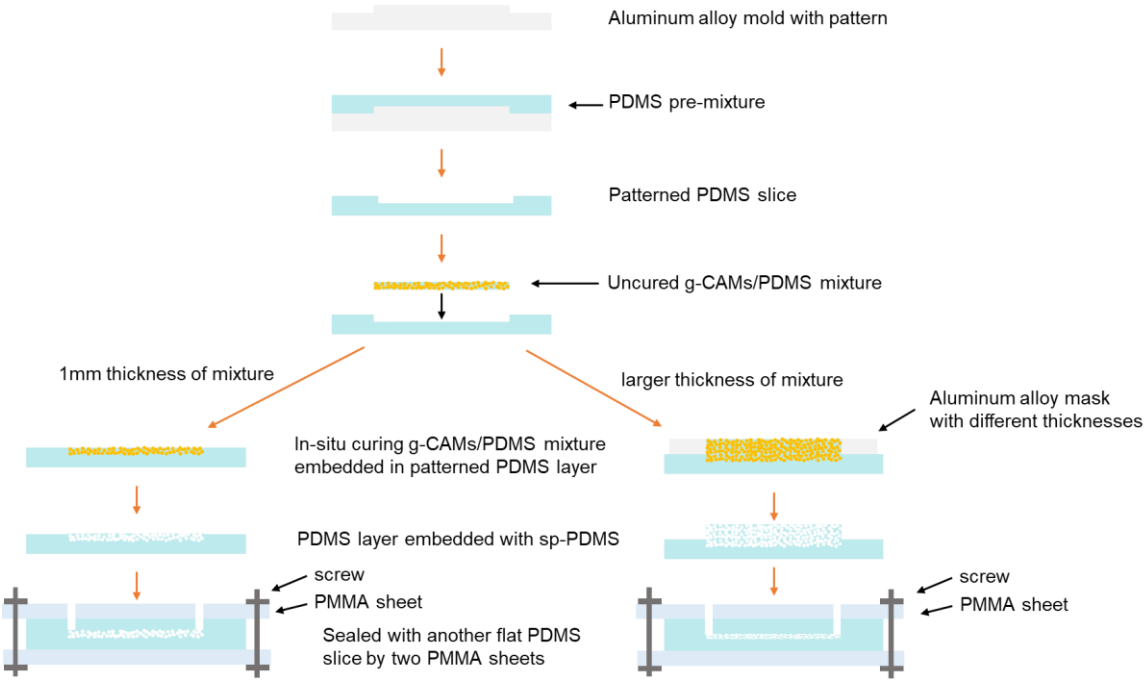

Figure 6.1 Process flow of the fabrication of sp-PDMS embedded microreactors.

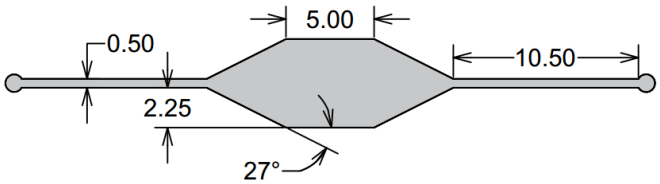

Figure 6.2 Design of the aluminum mold for PDMS pattern fabrication, the unit is mm.

6.2.2 Immobilization of RuBisCO into SPMRs

Polydopamine (PDA) was used to modify the inner surfaces of SPMRs before the RuBisCO immobilization. After oxygen plasma treatment and reactor sealing, 10% (v/v) APTES was immediately injected into the SPMRs and then kept at 50 ºC for 2 hours. Then, the SPMRs were washed by ethanol and dried on a hotplate at 125 ºC for 1 hour. After this, 1 mg·mL^{-1} dopamine in Tris-HCl buffer (0.1M, pH 8.8) was pumped into the SPMRs at 2.5 μL·min^{-1} on a hotplate at 65 ºC for 10 hours. The SPMRs were washed by Tris-HCl buffer (0.1M, pH 8.8) at 2.5 μL·min^{-1} followed by the injection of RuBisCO solution at 2.5 μL·min^{-1} for 4 h. At the end, the RI-SPMRs were rinsed by the reaction buffer at a flow rate of 2.5 μL·min^{-1} for 40 mins before they were ready for use. The procedures of RuBisCO immobilization on PDMS by PDA is shown in **Figure 6.3**.

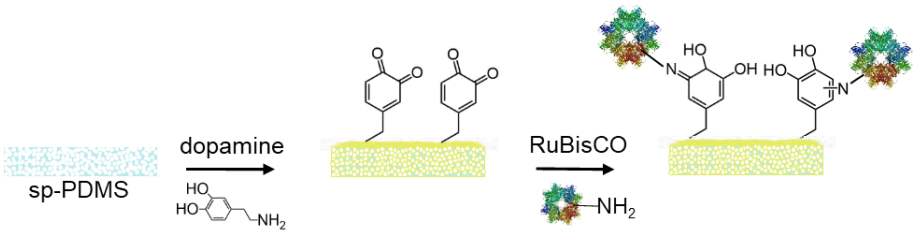

Figure 6.3 Illustration of the procedures for RuBisCO immobilization on SPMRs by PDA.

Here, another two different types of sp-PDMS were also prepared to fabricate the SPMRs for the comparison. The sp-PDMS prepared by in-situ method described above was regarded as 3# PDMS sponge. For 1# PDMS sponge, one large sp-PDMS block was cut into the same size of microreactor and then embedded into it. PDA was modified on the inner surface afterwards as mentioned before. While for the 2# PDMS sponge, the cut

sp-PDMS was modified with PDA first and then embedded in microreactor.

6.2.3 Determination of SPMRs volumes

The volume of the SPMRs (V_{spr}) is a very important parameter in the 3-PGA production reaction. It was determined by filling the microreactor with different solutions having different densities with the following equation:

$$m_{ri} = m_0 + \rho_i V_{spr} \tag{6.1}$$

where m_0 is the weight of the empty SPMRs, ρ_i is the density of the filled solutions (ρ_a is the density of air with the value of 0 g·cm^{-3}, ρ_e is the density of ethanol with the value of 0.789 g·cm^{-3}, $\rho_{0.5e}$ is the density of 50%(v/v) ethanol/water with the value of 0.893 g·cm^{-3}, ρ_w is the density of water with the value of 0.997 g·cm^{-3}, ρ_{NaOH} is the density of 2.8 M NaOH solution with the value of 1.11 g·cm^{-3}), m_{ri} is the weight of the SPMRs filled with the corresponding solutions. Then V_{spr} is calculated as the slope of the fitting line of the weight values as a function of the densities of the filled solutions.

6.2.4 Optimal condition investigation for RI-SPMRs fabrication

The protein loading efficiency and RuBisCO activity of the RI-SPMRs fabricated by using different g-CAM/PDMS ratios and sp-PDMS thicknesses were first compared. The concentration of the injected RuBisCO solutions was adjusted from 0.5 μg·μL^{-1} to 2 μg·μL^{-1}.

6.2.5 Feasibility of 3-PGA production with RI-SPMRs

The feasibility of producing 3-PGA with the RI-SPMRs was tested by injecting 0.5mM RuBP in the reaction buffer through a syringe pump in different flow rates. The production solution II was collected from the outlet for the determination of 3-PGA amount.

6.2.6 Reusability of RI-SPMRs

The reusability of the RI-SPMRs was evaluated by conducting the 3-PGA production reaction with one reactor for several cycles of reuse. Here, one cycle of reuse is V_{spr} of the RuBP solution passed through the RI-SPMRs for 3-PGA production. RuBisCO activity was measured from the collected production solution II for each cycle of reuse. The relative RuBisCO activity was calculated as a percentage of this highest activity, which was normalized to 100%.

6.3 Results and discussions

6.3.1 Characterization of SPMRs and RI-SPMRs

The dimensions of the bought CAM particles were in millimeter. They were grinded into micrometer size (**Figure 6.4** (a)) for the sp-PDMS fabrication. Then, the fabricated sp-PDMS would have relatively smaller pore size and larger surface area. The SEM images of the sp-PDMS fabricated by different g-CAM/PDMS ratios are shown in **Figure 6.4** (b), (c) and (d), demonstrating that the sp-PDMS is composed of the PDMS skeleton and the

air gaps. Larger g-CAM/PDMS ratio results in larger porosity. According to the results conducted by Prof. Jiang's group, the porosity of the PDMS sponge (5:1) can reach ~85% and the surface area is estimated to be ~57 mm^2/mm^3.

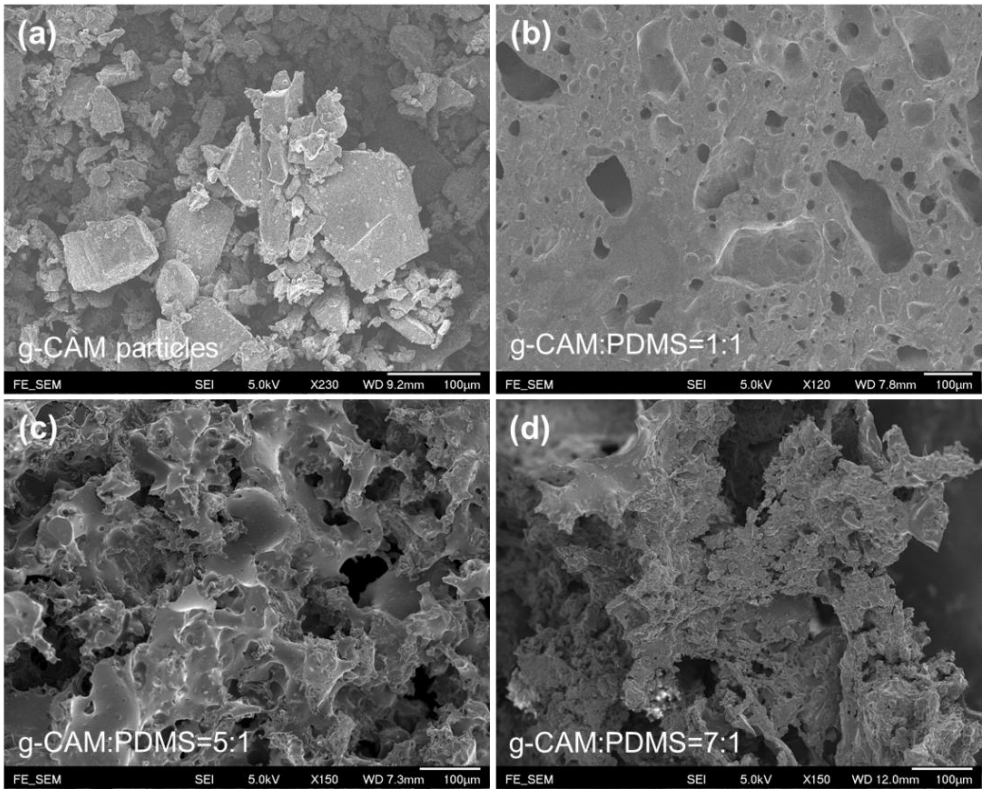

Figure 6.4 SEM images of (a) the g-CAM, porous PDMS sponge with the g-CAM to PDMS solution ratio of (b) 1:1, (c) 5:1 and (d) 7:1.

The similar PDA modification procedures in chapter 5 are used to modify the PDMS sponge for further RuBisCO immobilization. As shown in **Figure 6.5**, when the PDA modified PDMS sponge embedded microreactors are prepared in different procedure orders, their colors are in different shades, showing that different amounts of PDA would be coated onto the PDMS surface. The 1# reactor presents the least PDA amount modification. More PDA is modified in the 2# and 3# reactor than the 1# reactor and the

2# reactor presents the largest PDA amount modification. **Figure 6.5** (b) is the photograph of the fabricated RI-SPMRs.

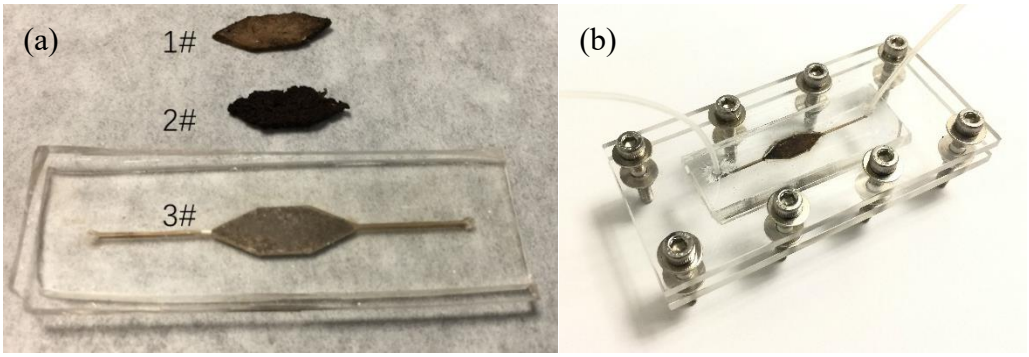

Figure 6.5 Photographs of the PDA modified-PDMS sponges in different procedure orders (a) and the RI-SPMRs (b). 1#: PDMS sponge was embedded first in microreactor then modified with PDA. 2#: PDMS sponge was modified with PDA first and then embedded in microreactor. 3#: PDMS sponge was formed in-situ in the microreactor and then modified with PDA.

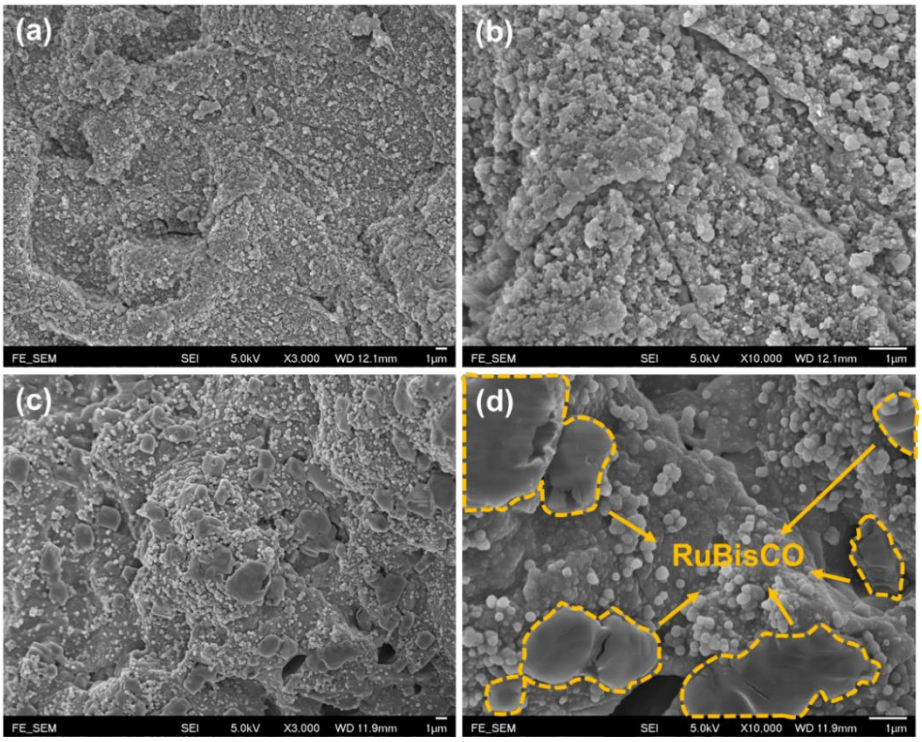

Figure 6.6 SEM images of the inner surfaces of (a), (b) the PDA-modified SPMRs and

(c), (d) the RI-SPMRs.

The SEM images (**Figure 6.6** (a) and (b)) show that after PDA modification, some PDA nanoparticles are formed into a coarse and rough layer to provide more active surface for RuBisCO immobilization. Consistent with our previous results in chapter 5, the further RuBisCO immobilization also gives rise to the blocks formation onto the PDA layer as shown in **Figure 6.6** (c) and (d). The blocks in yellow dotted circles should be the dried RuBisCO.

6.3.2 Determination of SPMRs volumes

By experiments, the volume of the SPMRs made by the in-situ method is determined by the weight changes as the filled solution is changed. As shown in **Figure 6.7** (a), the weights of SPMRs fabricated by different g-CAM/PDMS ratios are increased by the increasing density of the infused solution. According to Eq. 6.1, the calculated volumes of the SPMRs should be the slope of the fitted line. The coefficients of determination are all acceptable (> 0.99). After three replicate experiments, the volume of the SPMRs with 1 mm sp-PDMS can be estimated as 31.8 μL for that fabricated by the ratio of 3:1, 33.1 μL for 5:1 and 35.4 μL for 7:1. The SPMRs volume increases with the increase of the g-CAM/PDMS ratio, presenting higher porosity. When the thickness of the embedded sp-PDMS increase, the volume of the SPMRs would decrease, as shown in the solid bars of **Figure 6.7** (b), (c) and (d). When the thickness of sp-PDMS is 2 mm, the volumes decrease to 19.5 μL for 3:1, 25.6 μL for 5:1 and 27.7 μL for 7:1. When the sp-PDMS

thickness is 3 mm, the volumes are 17.8 μL for 5:1 and 20.2 μL for 7:1, respectively. When the sp-PDMS thickness is 4 mm, the volumes are 12.6 μL for 7:1. It is noted that when the g-CAM/PDMS ratio is relatively small and the thickness of sp-PDMS is relatively large, the experimental errors of the SPMRs volumes would be too large. Such cases are therefore not included in the subsequent experiments.

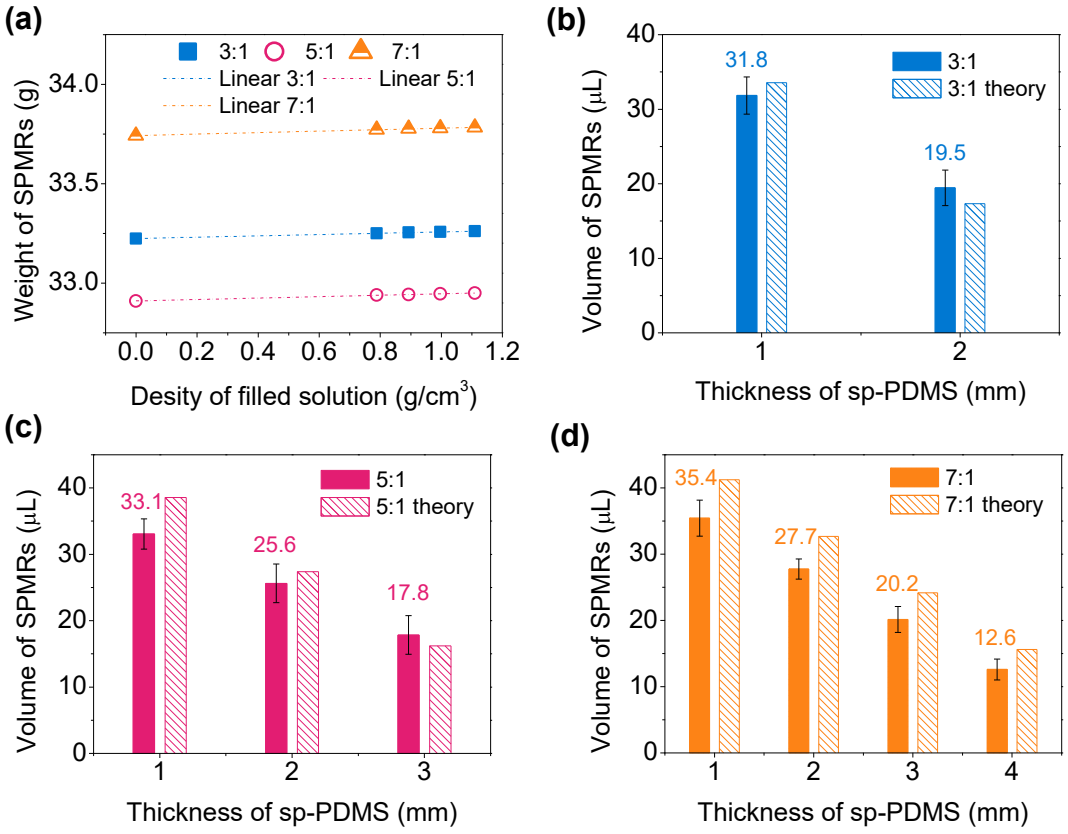

Figure 6.7 Volume determination of the SPMRs. (a) Weight change of SPMRs after infusion by different solutions having different densities. The thickness of the sp-PDMS used here is 1 mm. Calculation of the volumes of SPMRs fabricated by different thicknesses of sp-PDMS with the g-CAMs/PDMS ratio of (b) 3:1, (c) 5:1, (d) 7:1.

The volume of the microreactors can also be determined by theoretical calculation. Since the empty microreactor is filled with the mixture of g-CAM/PDMS, the volume of

the empty microreactor (V_r) can be calculated by:

$$nV_r = \frac{m_P}{\rho_P} + \frac{m_C}{\rho_C} \tag{6.2}$$

where m_P and ρ_P are the weight and density of PDMS, m_C and ρ_C are the weight and density of g-CAM particles, n is the height ratio of the mixture compared to the empty microreacgtor (n is 1, 2, 3, and 4). Since g-CAM and PDMS are mixed in the mass ratio of r (r can be 1, 3, 5, and 7), m_C equals rm_P. Therefore, the weight of PDMS composite will be

$$m_P = \frac{nV_r}{\frac{1}{\rho_P} + \frac{r}{\rho_C}} \tag{6.3}$$

and V_{spr} can be calculated by

$$V_{spr} = V_r - \frac{m_P}{\rho_P} = V_r - \frac{nV_r}{1 + \frac{\rho_P}{\rho_C} r} = \frac{r\rho_P - (n-1)\rho_C}{\rho_C + r\rho_P} V_r \tag{6.4}$$

where ρ_P is 1.064 g/cm^3, ρ_C is 1.542 g/cm^3, V_r is 49.75 mm^3 which is calculated from the CAD model. As shown by the open bars with the slash pattern in **Figure 6.7**, the theoretical results are consistent with the experimental results with acceptable operational errors. Therefore, the values of V_{spr} of different SPMRs are determined.

6.3.3 Optimal condition investigation for RI-SPMRs fabrication

As shown in **Figure 6.8**, the produced amounts of 3-PGA from different microreactors with different fabrication procedures are quite different from each other. The 1# reactor

presents the least 3-PGA production which is 0.063 nmol. The 2# reactor and the 3# reactor show larger 3-PGA production , which are 0.175 nmol and 0.140 nmol, respectively. Compared with the 1# reactor, the production in the 2# reactor and the 3# reactor increase about 2.8 folds and 2.2 folds, respectively. However, the results in the 2# reactor are hard to repeat due to the difficult in controlling the thickness of PDMS sponge by the cutting method. Therefore, in the following experiments, the RI-SPMRs are fabricated by in-situ embedding the sp-PDMS.

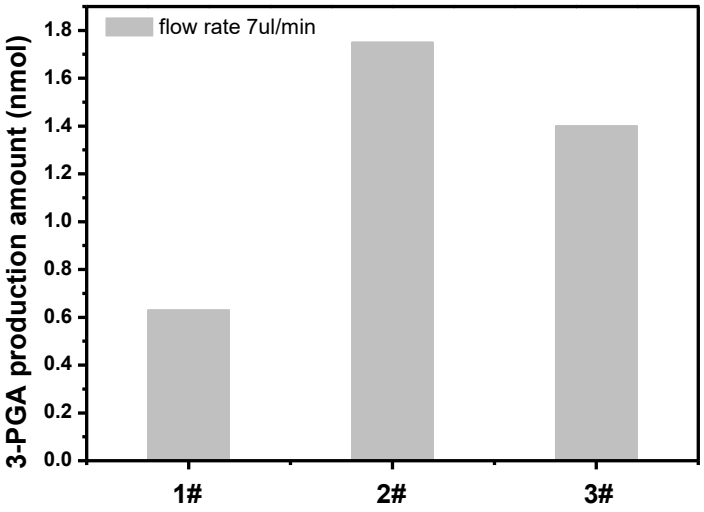

Figure 6.8 3-PGA production by RI-SPMRs fabricated in different procedures. The flow rate of injected RuBP solution was 7 μL·min^{-1}.

Some primary experiments are conducted to investigate the optimal condition for RI-SPMRs fabricated by the g-CAM/PDMS ratio of 5:1 in terms of the thickness of sp-PDMS and the concentration of the injected RuBisCO. As shown in **Figure 6.9** (a), the 3-PGA production increases with the increasing sp-PDMS thickness. When the injected

RuBisCO concentration is 1 μg·μL^{-1}, the 3-PGA production amount is 0.290 nmol for the microreactor without the embedding of sp-PDMS (0 mm). The 3-PGA production amounts are 0.948 nmol with 1 mm-thick sp-PDMS and 1.756 nmol with 2 mm-thick sp-PDMS, which respectively show 3.3-fold and 6.1-fold increase as compared to the production with 0 mm-thick sp-PDMS. The increasing thickness of sp-PDMS provides increasing surface area, allowing to immobilize more RuBisCO, which in turn results in larger 3-PGA production. In addition, the fluid in the porous structure would be more disordered compared with the fluid in the microreactor without sp-PDMS. The disordered flow may help the reactant to contact with the enzyme immobilized in the microreactor, therefore improving the overall reaction rate.

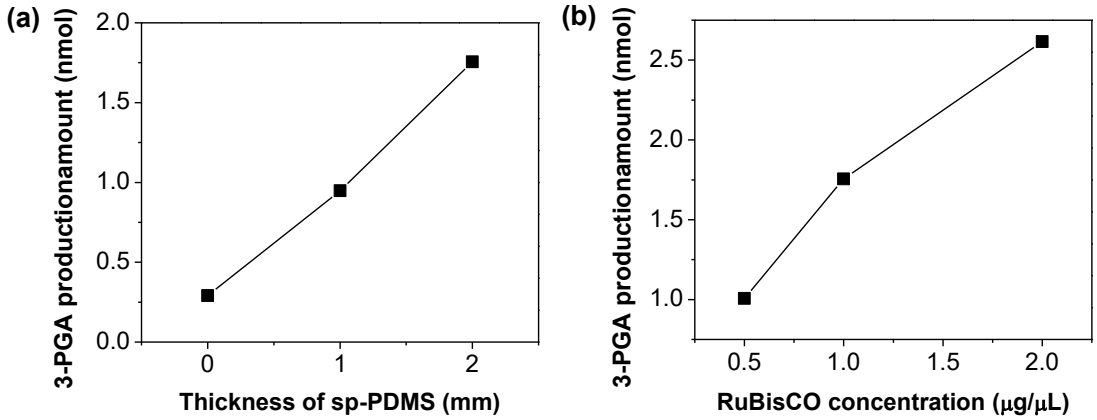

Figure 6.9 3-PGA production amount from the RI-SPMRs fabricated in different conditions with RuBP solution injected in 7 μL·min^{-1}. (a) 3-PGA production amount changes as a function of the thickness of sp-PDMS when 1 μg·μL of RuBisCO is injected for immobilization. (b) 3-PGA production amount changes as a function of the injected RuBisCO concentration by SPMRs fabricated with 2 mm-thick sp-PDMS.

The produced 3-PGA amount also increases with the increase of the injected

RuBisCO concentration, as shown in **Figure 6.9** (b) for the RI-SPMRs fabricated with 2 mm sp-PDMS. When the injected RuBisCO solution is 0.5 $\mu g \cdot \mu L^{-1}$, the produced 3-PGA amount is 1.007 nmol. It is increased by 2.6-fold when the injected RuBisCO solution is 2 $\mu g \cdot \mu L^{-1}$. And the 3-PGA production rate reaches 0.715 $nmol \cdot min^{-1}$ derived from the reaction time determined by the flow rate and the reactor volume. The enhancement of production rate is due to the increased amount of immobilized RuBisCO as a result of the increased concentration of the injected RuBisCO.

6.3.4 Feasibility of 3-PGA production with RI-SPMRs

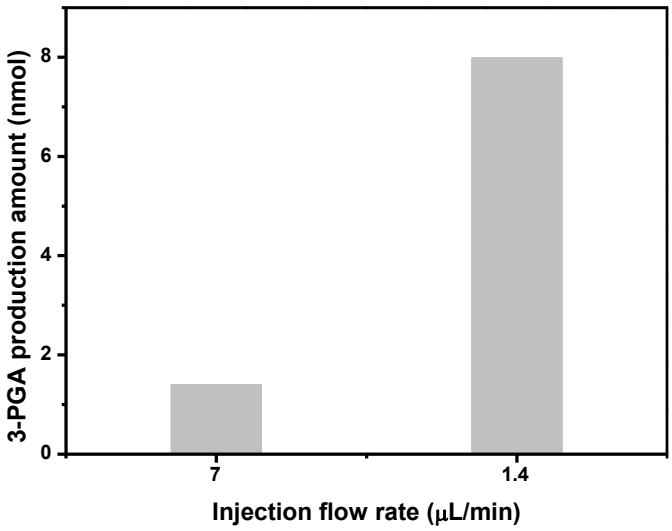

Figure 6.10 3-PGA production amounts when RuBP solution is injected at different flow rates. The thickness of sp-PDMS is 2 mm, RuBisCO concentration is 2 μg/μL.

The feasibility of the RI-SPMRs for 3-PGA production is verified by changing the flow rate of the injected RuBP solution. As shown in **Figure 6.10**, the produced 3-PGA amount is 0.140 nmol and 0.799 nmol respectively when the flow rate is 7 $\mu L \cdot min^{-1}$ and 1.4

μL·min^{-1}. The production is increased by 5.7-fold when the flow rate is decreased by 5-fold. As the injection flow rate decreases, the reaction time increases, which contributes to the production of a larger amount of 3-PGA. This result also proves the easy control of the 3-PGA production reaction in the RI-SPMRs.

6.3.5 Reusability of RI-SPMRs

Reusability of enzyme is very important for industrial usage. As shown in **Figure 6.11**, 90% of initial activity could be maintained after five cycles of reuse when the flow rate is 7 μL·min^{-1}. Compared with the reusability of the RI-PMRs (20.3%) and the RI-DPMRs (80%), the reusability is enhanced by 4.4-fold and 1.1-fold, respectively. The strong chemical bond between RuBisCO and PDA mainly contributes to the improved reusability. The slight activity loss may be due to the enzyme deactivation after the repeated uses and the enzyme detachment flushed off by the flowing solution [24].

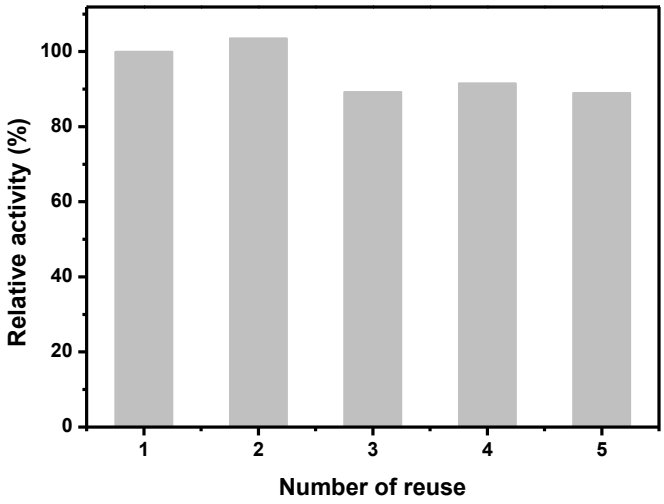

Figure 6.11 Reusability of the microreactor when the flow rate of the injected RuBP is set as 7 μL·min^{-1}. The thickness of sp-PDMS is 2 mm, RuBisCO concentration is 2 μg/μL.

6.4 Summary

In this chapter, the microfluidic reactors with monolithic porous structure were prepared in order to provide larger surface areas for the RuBisCO immobilization. The monolithic porous structure was prepared using the sp-PDMS fabricated by the sacrificial template method. The sp-PDMS was in-situ embedded into the microreactors for SPMRs fabrication. Even larger surface area was obtained by compressing a thicker sp-PDMS into the PMRs. Compared with the microreactors without the sp-PDMS in which RuBisCO was immobilized only on the inner surfaces, the RI-SPMRs obtained an increase of 4.8 folds in the amount of 3-PGA production. The 3-PGA production rate reached 0.715 $nmol \cdot min^{-1}$ with the 2 mm SPMRs when the injected RuBisCO solution was 2 $\mu g \cdot \mu L^{-1}$. The production rate was increased by 65.0-fold and 5.9-fold as compared to the RI-PMRs and the RI-DPMRs, respectively. This monolithic reactor greatly increases the enzyme loading therefore improve the overall reaction efficiency. In addition, the reusability was also enhanced. It attained up to 90% when the RuBP injection rate was 7 $\mu L \cdot min^{-1}$, which was 4.4 folds and 1.1 folds as compared to the RI-PMRs and the RI-DPMRs, respectively.

This in-situ sp-PDMS embedded microfluidic reactor provides a green solution to increase the surface area of microfluidics. Compared with the RI-DMPRs, the RI-SPMRs have a larger volume, ensuring a larger output in the same operation time. Therefore, a more promising method for the large amount of basic food material production is

accordingly offered.

6.5 References

[1] J. Qiao, L. Qi, X. Mu, and Y. Chen, "Monolith and Coating Enzymatic Microreactors of L-Asparaginase: Kinetics Study by Mce–Lif for Potential Application in Acute Lymphoblastic Leukemia (All) Treatment," *Analyst,* vol. 136, pp. 2077-2083, 2011.

[2] Y. Kang, J. He, X. Guo, X. Guo, and Z. Song, "Influence of Pore Diameters on the Immobilization of Lipase in Sba-15," *Industrial & Engineering Chemistry Research,* vol. 46, pp. 4474-4479, 2007.

[3] S. M. Santos, J. A. Cecilia, E. Vilarrasa-García, I. J. S. Junior, E. Rodríguez-Castellón, and D. C. Azevedo, "The Effect of Structure Modifying Agents in the Sba-15 for Its Application in the Biomolecules Adsorption," *Microporous and Mesoporous Materials,* vol. 232, pp. 53-64, 2016.

[4] H. Wang, Y. Jiang, L. Zhou, Y. He, and J. Gao, "Immobilization of Penicillin G Acylase on Macrocellular Heterogeneous Silica-Based Monoliths," *Journal of Molecular Catalysis B: Enzymatic,* vol. 96, pp. 1-5, 2013.

[5] M. Mathesh, B. Luan, T. O. Akanbi, J. K. Weber, J. Liu, C. J. Barrow*, et al.*, "Opening Lids: Modulation of Lipase Immobilization by Graphene Oxides," *ACS Catalysis,* vol. 6, pp. 4760-4768, 2016.

[6] J. Zhang, F. Zhang, H. Yang, X. Huang, H. Liu, J. Zhang*, et al.*, "Graphene Oxide as a Matrix for Enzyme Immobilization," *Langmuir,* vol. 26, pp. 6083-6085, 2010.

[7] D. Lee, J. Lee, J. Kim, J. Kim, H. B. Na, B. Kim*, et al.*, "Simple Fabrication of a Highly Sensitive and Fast Glucose Biosensor Using Enzymes Immobilized in Mesocellular Carbon Foam," *Advanced Materials,* vol. 17, pp. 2828-2833, 2005.

[8] D. S. Peterson, T. Rohr, F. Svec, and J. M. Fréchet, "Enzymatic Microreactor-on-a-Chip: Protein Mapping Using Trypsin Immobilized on Porous Polymer Monoliths Molded in Channels of Microfluidic Devices," *Analytical Chemistry,* vol. 74, pp. 4081-4088, 2002.

[9] D. S. Peterson, T. Rohr, F. Svec, and J. M. Fréchet, "High-Throughput Peptide Mass Mapping Using a Microdevice Containing Trypsin Immobilized on a Porous Polymer Monolith Coupled to Maldi Tof and Esi Tof Mass Spectrometers," *Journal of Proteome Research,* vol. 1, pp. 563-568, 2002.

[10] N. Brun, A. Babeau Garcia, H. Deleuze, M.-F. Achard, C. Sanchez, F. Durand*, et al.*, "Enzyme-Based Hybrid Macroporous Foams as Highly Efficient Biocatalysts Obtained through Integrative Chemistry," *Chemistry of Materials,* vol. 22, pp. 4555-4562, 2010.

[11] P. Li, J. A. Modica, A. J. Howarth, E. Vargas, P. Z. Moghadam, R. Q. Snurr, *et al.*, "Toward Design Rules for Enzyme Immobilization in Hierarchical Mesoporous Metal-Organic Frameworks," *Chem,* vol. 1, pp. 154-169, 2016.

[12] Y. Du, J. Gao, L. Zhou, L. Ma, Y. He, Z. Huang, *et al.*, "Enzyme Nanocapsules Armored by Metal-Organic Frameworks: A Novel Approach for Preparing Nanobiocatalyst," *Chemical Engineering Journal,* vol. 327, pp. 1192-1197, 2017.

[13] P. Li, Q. Chen, T. C. Wang, N. A. Vermeulen, B. L. Mehdi, A. Dohnalkova, *et al.*, "Hierarchically Engineered Mesoporous Metal-Organic Frameworks toward Cell-Free Immobilized Enzyme Systems," *Chem,* vol. 4, pp. 1022-1034, 2018.

[14] S.-J. Choi, T.-H. Kwon, H. Im, D.-I. Moon, D. J. Baek, M.-L. Seol, *et al.*, "A Polydimethylsiloxane (Pdms) Sponge for the Selective Absorption of Oil from Water," *ACS Applied Materials & Interfaces,* vol. 3, pp. 4552-4556, 2011.

[15] B. Liu, L. Wu, X. Zhou, H. Wu, and B. Zheng, "Porous Polydimethylsiloxane Monolith for Protein Digestion," *Journal of Materials Chemistry B,* vol. 6, pp. 824-829, 2018.

[16] S. Wu, J. Zhang, R. B. Ladani, A. R. Ravindran, A. P. Mouritz, A. J. Kinloch, *et al.*, "Novel Electrically Conductive Porous Pdms/Carbon Nanofiber Composites for Deformable Strain Sensors and Conductors," *ACS Applied Materials & Interfaces,* vol. 9, pp. 14207-14215, 2017.

[17] D. Zhu, S. Handschuh-Wang, and X. Zhou, "Recent Progress in Fabrication and Application of Polydimethylsiloxane Sponges," *Journal of Materials Chemistry A,* vol. 5, pp. 16467-16497, 2017.

[18] S. Liang, Y. Li, J. Yang, J. Zhang, C. He, Y. Liu, *et al.*, "3d Stretchable, Compressible, and Highly Conductive Metal - Coated Polydimethylsiloxane Sponges," *Advanced Materials Technologies,* vol. 1, p. 1600117, 2016.

[19] X. Zhao, L. Li, B. Li, J. Zhang, and A. Wang, "Durable Superhydrophobic/Superoleophilic Pdms Sponges and Their Applications in Selective Oil Absorption and in Plugging Oil Leakages," *Journal of Materials Chemistry A,* vol. 2, pp. 18281-18287, 2014.

[20] X. He, X. Mu, Q. Wen, Z. Wen, J. Yang, C. Hu, *et al.*, "Flexible and Transparent Triboelectric Nanogenerator Based on High Performance Well-Ordered Porous Pdms Dielectric Film," *Nano Research,* vol. 9, pp. 3714-3724, 2016.

[21] M. Chen, L. Zhang, S. Duan, S. Jing, H. Jiang, and C. Li, "Highly Stretchable Conductors Integrated with a Conductive Carbon Nanotube/Graphene Network and 3d Porous Poly (Dimethylsiloxane)," *Advanced Functional Materials,* vol. 24, pp. 7548-7556, 2014.

[22] S. Kang, J. Lee, S. Lee, S. Kim, J. K. Kim, H. Algadi, *et al.*, "Highly Sensitive Pressure Sensor Based on Bioinspired Porous Structure for Real‐Time Tactile Sensing," *Advanced Electronic Materials,* vol. 2, p. 1600356, 2016.

[23] C. Yu, C. Yu, L. Cui, Z. Song, X. Zhao, Y. Ma, *et al.*, "Facile Preparation of the Porous Pdms Oil‐Absorbent for Oil/Water Separation," *Advanced Materials Interfaces,* vol. 4, p. 1600862, 2017.

[24] C. Chao, J. Liu, J. Wang, Y. Zhang, B. Zhang, Y. Zhang, *et al.*, "Surface Modification of Halloysite Nanotubes with Dopamine for Enzyme Immobilization," *ACS Applied Materials & Interfaces,* vol. 5, pp. 10559-10564, 2013.

CHAPTER 7
CONCLUSIONS AND FUTURE WORK

This PhD research aims to produce basic food materials by realizing Calvin cycle *in vitro* using microfluidic reactors. The first enzyme in Calvin cycle, RuBisCO, was immobilized into the microreactors with three designs. The idea enables to overcome the long-standing problems of enzymes such as limited reaction efficiency, low thermal stability, decreasing activity in storage and poor reusability. In addition, the merits of microfluidics such as fine flow control, large surface-area-to-volume ratio, and low consumption are inherited at the same time with the advantages of enzyme immobilization.

Table 7.1 Comparison of the microfluidic reactors developed in this PhD research.

	Microstructure	SAV ratio		Protein loading efficiency		3-PGA production rate		Reusability [&]	
		Result (mm^2/mm^3)	Enhancement factor[※]	Result (%)	Enhancement factor	Result ($nmol \cdot min^{-1}$)	Enhancement factor[※]	Result (%)	Enhancement factor[※]
Design 1: RI-PMRs		52.5	-	20.5	-	0.011	-	20.3	-
Design 2: RI-DPMRs		52.5N[$]	N-fold	52.3	2.6-fold	0.237	21.6-fold	80	4-fold
Design 3: RI-SPMRs		57N	1.1N-fold	-	-	0.715	65-fold	90	4.5-fold
		114N	2.2N-fold						

[$] N is the enhancement factor induced by PDA coarse layer

[&] Reusability is the remaining relative activity after 5 cycles of reuse at the flow rate of 7 $\mu L \cdot min^{-1}$.
[※] The enhancement factors refer to the factor of the performance in Design 2 and Design 3 as compared to that in Design 1.

The first design (RI-PMRs) is a wall-coated type microfluidic reactor with RuBisCO directly immobilized on the PDMS inner surface by physical adsorption. The

immobilized RuBisCO amount is very limited, leading to a low 3-PGA production rate at 0.011 nmol·min^{-1}. The reusability of RI-PMRs is only 20.3%, which is not good enough for industrial usage.

The second design (RI-DPMRs) is also a wall-coated type microfluidic reactor. In this case, PDA is utilized to modify the PDMS surface of microreactors for RuBisCO immobilization via covalent binding. The PDA layer functionalized on the PDMS surface provides more active surface for the RuBisCO immobilization from the nanoscopic aspect. Therefore, more RuBisCO is immobilized, and a larger 3-PGA production rate (0.122 nmol·min^{-1}) is obtained. The bonding between RuBisCO and the support by PDA is much stronger compared with the physical adsorption in RI-PMRs, resulting in a remarkably enhanced reusability. When the flow rate of injected RuBP is 7 μL·min^{-1}, the reusability is about 80%. It can reach to 90% of the reusability when the flow rate is decreased to 1.4 μL·min^{-1}. Moreover, the RI-DPMRs enable to continuously produce 3-PGA with little RuBisCO, which maximize the efficiency of RuBisCO in a cheap, convenient and durable way for food material production.

The third design (RI-SPMRs) is a porous PDMS monolithic microreactor. The RuBisCO immobilization is also achieved by the PDA functionalization on PDMS surface. This structure provides an even larger specific area for RuBisCO immobilization from the microscopic aspect, therefore ensuring the highest 3-PGA production rate (0.715 nmol·min^{-1}) of the three designs. The reusability is also best (~90% when the flow rate of

injected RuBP is 7 μL·min^{-1}). In addition, the large volume of this design of microreactor guarantees a large amount of reactant to react with the enzyme, thereby greatly saving the operation time.

For comparison, the performances of the 3 designs of microfluidic reactors are listed in **Table 7.1**. In the aspect of the 3-PGA production rate, the second design RI-DPMRs and the third design RI-SPMRs present 11.1 folds and 65 folds of enhancements, respectively as compared to the first design RI-PMRs. In term of reusability, they are enhanced by 4 folds and 4.5 folds as well.

Nevertheless, there are still some limitations in this work. For example, the RuBisCO immobilization via PDA modification always affects the RuBisCO activity. In addition, there is still plenty of room for the increase of surface area if nanostructures are applied.

In the future, more research efforts can be put in the following topics:

(1) A better immobilization method may be developed to maximize the RuBisCO activity, such as the hydrogel encapsulation method, which can maintain the microenvironment of enzymes active sites.

(2) Some new micro- or nano-structures with large surface area can be considered for the microfluidic reactors.

(3) The reactor can be scaled up and more functionalities can be integrated, such as

deoxygenation, temperature control of individual reaction, etc.

(4) Other enzymes for the constitution of the full NPS pathway can also be employed in the reactor.

With the success of the above research efforts, a promising industrial route will be ready to produce large amount of basic food material and to relieve the food crisis. It eventually lifts the restrictions of labor, weather and land resources to the food production and prepares for the future space colonization. Moreover, the methods are very easy to be extended to other bio-enzymatic systems, therefore expanding the application of enzyme engineering and microfluidics in industry.